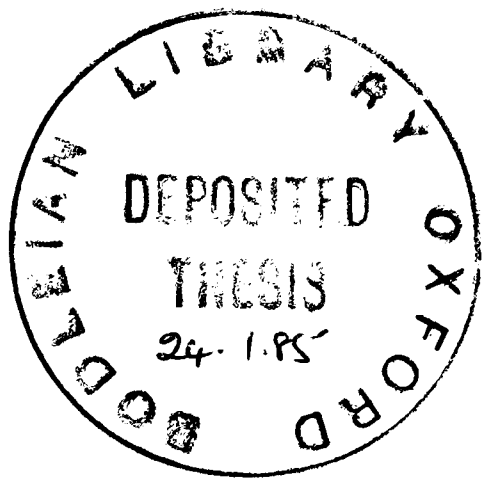
Kinetics and Energy Transfer Studies using a Shock Tube and Probe Laser



A Thesis submitted for the degree of Doctor of Philosophy

by

John A. Chenery

University College,
Oxford

Trinity Term
1984

Kinetics and Energy Transfer Studies using a Shock Tube and Probe Laser

A Thesis submitted for the degree of Doctor of Philosophy

by

John A. Chenery

University College,
Oxford

Trinity Term
1984

ABSTRACT

A continuous wave infrared CO laser has been used to monitor kinetic processes occurring behind shock waves. Studies have been made of both vibrational energy transfer and reaction kinetics.

It has been demonstrated that, following shock-heating, the vibrational levels of CO and DCl relax via a continuous series of Boltzmann distributions into the final Boltzmann equilibrium distribution at the translational temperature. This is shown to be in accord with the established theory, and it is proposed that all diatomic molecules relax in this manner. Previous results for HI, which suggested otherwise, are questioned, and the theoretical arguments used to explain these results are shown to be misconceived. A new method is developed to calculate vibrational relaxation times from any laser absorption trace.

The initial vibrational distribution of CO formed in the unimolecular decomposition of OCS at 4000 K has been investigated. It has been found that at least 90 % of the CO is born in the lowest vibrational level v=0, when 50 % would be in v=0 at equilibrium. This result is explained in terms of the dynamics of the reaction.

The kinetics of the isotope exchange reaction $^{12}C^{18}O + {}^{13}C^{16}O \rightleftharpoons {}^{12}C^{16}O + {}^{13}C^{18}O$ have been investigated. The results have been shown to be consistent with an atomic chain mechanism, in conflict with the conclusions of earlier work. Reasons for this are discussed.

A general account of the principles of operation of the apparatus is given, and conclusions are arrived at for the most profitable directions of future work.

ACKNOWLEDGEMENTS

Stephen Simpson, my supervisor, has been a fount of enthusiasm and ideas. This is just part of his long-term research programme.

I must also thank my fellow shock tube workers Tony Aherne, Mark Buckingham, John Buxton, Asghar Fakhr, Rupert Sohm and Malcolm Wood. I will remember them when I have forgotten physical chemistry.

For help with computing I thank the National Algorithm Group, the Oxford University Computing Service, Ivan Powis and my Simpsonite contemporary Tom Wickham-Jones. They may have had some influence on my future career.

Stephen, John, Mark and brand-new shock tube worker Richard Tossell generously allocated time to reading this manuscript at some stage in its development. (John, when I say 'at very early times', I do not mean the pre-Cambrian era.) The thesis was word-processed on the P.C.L.'s Onyx computer and printed on the N.E.C. spinwriter.

Figures 3.2 is adapted from Jean-Pierre Martin's thesis, 3.3 from Les Dolby-Glover's Part Two thesis, 6.2 to 6.6 from Mark Buckingham's Part Two thesis and 10.3 from Tony Aherne's Part Two thesis. Figures 2.1, 3.1 and 3.4 were produced on an Epson FX-80 lineprinter connected to a North Star Advantage computer running my program DRAWIT.

Finally I thank everyone associated with the P.C.L. for making it a place of which I am glad to have been a part.

To my parents

Also to Jayne, Mike, Rosemary and Sarah

CONTENTS

Chapter 1. Introduction. 1.

PART ONE. APPARATUS AND PRINCIPLES.

Chapter 2. Shock Tubes. 5.

Chapter 3. The P.C.L. Shock Tube and its Instrumentation. 26.

Chapter 4. Shock Tube and Infrared Absorption Theory. 44.

PART TWO. EXPERIMENTS ON ENERGY TRANSFER.

Chapter 5. Vibrational Relaxation following Shock-Heating. 62.

Chapter 6. Experimental Work on Carbon Monoxide. 102.

Chapter 7. Experimental Work on Deuterium Chloride. 124.

Chapter 8. Determination of Vibrational Relaxation Times from Single Laser Absorption Traces. 130.

PART THREE. EXPERIMENTS ON REACTION KINETICS.

Chapter 9. The Decomposition of Carbonyl Sulphide. 141.

Chapter 10. The CO Isotope Exchange. 159.

Chapter 11. Current and Future Work. 183.

References. 199.

CHAPTER ONE - INTRODUCTION

This thesis comprises an account of experimental work on gas-phase chemical kinetics at high temperatures (700-5000 K). A shock tube provides rapid heating and time-resolved infrared absorption spectroscopy is used to observe the chemical events which follow. The infrared source is a continuous wave carbon monoxide laser. The work may be conveniently subdivided into two areas: research into the kinetics of energy transfer and into the kinetics of reactions.

The former investigations are concerned with the transfer of energy from the translational and rotational degrees of freedom into vibration which occurs following the shock-heating of diatomic gases. Knowledge of the rate of population of the different vibrational levels is essential for an understanding of reactions in which vibrational energy is postulated to play a crucial role. Examples are provided by the dissociation of diatomic molecules and isotope exchange reactions.

The gases studied are CO [reference 1] and DCl [2], diluted in inert gas. The population growth curves of individual vibrational levels (v=1,2,3,4) are recorded. Theory [3,4] is clear in predicting the shape of these curves: the levels should relax via a continuous series of Boltzmann distributions. This is for a gas comprised of simple harmonic oscillators, which is a good description for the lowest vibrational levels. The results of Chow and Greene on HI [5] directly contradict the theory but this was not emphasised, so there has been some confusion in the literature. Thus the experiments reported here are important.

Also, a new method is developed to calculate vibration-translation energy transfer rate constants from laser absorption traces, and is applied to the case of CO-He over the temperature range 900-2300 K.

These studies complement the work on energy transfer carried out with this shock tube for many years; they are the first studies to be completed which make use of the CO probe laser.

The investigations on reaction kinetics reported here are the first to be made with this shock tube. A variety of systems is studied, partially in order to determine in which areas future work might most usefully be done. The initial vibrational distribution of carbon monoxide produced in the decomposition of carbonyl sulphide, OCS -> CO + S, is deduced [6] and similar investigations are begun for larger molecules. This is the first time such information has been obtained directly for thermally initiated reactions to our knowledge, though work has been done on similar systems initiated photochemically [7-9]. The mechanism of the isotope exchange reaction

$$^{13}C^{16}O + {}^{12}C^{18}O \rightleftharpoons {}^{12}C^{16}O + {}^{13}C^{18}O \qquad (1.1)$$

is also investigated. The major points of interest here concern the role of vibrational energy of the reactants and whether a four-centre transition state is involved.

Computer calculations are presented which model the systems studied, other work in the field is reviewed, and suggestions are made for further work.

Part One of the thesis is an introduction to the shock tube field. In chapter two an account is given of different types of shock tube and of elementary theory. In chapter three the apparatus used here is described, and past work carried out with it is reviewed. In chapter four the detailed shock tube theory and infrared absorption theory necessary for what follows are described.

In Part Two the work on energy transfer is discussed. Chapter five develops the relevant theory and considers past work. Chapters six and seven give an account of the experiments on CO and DCl respectively. Chapter eight describes how rate constants can be obtained from a single laser absorption trace, and presents results for the CO-He system.

In Part Three the experiments on reaction kinetics are discussed. Chapter nine is a discussion of the OCS decomposition experiment. Chapter ten presents the work done on the isotope exchange (1.1). Chapter eleven closes the thesis with an account of current and future work.

PART ONE

APPARATUS AND PRINCIPLES

CHAPTER TWO -SHOCK TUBES

2.1 Introduction

Shock tubes are divided into two sections,the driver and driven sections. These are separated by a burstable diaphragm. The driver section contains a higher pressure of gas than the driven section. When the diaphragm bursts, a shock wave passes into the driven section, compressing and heating its contents, and a train of expansion waves passes into the driver section, cooling its contents. There is often a third section separated from the driven section by another diaphragm. It is called the expansion section, dump tank or damp tank. When the second diaphragm bursts, the contents of the driven section expand into the expansion section and cool.

Experiments in this laboratory are carried out in the driven section on gases, but experiments have been done in all three sections and on liquids as well as gases. For example, Driels [10] has studied bulk cavitation in a vertical water-filled shock tube during research on underwater explosions. Barschdorff [11] has observed the condensation of water droplets caused by the expansion of a vapour in the driver section; Hodgson and Mackie [12] did a similar experiment in the expansion section on cyclohexane vapour. Beck and Mackie [13] observed the three-body recombination of iodine atoms in the expansion section. Henceforth we shall only be concerned with gas-phase work in the driven section (which therefore will be referred to as the test section), but, before discussing the scope of that work, the introduction of some theory is necessary.

2.2 Production of the Shock Wave

When the diaphragm bursts, the pressure in the driver section must be greater than the pressure in the test section in order for a shock wave to pass into the test section. In some designs the diaphragm is burst by pricking it with a needle (e.g. [14]), but more often is allowed to burst spontaneously as a result of an increase of pressure in the driver section. This increase in pressure may be brought about in the following ways:

i)Further driver gas is added to the driver section until the diaphragm bursts, as is done in this work. This is the conventional method for chemical applications.

ii)The driver gas is heated by a filament (e.g. [15]).

iii)The driver gas is heated by an electric discharge - an 'arc-driven' shock tube (e.g. [16]).

iv) An explosive gas mixture is used in the driver section (e.g. [17]).

v) The driver gas is compressed with a piston [18].

To give some idea of the temperature range available, Dannerberg [16], using an arc-driven shock tube, has obtained a shock-speed in air 60 times greater than the speed of sound, which corresponds to a post-shock temperature in excess of 200,000 K.

At the other extreme, Simpson et al [19] have obtained results down to 320 K. A shock tube cooled with liquid helium to 30 K has been used to obtain results after shock-heating to 130 K [20] (and the condensation of argon in the driver section of a liquid-nitrogen cooled shock tube has been studied at 47 K [21]), but usually there are more convenient techniques for getting results below room temperature.

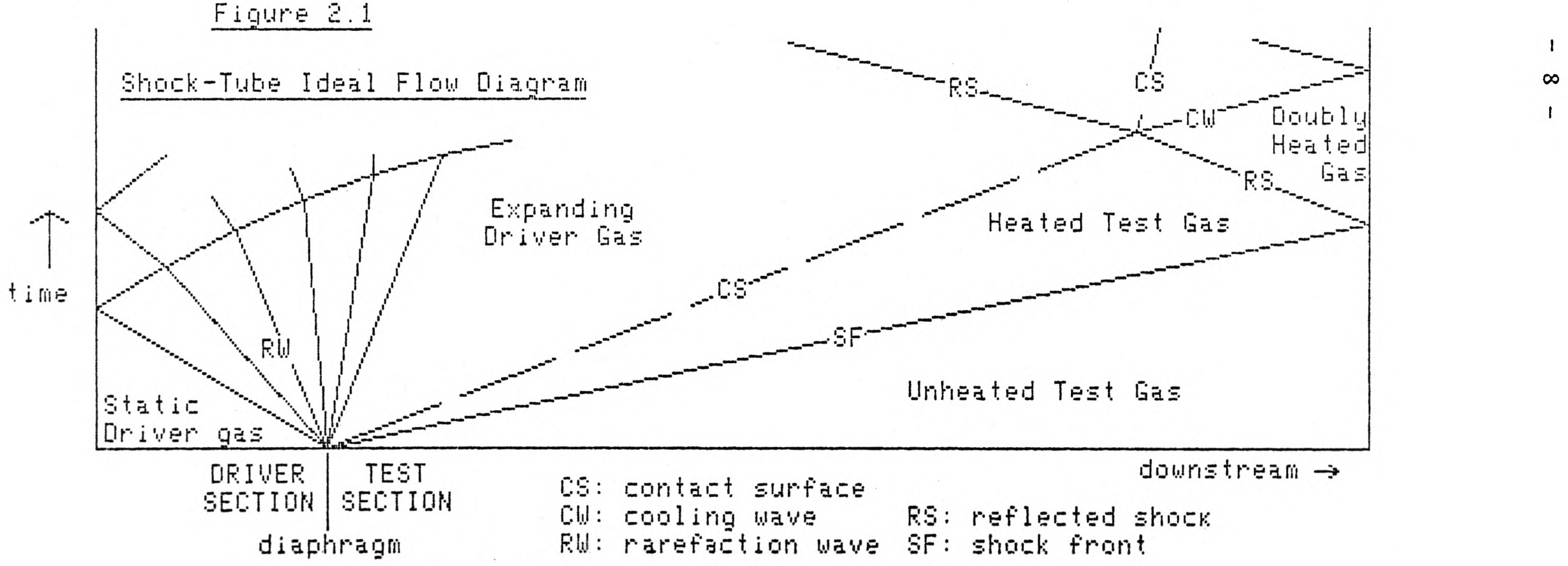
The mechanism of the formation of the shock wave may be discussed in the following manner:

The instant the diaphragm bursts, the driver gas begins to expand into the test section. A compression wave travels ahead of it into the test gas. The expansion continues so further compression waves follow. Each compression wave raises the temperature of the test gas. The speed of sound varies as the square-root of temperature, so every wave travels faster than its predecessor. The result is that they catch up with each other to form a sharp discontinuity called a shock front, behind which temperature, pressure and density are elevated. A shock wave consists of this one sharp jump, completed in 5 to 10 collisions, and is so contrasted from a sinusoidal sound wave. It is supersonic in the sense that it travels faster than the speed of sound of the unheated gas in front of it, but it travels at the speed of sound of the heated gas immediately behind it.

2.3 Ideal Flow Diagram

Meanwhile, a series of expansion (or rarefaction) waves propagate into the driver section. Because these cool the gas, they do not form a sharp discontinuity but spread out. Behind the shock front the body of heated test gas moves down the tube, since it is being compressed. It moves more slowly than the shock front, which is the signal which 'tells' the test gas that it is being compressed. The boundary between the heated test gas and the expanding driver gas is called the contact surface. In the region between the contact surface and shock front, temperature, pressure and density are constant in the absence of chemical events, for ideal flow. The shock tube ideal-flow diagram (Figure 2.1) is a time/distance graph. This diagram assumes an instantaneous removal of the diaphragm, and no interaction of the shock

Figure 2.1


Shock-Tube Ideal Flow Diagram
RS
CS
CW
Doubly Heated Gas
RS
Expanding Driver Gas
Heated Test Gas
time
CS
RW
SF
Static Driver gas
Unheated Test Gas
DRIVER SECTION
TEST SECTION
downstream →
diaphragm
CS: contact surface
CW: cooling wave
RW: rarefaction wave
RS: reflected shock
SF: shock front

wave with the tube walls. The real situation will be discussed in section 2.6; the diagram remains a very useful guide. When the shock front reaches the end of the test section it reflects, and brings into existence a region of doubly-heated gas. Experiments may be carried out behind the incident or reflected shock. The measurements discussed here are made behind the incident shock, but many workers use the doubly-heated region. The advantages and disadvantages of this are discussed in section 2.9.

If there is a second bursting diaphragm between the test section and expansion section (i.e at the extreme right-hand end of figure 2.1), the situation will be different. A reflected shock still occurs, but, as the diaphragm breaks, new expansion waves propagate and the test gas moves into the expansion section. Reflected shock workers employ an end wall rather than the second diaphragm.

2.4 Real-time and lab-time

This is a convenient point to introduce the distinction between real time and laboratory time for experiments behind the incident shock. Consider an observer studying the small segment of test gas passing at an instant in time. To obtain any rate data, he or she needs to know the time, t_r, 'real time', since the segment of gas was heated. This event occurred when the shock front and segment were at the same place. Let the shock front be travelling with velocity u_1 and the test gas at $u_1 - u_2$ (u_2 is then the velocity of the test gas relative to the shock front). The shock front has passed the observer, who recorded the event, and is now distance x away. The segment is passing the observer now. t_r seconds ago the shock front was $u_1 t_r - x$ distance from the observer, while the segment of test gas was $(u_1 - u_2)t_r$ from the observer. Thus, as they were at the same place $u_1 t_r - x = (u_1 - u_2)t_r$

i.e. $t_r = x/u_2$.

The time that the observer can measure directly (on an oscilloscope or transient recorder timebase), 'laboratory time', is the time since the shock front passed i.e. x/u_1. So to convert laboratory time into real time, as is desired, the former must be multiplied by $(x/u_2)/(x/u_1) = u_1/u_2$. As u_1 is greater than u_2, real time is longer than laboratory time. This is an alternative to the usual explanation given from the point of view of a hypothetical observer travelling on the shock front.

2.5 Position of Observation Windows for Experiments behind Incident Shock

The observer wishes to monitor the heated test-gas for as long as possible under the constant conditions behind the incident shock. Two events can bring about the end of these conditions: the arrival of the reflected shock at the observation point, and the arrival of the contact surface. Maximum observation time is obtained at the point where the contact surface and reflected shock meet. This is a function of u_1/u_2 which varies from experiment to experiment so the observation windows are fixed at the optimum point for an average experiment. This point is some distance upstream from the end wall (very close to which the reflected shock worker places his windows). A third event which could conclude the uniform post-shock conditions is the leading rarefaction wave arriving after reflecting from the end of the driver section. The driver section is made sufficiently long that this does not happen. Too long a driver section uses an unnecessary quantity of driver gas and increases the ultimate post-experiment pressure in the whole tube.

2.6 Real Flow

The diaphragm is not removed instantaneously and the shock wave does interact with the walls. As a result of the former the shock wave takes time to accelerate to its maximum speed; as a result of the latter, it then decelerates [22]. The shock is curved initially but becomes planar by Mach reflections from the shock tube walls within 10-20 tube diameters, and is almost exactly perpendicular to the walls. The wall interactions (which occur because real gases have finite viscosity and finite thermal conductivity) cause the formation of a boundary layer of cooler gas along the walls. As a result the shock front becomes slightly curved at the edges.

As the shock wave decelerates the contact surface accelerates and this continues until they have reached the same speed [23]. Thereafter the distance between them remains constant, so there is no advantage in observation time to be gained by increasing the length of the test section indefinitely.

A discussion of the consequences of the boundary layer in this work will be found in section 4.9, and the work done in this shock tube on diaphragm opening times in section 3.11.

2.7 Range of Experiments carried out in Shock-Tube Driven Sections

This is a thesis on chemical kinetics, but we shall pause briefly to consider the range of other work done. A closely related application is spectroscopy. Spectroscopic techniques are used by kineticists to follow reactions in shock tubes, but can also be used by spectroscopists to determine absorption coefficients and lineshapes at high temperatures and pressures. For example Lesage et al [24] studied the Stark-broadening of Si^+ at up to 12,500 K behind reflected shocks. The work

of Weisbach and Chackerian [25] on CO is of direct relevance to our work and will be discussed in chapter 4.

The test gas can contain solid particles, either formed in a chemical reaction or injected into the tube beforehand. Nakajima et al [14] shock-heated metal oxide particles and looked at the atomic emission lines resulting. They proposed this as an analytical technique for determining the composition of mixed metal oxide particles. Frenklach et al [26] measured the size of soot particles formed in the pyrolysis of toluene by a laser technique. Seeker et al [27] placed a 20 mg lump of coal inside the shock tube and observed its ignition and burnout. Nasser and East [28], using a shock tube to dissociate hydrogen, observed the heat transfer from the H atoms to a catalytic nickel surface inside the tube. Finally, Fujikawa et al [29] found a use for the boundary layer that grows on the end wall after the passage of a reflected shock. A vapour cooled in the boundary layer and a thin liquid film formed on the end wall: this was a study of a liquid-vapour phase change.

We shall now look at the range of instrumentation used in kinetics experiments.

2.8 Instrumentation in a Shock Tube Experiment

The instrumentation in use in our laboratory will be discussed in detail in chapter 3. The shock tube itself can be a simple apparatus. Shock tubes have been made from steel, brass and pyrex. With pyrex the observation point may be varied. The cross-section of the tube may be circular, which is cheaper, or rectangular, which allows easy fitting of gauges and windows. Special features that have been employed will be discussed in section 2.20. We shall now concentrate on the techniques used to determine the actual kinetics. First we must discuss the

advantages and disadvantages of working behind the incident and reflected shocks.

2.9 Incident or Reflected Shock?

The greatest differences in carrying out experiments behind the incident and reflected shocks are:

i)Higher temperatures are reached behind the reflected shock (for the same driver conditions).

ii)The test gas is stationary behind the reflected shock.

By themselves these statements appear to favour the reflected shock technique. It is essential to use the reflected shock technique for work at temperatures approaching, or greater than, 10,000 K (for conventionally-driven shock tubes). At lower temperatures there is a choice. It requires less extreme driver conditions, and less test gas, to reach a given temperature and pressure if the reflected shock is employed. On the other hand, at very low temperatures where weak shocks are required, the incident shock technique is easier.

Because the test gas is stationary behind the reflected shock,it may be removed for analysis. This is impossible behind the incident shock.

For the case of ideal flow, it is no more difficult to calculate post-shock conditions behind the reflected shock than behind the incident shock, from a measurement of the shock speed. However, flow irregularities have a magnified effect behind the reflected shock. For example, deceleration of the incident shock between the region where the speed is measured and the end wall causes an overestimation of the speed of the reflected shock and hence an overestimation of the temperature

and pressure. The most serious drawback is the complex interaction of the reflected shock and side-wall boundary layer left behind the incident shock. Also the reflected shock may 'scrub' impurities off the shock tube walls and into the test gas. The effects can be allowed for to some extent but introduce greater uncertainty in the rate constants determined. Thus many workers prefer working behind the incident shock.

The difficulties behind the reflected shock are probably best avoided by using an optical technique very close to the end-wall, e.g. [30].

Methods involving analysis of the test gas from the shock tube require the reflected shock technique; other analytical methods may be performed behind incident or reflected shocks.

2.10 Single-Pulse Shock Tube

A shock tube designed for the determination of rate constants by product analysis, after the reaction is complete, is called a single-pulse shock tube. Use of this method demands that:

(i) The reaction is initiated rapidly.

(ii) At the end of the reaction time, it is quenched rapidly.

(iii) The reaction does not restart i.e. it is 'single-pulse'.

(iv)The time for which the reaction takes place is well known.

The reaction is initiated by shock-heating which is very rapid (5-10 collisions). However the gas has already been heated by the incident shock to approximately half the final temperature. In order that this pre-heating causes negligible extent of reaction, the reaction studied must have a large activation energy. This also means that the cooling process quenches the reaction more rapidly, although secondary reactions with small activation energies will not be quenched so

rapidly.

Lifshitz, Bauer and Resler [31] describe how the shock tube is designed to maximise the cooling rate. When the reflected shock meets the contact surface, a cooling wave is generated and heads back through the test gas, as shown in figure 2.1. (The reflected shock continues towards the driver section and the contact surface is brought approximately to a halt [22].) The rarefaction wave from the original bursting of the diaphragm, having reflected off the end of the driver section, will also cool the test gas when it catches it. The optimum cooling rate is obtained by arranging to adjust the length of the driver section so that the reflected shock meets the contact surface and rarefaction wave at the same time.

If the reflected shock reflects again from the end of the driver section and returns, it can restart the reaction. A special tank, joined to the side of the test section near to the diaphragm, effectively quenches the reflected shock but only slightly attenuates the incident shock.

Condition (iv) is most problematical. The reaction time is from the arrival of the reflected shock to the arrival of the cooling wave (figure 2.1). Yet this time, the 'dwell-time', varies along the tube, from a maximum at the endplate to zero at the other extent of the doubly-heated region. Considering real flow, the problem is made worse by the finite diaphragm opening time. This causes some mixing of the driver and test gases, so that some of the test gas is not heated by the shock wave. If this unheated gas gets into the sample to be analysed, the measured extent of reaction will be too low.

It is common for the test gas to be largely argon diluent. Bar-Nun and Lifshitz [32], placed a valve in the middle of the test section. On

the diaphragm side of the valve, the test section was filled with pure argon and only on the other side with the full reactive mixture. The valve was opened (a slider valve was used) immediately before the shock was fired. None of the reactive mixture mixed with the driver gases. This idea can be extended so that the reactive mixture is confined to a very small part of the test section by two valves, constituting a 'reactive slug' so that the dwell-time is very nearly the same for all the reactive mixture.

To avoid the uncertainties of absolute rate constant measurements, Tsang [33] has developed a comparative technique, utilizing for standards reactions whose rate constants have been established by another method.

The analysis of the sample may be done by gas chromatography [31] or mass spectrometry [32]. The post-shock conditions are calculated either from a measurement of the reflected shock speed or from the incident shock speed but taking into account deceleration.

With this method, for each run, just one measurement of the concentration of each species at one time is produced. Thus no information is gained on the time dependence of the concentration. To obtain a rate constant, a rate law must be assumed - usually it is assumed that product growth is single-exponential. If there is an induction period, it will not be seen. This is a serious disadvantage for the study of a reaction of uncertain mechanism.

There is a useful summary of the single-pulse technique in an article by Khandelwal and Skinner [34].

2.11 Time-of-flight Mass Spectrometry

This is a useful technique for studying the variation of the concentration of a species with time when there is no suitable spectroscopic technique. The technique can only be applied behind the reflected shock. Taking as an example the apparatus of Kern and coworkers [35], gas flows through a nozzle, which protrudes approximately 1 mm into the shock tube from the end wall, into an ion source. The protrusion is necessary to avoid the sampling of gas cooled prematurely by the boundary layer on the end wall. In the ion source the gas is ionised at 20 μs intervals for a typical reaction period of 500 μs. Optical spectroscopic methods give a more continuous record of species concentration, but the time-of-flight method is a great improvement on the single-pulse shock tube in this respect. The employment of a mass spectrometer always leads to doubts that some reactions might be occurring in the spectrometer itself and distorting the results. Optical spectroscopic methods are in situ by nature and to be preferred but time-of-flight is good for the observation of several species at once in a complex reaction.

2.12 Interferometry

This technique and the laser schlieren technique determine bulk properties of the test gas. Interferometry gives a record of the variation of the density of the test gas with time. The density drops when an exothermic reaction is occurring and rises during an endothermic one. A beam of light passing through the test gas is made to interfere with a beam which has by-passed the shock tube. The fringe-shift changes as the density does. The resulting pattern is recorded photographically. The light beam must cross at right angles to the shock tube, i.e. parallel to the shock front, for optimum time

resolution. (This applies to all optical methods.) The earliest experiments on the shock tube used in this work were completed using a Mach-Zehnder interferometer, using a short-duration spark light source [36]. Some more recent work of Glass and Liu [17] uses a ruby laser as a light source.

2.13 Laser Schlieren

This technique relies on the refraction of light caused by a change in density of the medium it is traversing, which is the phenomenon that produces mirages. A laser beam is made to traverse the shock tube, and its deflection in the horizontal plane is monitored using a partially blocked or divided (differential) photomultiplier or photodiode. What is obtained is a record of the variation of density-gradient behind the shock front with time. Although this is the only variable followed in a laser schlieren experiment, the technique has high sensitivity and resolution [37], and information can be gained on reactions with complex mechanisms containing many steps [38] e.g. the pyrolysis of propene [39].

Laser schlieren and interferometry are unsuitable for reactions which are very close to thermoneutrality such as an isotope exchange e.g. equation (1.1). This also applies to thermoneutral steps within a complex mechanism and can be advantageous. The schlieren experiment obtains information on the other step(s) without interference from the thermoneutral ones. The laser schlieren technique superseded interferometry in this laboratory [40,41] and was used until the advent of our CO laser. It is able to determine rate constants for faster processes than other techniques, and has recently been reviewed by Kiefer [42].

2.14 X-Ray Absorption

This is an alternative technique to interferometry for measuring density changes [43]. X-ray absorption is unaffected by chemical reaction.

2.15 Ultra-violet and Visible Emission

Quartz windows in the shock tube walls allow the observation of emissions from the excited gas. Optics must be arranged to restrict the segment of heated gas from which the emissions are collected, in order to optimise the time resolution. Many species are amenable to this technique. A monochromator is used to cut out emissions from other species. Usually intermediates, formed in electronically excited states, are observed e.g. CH^*, C_2^* [44], OH^* [45]. 'Flame-band' emission from recombined CO_2 is used as a diagnostic for CO and O [46]. Its intensity is proportional to the product of the concentrations of those species. Thus a known concentration of CO is often added to a reaction mixture which forms O atoms.

2.16 I.R Emission

This is a very commonly used shock tube diagnostic technique for species such as CO [47], CH_2O and CO_2 [46], and HCl and DCl [48]. Problems from overlapping bands can be overcome to some extent by using filters but it is not possible to resolve different vibrational bands of CO (1->0, 2->1, 3->2 etc) because they overlap [49]. To remove interference from other vibrational bands, it would be necessary to look at a single vibrotational line but the necessary resolution is not available in emission. However useful information can be obtained by looking at the fundamental ($\Delta v=1$) and overtone ($\Delta v=2$) bands separately [50].

Emission techniques require less instrumentation than absorption ones, and are the only alternative if no suitable laser or other light source is available.

2.17 U.V. and Visible Absorption

This is another popular technique. A narrow light-beam is passed across the shock tube. The light-source may be a discharge lamp; in this case the beam is often not made monochromatic until after passing through the shock tube [5]. The beam crossing the tube is then relatively powerful so there is a danger of it acting as a 'pump' rather than a 'probe', and disturbing the kinetics it is being used to investigate.

A more monochromatic source is provided by utilizing atomic resonance absorption spectroscopy (ARAS) [51-53]. Sources are designed to emit an atomic line. Hydrogen atom (using the Lyman-α line) and oxygen atom concentrations can be followed using this technique. The absorption coefficients of such lines are very large, so very small concentrations (a few p.p.m.) of atoms may be observed. It is thus possible to do experiments on very high dilutions of reactants in argon, which greatly simplifies the kinetics by eliminating many secondary reactions. Working with such large dilutions necessitates correspondingly low impurity concentrations so an ultra-high-vacuum shock tube is necessary. With ARAS, larger concentrations of reactants in a less clean shock tube do not constitute a viable alternative as 100 % absorption will then occur when the extent of reaction is very low.

Hanson et al [54] have used a dye laser to study OH radicals formed in the H_2/O_2 reaction in a feasibility study. Such an apparatus is very expensive but they point out that use of a fibreoptic link enables a

central laser to be shared by several research groups.

2.18 Infra-red Absorption

This is the technique used here, and will be discussed in detail in the next chapter. The infrared source is invariably a laser and an individual vibrotational line is observed. As well as CO lasers, a CO_2 laser has been employed [55]. Hundreds of frequencies can be obtained from a CO laser (use of isotopic CO adds to the range) but it is not continuously tunable as a diode laser is. Hanson [56] has used a rapidly tunable diode laser, to sweep across a single vibrotational line of CO during the the time the CO is heated by an incident shock, and thus to compare experimental and theoretical line shapes.

The other users of CO lasers with shock tubes have been Hanson and coworkers [57,58], Weisbach and Chackerian [25,59], and Dibble and Bowen [60]. Only the Simpson group has monitored CO (v=0) using the 1->0 vibrational band.

2.19 Advanced Spectroscopic Techniques

Where possible, the simpler techniques are to be preferred, but any spectroscopic technique should be considered for shock-tube use. A requirement of any new technique is that the relationship between signal and species concentration is known.

Shock-tube intracavity dye laser spectroscopy (SIDLS c.f. [61]), in which the shock tube would be inside the laser cavity, is under consideration by this research group, and is believed to be feasible [62]. Intracavity absorption spectroscopy has the advantage of being more sensitive than conventional absorption spectroscopy by several orders of magnitude. Thus species with very weak absorption bands may

be studied e.g. HCO. There is a recent review of intracavity spectroscopy by Harris [63]. The dependence on species concentration is linear.

Laser fluorescence has been used with a shock tube by Bott and Cohen [64]. This was a conventional laser fluorescence experiment (see for example [65]) on energy transfer in HF (the deactivation of the v=1 level) with the shock tube being employed to supply a high translational temperature, rather than the use of laser induced fluorescence (LIF) as a diagnostic for a species formed in a shock-initiated reaction. (Conventionally laser induced fluorescence refers to excitation to another electronic state, laser fluorescence within the ground electronic state.)

Spontaneous Raman spectroscopy has also been used with a shock tube [66], but only as a means of establishing the equilibrium temperature and density of partially ionised nitrogen gas. The technique was said to be at the limits of its applicability.

Indeed pulsed laser techniques such as LIF and the various Raman techniques are generally unsuitable for use with a shock tube for the following reasons:

(i) They normally employ signal-averaging, as the inherent signal-to-noise is low. This is not possible with a shock tube as the repetition rate of shocks is low, typically two per hour, and the shocks are not exactly reproducible. The shock tube technique is single-shot by nature.

(ii) As for the single-pulse shock tube, only one measurement of species concentration at any one time is made in each experiment.

Also any technique involving measurement at a surface cannot be used because of the existence of the boundary layer. This rules out the

opto-galvanic effect.

2.20 Special Shock-Tube Features

'Ultra-clean' shock tubes are necessary in some cases. When ARAS (section 2.17) allows very low concentrations of reactants to be used, impurity levels must be exceedingly low. Also, certain processes are catalysed by atoms produced from impurities via chains e.g. $H_2 + D_2 \rightarrow 2HD$ [67]. Hydrogen atoms represent a special problem as they can be formed from hydrocarbon molecules which have backstreamed from the pump-oil. Therefore in an ultraclean shock tube great effort is made to exclude pump-oil [67]. Such a shock tube is bakeable to 300-400 ^{o}C which necessitates the design of special windows [68]. To minimise degassing from the shock-tube walls, all rubber and plastic parts are excluded and the test section is made from seamless steel. The sharp corners of a rectangular shock tube are undesirable. Myerson and Watt [51] rounded their corners off; an entirely cylindrical tube can be used. Great attention is paid to test-gas purity. Myerson and Watt were able to pump down to less than $1x10^{-7}$ torr without baking and had a degassing rate of $1-5x10^{-9}$ torr/min. For conventional shock tubes equivalent figures are $1x10^{-5}$ torr and $2x10^{-4}$ torr/min. Fortunately extreme precautions are not necessary for the study of all reactions.

Another special design is the discharge-flow / shock-tube, for example as described by Borrell et al [69]. Test gas flows through the test section of the shock tube continuously but this does not disturb the formation of the shock wave in an otherwise conventional tube. The technique allows excited intermediates, generated in the flow before it enters the test section, to be studied as reactants. An example is $O_2(^1\Delta_g)$ generated in a microwave cavity [69]. The reactions which remove the intermediate must be slow enough at room temperature for

there to be an observable concentration of the intermediate at the shock tube observation point, but fast enough at the post-shock temperature for the decay of that concentration to be observable.

2.21 Alternatives to Shock Tubes for Studying High Temperature Reactions

As the temperature range studied approaches room temperature, more techniques become available. We shall restrict ourselves here to techniques used at over 1000 K.

Heated flow systems [70,71] offer the advantage of steady-state conditions. The high temperature fast flow reactor of Fontijn et al. provides results up to about 2000 K.

The technique of rapid compression [72] increases pressure and temperature like the shock tube. However the resultant conditions are not so simple to deduce. The compression is produced by a piston, as in the internal combustion engine. Temperatures of up to ~1400 K may be reached. Advantages are that reactions may be studied for tens of milliseconds, longer than in shock tubes, and that conditions are similar to those in working combustion systems such as engines.

An area in which much work is being done is flame studies. A flame is simple to produce. The burner is designed so that the flame is stable - the system is then in a steady state. However species concentrations depend on diffusion equations as well as chemical equations (and the former often dominate) and heavy dilution in an inert gas to simplify the kinetics is not viable. The shock tube is to be preferred for the study of elementary reactions. Flames are unlikely to be employed in order to study reactions which do not themselves occur in flames of practical importance, e.g. CH_4/O_2 which is an extremely complex system. Nevertheless that practical importance is enormous so a

very large amount of work is done by this technique. An example of modern flame work is that of Kychakoff et al [73].

2.22 The Advantages of Shock Tubes

With shock tubes the attainable temperature range is from 320 K to as high as might be desired in a chemical experiment. It is a simple matter to adjust test-gas composition, diaphragm and driver gas to reach the desired conditions. The heating is extremely rapid ($\leq$ 10 ns) and conditions then remain constant (ignoring the effect of chemical reactions) for 50-1,000 μs (depending on the exact conditions). This is long enough for most processes of interest to be observed, and short enough for interactions of molecules with the walls to be unimportant. The essential apparatus is relatively simple, as is the calculation of the post-shock conditions.

This completes the discussion of shock tubes in general. In the next chapter, one shock tube in particular, that used in this work, will be described.

CHAPTER THREE - THE P.C.L. SHOCK TUBE AND ITS INSTRUMENTATION

3.1 The Shock Tube

The shock tube was designed and built at the National Physical Laboratory in 1963/1964 and transported to Oxford in 1969. The experiments carried out with it prior to the present work will be described in section 3.11.

The shock tube is conventionally driven (see section 2.2) and makes use of spontaneously bursting diaphragms. It is designed for measurements to be carried out behind the incident shock. The apparatus is outlined in figure 3.1.

The driver section is a chromium-plated steel cylinder of length 1.9 m and internal diameter 10.8 cm. A 15 cm long stainless-steel change-shape section leads to the test section.

The test section is 3.7 m long and has a rectangular cross-section. The internal dimensions are 7.62 cm (width) and 5.08 cm (height). Details of the construction of the test section are given by Simpson, Chandler and Clutterbuck [74]. It is formed from 4 bars, sealed together with O-ring cord. All fittings are ground flush with the inner walls.

At the end of the test section is the dump tank, a cylinder of length ~1.3 m and diameter ~0.8 m, separated from the test section by a second diaphragm. It serves as a reservoir to reduce the post-experiment pressure and any solid particles formed behind the shock front are swept into it rather than left to pollute the test section walls.

The driver section and dump tank are held against the test section

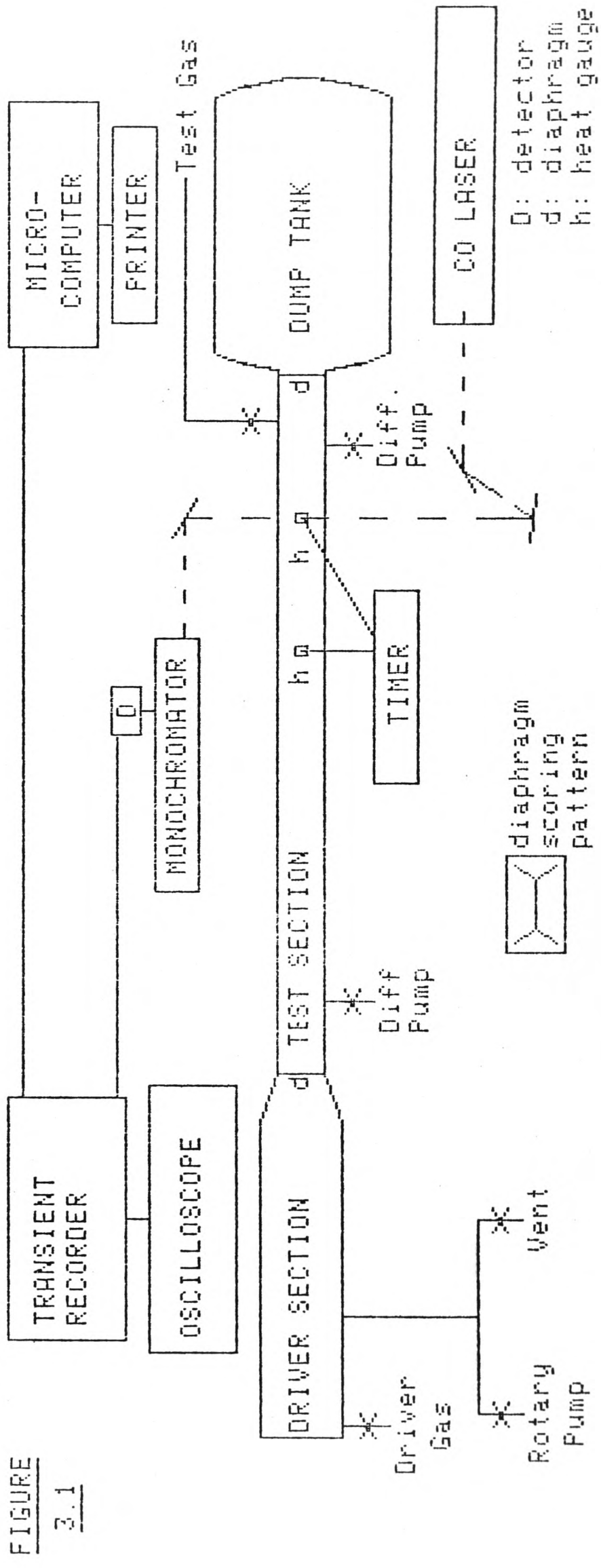

MICRO-
COMPUTER
PRINTER
Test Gas
DUMP TANK
CO LASER
D: detector
d: diaphragm
h: heat gauge
Diff.
Pump
h
d
h
TIMER
D
MONOCHROMATOR
diaphragm
scoring
pattern
TRANSIENT
RECORDER
OSCILLOSCOPE
DRIWER SECTION
d
TEST SECTION
Diff
Pump
Vent
Driwer
Gas
Rotary
Pump

FIGURE 3.1

with 100 ton and 20 ton hydraulic rams respectively. The oil pressure used in practice is 2,000 P.S.I. and 1,000 P.S.I. respectively giving loads of about 50 and 5 tons. When the pressure is released, coil springs pull the driver section and dump tank away and allow the diaphragms to be changed. O-rings on each side of the diaphragm act as the vacuum seal.

The test section is evacuated by two 3-inch oil diffusion pumps, backed by a rotary pump. A second rotary pump is used to evacuate the driver section and dump tank. Liquid nitrogen traps prevent the backstreaming of pump-oil. In the event of a post-experiment pressure in excess of atmospheric pressure, these sections may be connected directly to the atmosphere outside. The controls for evacuation, ventilation and filling of the driver section are situated on the outside of a 3 m tall steel 'house', which encloses that section. The 'house' is connected to the outside atmosphere via a ventilation shaft and exists as a safety measure in the event of an escape of high-pressure H_2 driver gas. Driver pressures greater than 300 P.S.I. have not been used in this work, and these precautions were only essential in the past.

3.2 The Diaphragms

Throughout this work, half-hard aluminium diaphragms have been used, of thickness 0.005, 0.010, 0.018, 0.023, 0.030 or 0.046 inches. The diaphragms are pre-scored using a press-tool in the Dennison ram of the University of Oxford Department of Engineering Science. The pattern cut by the press-tool is shown in figure 3.1. This pattern has been found to give reproducible, planar shock waves with constant velocity in the observation region. Flanges built into the test section catch the aluminium 'petals' of the diaphragm, to prevent them rebounding and

distorting the flow. The scoring of the diaphragm is to between 1/3 and 2/3 of its thickness. An 18/10 diaphragm for instance is 0.010 inches thick at the score-lines and 0.018 inches thick elsewhere. How an appropriate diaphragm is chosen for a given set of desired experimental conditions will be explained in section 4.11.

3.3 Measurement of Shock Speed

The shock speed is calculated by determining the time taken for the shock front to travel between two thin-film platinum resistance heat gauges. These gauges act as very sensitive resistance thermometers. They consist of strips of platinum about 0.25 mm wide, partially fused into the surface of pyrex rods held in a fitting whose surface is flush to the shock tube wall. The fittings in use at present are at the observation window and 15 cm upstream of it; the platinum strips are 150.0 mm apart. The gauges are connected to a high-gain amplifier (trigger gauge) which produces a 5 V pulse when the gauge resistance drops. The pulses start and stop a Racal 9900 Universal Counter Timer. The response time of the heat-gauge / timer combination is less than 0.1 μs.

3.4 Test-gas Handling

The test gas is admitted to the shock tube via a valve just upstream of the dump tank diaphragm from a metal and glass gas-handling line. The pressure of the test gas is currently measured by a an M.K.S. 170M-6C Baratron capacitance manometer with a 310CHS 100 torr head, or a Wallace and Tiernan pressure gauge, reading up to 1500 torr. Earlier in this work an M.K.S. type 77 Baratron reading to 10 torr and other Wallace and Tiernan pressure gauges were used. Gas mixtures are made up in glass bulbs, which have been pumped to 1×10^{-5} torr, and left for

several hours to mix before use.

3.5 The CO Laser

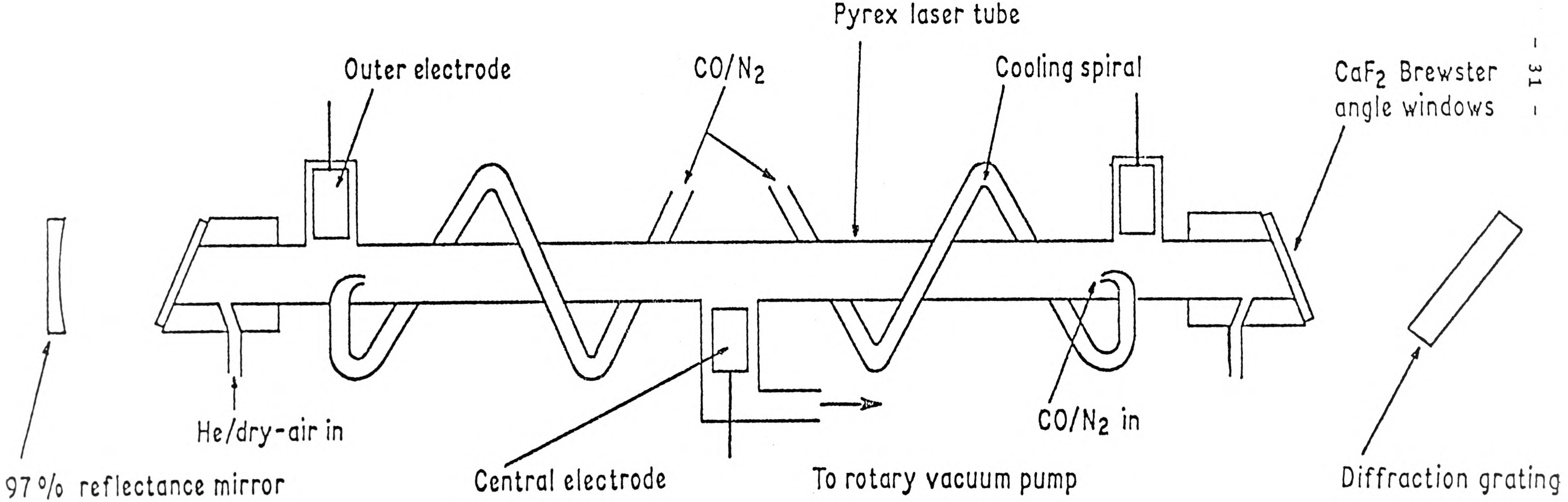
The laser is shown in figure 3.2. It consists of a pyrex tube, 1.9 m long and 3 cm in diameter, along which gas flows from the ends to the middle, and through which an electric discharge is struck, again from the ends to the middle. The tube is immersed in a stainless steel tank containing liquid nitrogen. This is necessary for operation on transitions between the lowest vibrational levels. The tank is surrounded by thermally insulating material. The whole assembly rests on a beam alongside the dump tank.

The laser runs on a mixture of CO, N_2 and He. The CO constitutes less than 1 % of the mixture. It can now be run without including dry air in the mixture, as was found necessary in the past. The rates of flow of gases are controlled by needle valves. The N_2 and He rates are monitored with a flow-meter; the CO flow is too small for that to be possible. The CO and N_2 are precooled by flowing through a spiral around the laser tube, and enter just downstream of the end electrodes. The He enters at the end windows. This arrangement prevents the build-up of CO (v=0) between the end windows and the electrodes which would prevent lasing on the 1->0 vibrational band. The flow is maintained by an 80 l/min rotary pump, via a 50 l bulb which smooths out pressure fluctuations. Strips of copper foil in the bulb remove any active species, in particular O_3, before they reach the pump.

The end electrodes are positioned 0.82 m from the central one. The voltage between them is typically 12-15 kV. The power supply is designed so that the discharge current remains constant (usually at 20 mA) as the voltage fluctuates. This is necessary for stable operation.

FIGURE 3·2

THE CO LASER



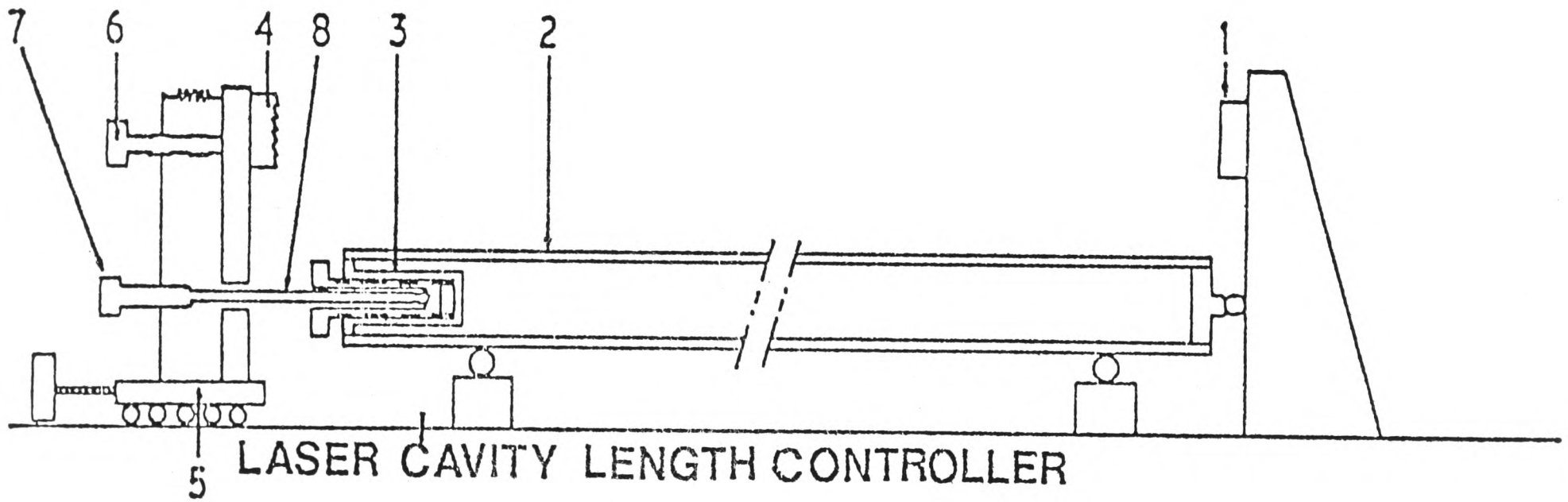
The laser windows are made from calcium fluoride, 5 mm thick. They are held at Brewster's angle by 'tufset' plastic window-holders. Previously perspex or aluminium window-holders were used. The former are liable to crack at low temperatures; the latter are poor thermal insulators and also become electrically live during operation creating a hazard. The windows are removed for cleaning periodically. This is especially important for 1->0 operation. The space between the metal tank and window-holders is well thermally insulated to prevent condensation on the windows.

The optical cavity is enclosed by a 97.5 % reflecting germanium output coupler of radius of curvature 8 m and a 240 lines/mm Bausch and Lomb diffraction grating blazed at 3.75 μm. The cavity is 2.25 m long. For satisfactory operation, the laser power must be steady. This is ensured by a silica-tube / brass-rod differential expansion arrangement which stabilises the cavity length and ensures single longitudinal mode operation. Cavity-length stabilisation is superior to electronic feedback arrangements which had been used in previous designs [75]. The laser described here is that with which single-line laser action for a 1->0 line was first achieved.

The cavity-length stabilisation arrangement is shown in figure 3.3. The output coupler is fixed but the diffraction grating is mounted on a low-friction trolley with high-precision roller bearings which can move parallel to the optical axis. The length of the silica tube and brass rod are such that as the temperature changes they expand in length by the same amount, but in opposite directions. Thus the cavity length is not affected by small fluctuations in temperature.

The laser, its optics (with the exception of the shock tube windows), and the monochromator rest on beams on anti-vibration mounts to further enhance stability. The mounts consist of inflated Firestone

FIGURE 3·3



Key: 1. Output Coupler 2. Silica tube 3. Brass rod 4. Diffraction Grating
5. Trolley 6,7. Micrometers which adjust cavity length. 8. Silica rod

'tyres' connected to a central reservoir so that the relative orientation of the optics is maintained.

3.6 Theory of CO Laser

A brief summary will be given here. For a fuller treatment, see references [76-78].

In the electric discharge, vibrationally excited molecules are formed, as follows. The bond-length of N_2^- is greater than that of N_2, so when N_2^- loses an electron, the N_2 is formed in a high vibrational state. (Instead of N_2^- formation/ionisation this can alternatively be seen as a one-step energy transfer process between $N_2(v)$ and an electron.) If the temperature is low, vibration-translation (VT) energy processes are extremely slow, so the energy remains in vibration. Near resonant (VV) processes however have large rate constants at low temperatures so the energy is distributed amongst the vibrational levels of N_2. N_2-CO (VV) processes such as

$$N_2(v=7) + CO(v=0) \rightleftharpoons N_2(v=6) + CO(v=1) \quad \Delta E=13\ cm^{-1} \qquad (3.1)$$

are also near-resonant and fast so the CO too has an excess of vibrational energy. At very low temperatures, the anharmonicity, $x_e\omega_e$, becomes comparable to kT and affects the distribution of molecules between different vibrational levels v. The situation is treated by the theory of Treanor at al [79]. This was modified by Caledonia and Center [80] to take account of (VT) processes and radiative decay (which will only be important for high levels and high temperatures) but the essential conclusions remain the same:

(i) When the energy in vibration is greater than it would be at thermodynamic equilibrium at the translational temperature, the

population ratios n_{v+1}/n_v will be greater than they are for a Boltzmann distribution at that temperature, and there may even be an overpopulation ($n_{v+1} > n_v$).

(ii) The effect is enhanced the larger the amount of vibrational energy and the lower the translational temperature.

(iii) When a mixture of two diatomic gases is present, a disproportionately large fraction of the total vibrational energy is in the gas with the smaller separation between the vibrational levels (smaller ω_e). This favours CO in the presence of N_2. The process

$$N_2(v=1) + CO(v=0) \rightleftharpoons N_2(v=0) + CO(v=1) \qquad (3.2)$$

is exothermic by 188 cm^{-1} so the equilibrium is very much to the right ($e^{-\Delta E/kT} = 15$ at 100 K).

The form of Treanor distributions is discussed further in section 5.15.

The addition of N_2 is also thought to lower the electron 'temperature' and so promote the excitation of low vibrational levels of CO [78]. N_2 is absolutely necessary for lasing on the 1->0 transition.

For lasing to occur, it is not necessary to have a complete vibrational overpopulation. In explaining this, we shall also explain why lasing occurs on P-lines but not R-lines. Consider for example the 1->0P(9) line. This is a transition between v=0,J=9 and v=1,J=8. The lasing condition is $n_u/g_u > n_1/g_1$ where n_u, g_u, n_1 and g_1 are the populations and degeneracies in the upper and lower levels. The degeneracy of a vibrotational line is given by (2J + 1). For a P-line $g_1 > g_u$ (19 and 17 in our example) so it is not necessary that $n_u > n_1$. But for R-lines $g_1 < g_u$. Further, considering P- and R- transitions

from the same upper state, e.g. P(9) and R(7), the energy difference between levels connected by the R-line is greater than that between levels connected by the P-line, so n_u/n_1 (P-line) > n_u/n_1 (R-line).

The helium is essential for the laser to work. Its role is thought to be to alter the electron energy distribution to promote the vibrational excitation of N_2.

3.7 Output Characteristics of the CO Laser

An iris placed in the cavity in front of the diffraction grating restricts the laser to a single transverse mode, Gaussian in profile, and so prevents instability due to transverse mode-hopping.

By rotating the diffraction grating, single lines from the 1->0 band to the 25->24 band have been obtained. No exhaustive attempt has been made to reach higher lines, but it is probable that by altering the gas mixture and perhaps changing the grating, lines up to 36->35, as was achieved by Brechignac and Martin [75], could be obtained.

Lasing is readily obtained on the P(7) to P(13) lines of each band (but not P(7) and P(8) of 1->0). The laser can thus produce about 200 lines, each about 4 cm^{-1} apart, in the region 1500-2120 cm^{-1} (6.7 to 4.7 μm). That is 200 lines for each isotope of CO used in the laser. $^{12}C^{16}O$ and $^{13}C^{16}O$ (90 %, supplied by Prochem) have been used in this work.

On single-line operation, the laser power used is never more than about 2 mW, to avoid saturating the detector. Using a mirror in place of the diffraction grating so that the laser operates multi-line, the power is orders of magnitude higher. With a 10 % reflecting output coupler, the power has been sufficient to burn a hole in a brick.

The optimum gas mixture is very different for multi-line and single-line operation. Lasing on the 1->0 band is the most difficult to achieve, being very sensitive to mixture composition. Only for this band is the removal (by excitation) of the ground-state CO crucial. The tiniest trace of CO in the laboratory atmosphere (e.g from glass-blowing) prevents the laser from working on the 1->0 band.

3.8 The Optics

The optics are shown in figure 3.4. Having emerged from the laser cavity, the laser beam is focussed by a CaF_2 lens L_1 (focal length 150 mm) through a 200μm pin-hole P which improves the mode-structure of the beam. A second lens L_2 (focal length 200 mm) focuses the beam so that its average width within the shock tube is minimised: the width within the tube is 0.8-0.9 mm. The width is diffraction-limited [42].

Between the lens and the shock tube, the beam is reflected by two mirrors, M_1 and M_2, in the form of a periscope, and crosses the shock tube perpendicularly in the horizontal plane. This is necessary for maximum time resolution. It crosses at an angle of 5^o in the vertical plane, to avoid interference effects.

The shock tube windows are calcium fluoride discs. Windows 3 mm thick and 44 mm in diameter have recently been replaced by ones 3 mm thick and 20 mm in diameter. These latter rest on ledges and have been tested hydraulically: a pressure of 5000 P.S.I. was required to break them. Both sets of windows are mounted flush to the shock tube wall.

The observation windows are 3 m downstream from the diaphragm. They are in the ideal position for a shock for which $u_1/u_2 = 3$ (see section 2.5).

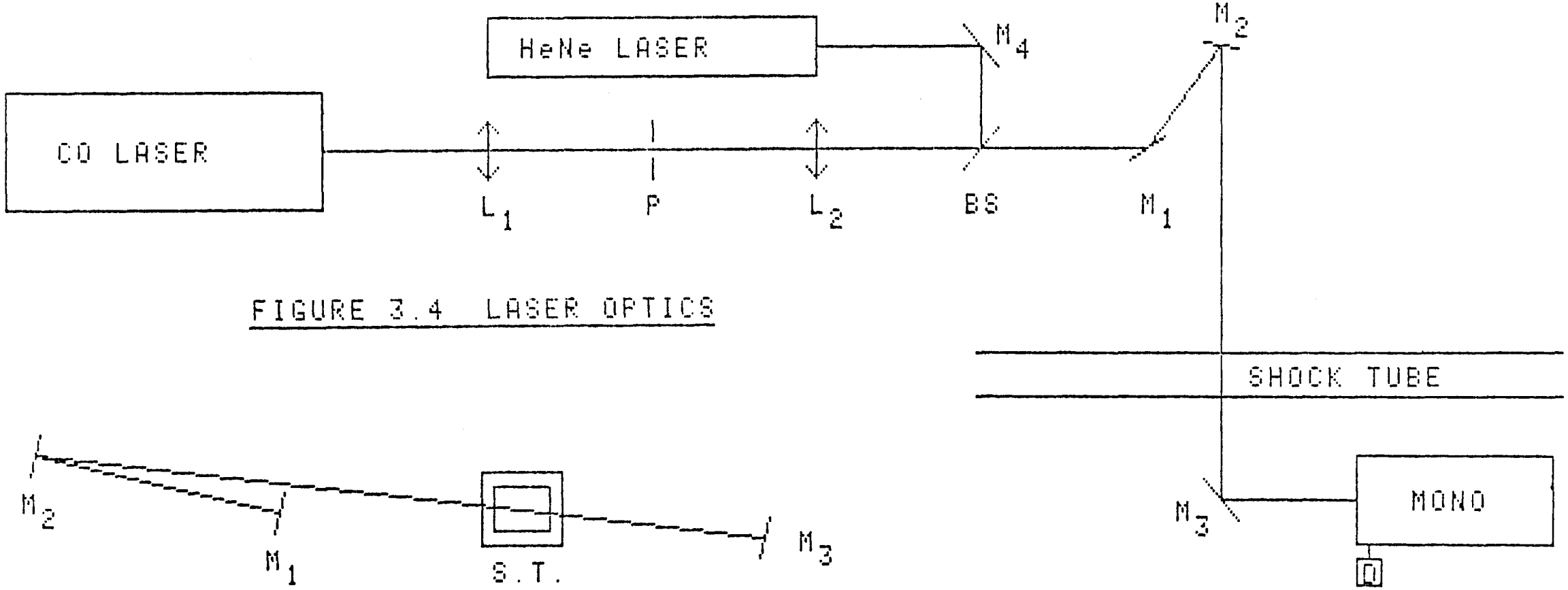


FIGURE 3.4 LASER OPTICS

On the far side of the shock tube the laser beam reflects off a mirror M_3 through a 1 m monochromator onto a liquid-nitrogen cooled Judson indium antimonide photovoltaic detector. The monochromator identifies the line being used and cuts out emission at other frequencies which would distort the trace. Spontaneous emission from that transition in the direction of the laser beam is negligible; stimulated emission is allowed for in the treatment of the results.

The monochromator is calibrated using the 7th and 8th order diffractions, from the monochromator grating, of a HeNe laser. This laser is also used for lining up the invisible CO laser beam. Mirror M_4 and beam-splitter BS are used for making the 2 beams coaxial.

3.9 Electronics

The signal from the detector is fed via a Perry pre-amplifier into a Data Laboratories DL 912 transient recorder. This records 4096 points at intervals of 0.05 μs or greater. The digitised signal is passed to a Gould 05260 oscilloscope for immediate display and a North Star Advantage microcomputer for analysis, via its PIO (parallel input/output) board. The interface is controlled by subroutine 'SHOCK' of program 'SHOCKIT'. The data analysis will be described in subsequent chapters. The computer and transient recorder were installed in late 1983; previous results were obtained by photography of a trace on the Gould oscilloscope and subsequent expansion of the image onto graph paper using an epidiascope. Data points were taken and fed into a computer (DEC LSI-11) by hand.

The laser power is recorded immediately before each shock using a 110Hz Edinburgh Instruments chopper placed in the beam.

3.10 Shock Procedure

The test section is evacuated to about $1x10^{-5}$ torr, measured with a Penning gauge, before the shock is fired. Once the test section is sealed off from the pumps, the shock is fired as soon as possible. Because of the necessity to ensure that the laser is stable, this may take slightly longer (3 or 4 minutes) than was the case for the interferometry and laser-schlieren experiments. The gas mixture is admitted to the shock tube, the trigger gauges are switched on, and the transient recorder armed. Either an internal or an external (from the trigger gauge which stops the timer) trigger may be used in the recorder. The recorder is used in pretrigger mode, so that a portion of the baseline is recorded before the arrival of the shock-front. The point at which the recorder was triggered is shown by a bright spot when the trace is displayed on the oscilloscope.

Once the laser is stable the shock is fired. The initial pressure p_1 is read from the MKS Baratron, the initial temperature T_1 is read from a mercury thermometer mounted on the test section, and the shock speed u_1 deduced from the time displayed on the timer. Program 'SHOCKIT' is run to feed the data into the computer and onto a floppy disk. Following the experiment, the whole shock tube is evacuated via the dump tank, so that gas flow is always from the test section to the dump tank. The tube is then filled with Air Products oxygen-free nitrogen to slightly over atmospheric pressure, and the hydraulic rams released to open the shock tube and change the diaphragms. The overpressure of nitrogen prevents wet air entering the shock tube. The three shock tube sections are now evacuated ready for the next shock.

For shocks in which no undesirable products, which might pollute the test section walls, are formed, a thick non-bursting dump tank diaphragm may be employed to conserve nitrogen.

3.11 History of the Shock Tube and Experiments carried out in it

As the shock tube is now over 20 years old, and to help put the present work in context, it is useful to include at this point a review of the previous shock tube work of Simpson and coworkers.

The earliest work studied the characteristics of the shock tube itself. The first paper to be published [81] was on the effect on shock trajectory of the opening time of the diaphragm. Twelve heat gauges were used to measure the shock speed along the length of the test section. It was found that the greater the opening time t, the greater was the distance L over which the shock accelerated before reaching its maximum speed s. The equation L=2st gives a rough guide. t is of the order of 100 μs. Different diaphragms were tested, and it was found that half-hard aluminium or half-hard brass gives an almost constant shock velocity for some distance upstream of the observation point. This is important as it ensures that all the gas observed at different times has been processed by a shock of the same strength. Comprehensive studies such as this have not been carried out for many shock tubes. The flanges which catch the diaphragms and prevent them from rebounding are important also. Without them there may be a series of density gradients behind the shock front [82].

The first experimental papers, published in 1968, were on the vibrational relaxation of CO_2 [36] and N_2O [19] studied by the interferometry technique. The CO_2 paper fully describes the method. At this time, the combined leaking and degassing rate of the shock tube was established to be 2×10^{-4} torr/min. Using a thermocouple, it was also established that the test gas reaches the temperature T_1, given by the thermometer mounted outside the tube, in the time taken to fill the shock tube to pressure p_1. It was concluded that all three vibrational modes of CO_2, and of N_2O, relax together. A point of contention at this

time was whether the relaxation time depended on the distance from equilibrium as well as the temperature. It was found to depend only on temperature.

After these two papers had been published, the laser schlieren technique, which had been developed by Kiefer and Lutz [83], was introduced. The paper which describes the technique [84] confirmed the interferometry results for CO_2, extended the work to higher temperatures, and gave results for CO_2 /Ar mixtures.

Reference [85] contains the fourth and last set of results obtained at the N.P.L. This was the first of a series of papers [85-92] on the relaxation of CO_2, OCS, and N_2O, in the presence of collision-partners Ar, Ne, ^4He, ^3He, n-D_2, o-D_2, HD, n-H_2 and p-H_2. Emphasis was placed on determining the role of rotation of the collision partner. (VR) energy transfer rate constants were evaluated. In some cases (RT) excitation of the collision-partner was found to be rate-limiting.

A brief departure from triatomic molecules saw a measurement of vibrational relaxation times in HD/Ar mixtures [93]. HD was found to relax faster than H_2 or D_2 which suggests rotational involvement in the vibrational excitation process. (Earlier work on the vibrational relaxation of N_2 [94] was never published in full.)

There are two further papers on triatomics. In one [95] O_2 was found to be a more efficient collision-partner than N_2 in the vibrational relaxation of CO_2, despite its lower mass. In the other [96] N_2O/CO_2 mixtures were studied. Fast (VV) processes were shown to cause the two molecules to relax together.

CF_4 and CH_4 vibrational relaxation and (VV) energy transfer between these gases and CO were studied [97].

The carbon monoxide laser was designed and built by Jean-Pierre Martin and Stephen Simpson in 1978. Some laser schlieren work continued until 1980 since when all work has used the infrared absorption technique.

It can be seen that the shock tube has always been used to gain mechanistic information as well as rate constants, and the work to be described here continues in that tradition.

CHAPTER 4 - SHOCK-TUBE AND INFRARED-ABSORPTION THEORY

4.1 The Rankine-Hugoniot Equations

The passage of the shock front causes the temperature T, pressure p and density ρ to rise very rapidly (three orders of magnitude quicker than the time resolution of our experiment) to new values. The calculation of these new values, and the values after any subsequent vibrational relaxation or chemical reaction, is achieved using the Rankine-Hugoniot equations [22].

These are the laws of the conservation of mass, momentum and energy expressed per unit time for a flowing system. Constant cross-sectional area is assumed and, for convenience, velocities are expressed relative to the shock front. In this frame of reference the unheated test gas approaches the shock front at velocity u_1; the shock-heated test gas leaves the shock front at velocity u_2. Subscripts 1 and 2 always refer to unheated and heated test gas, respectively.

Because the gas has been compressed, u_2 must be less than u_1. This is expressed by the first Rankine-Hugoniot equation (conservation of mass):

$$\rho_1 u_1 = \rho_2 u_2 = m \tag{4.1}$$

In expressing the conservation of momentum, account must be taken of pressure terms:

$$\rho_1 u_1^2 + p_1 = \rho_2 u_2^2 + p_2 = i \tag{4.2}$$

Similarly, enthalpy must be included in the expression for the conservation of energy:

$$u_1^2/2 + h_1 = u_2^2/2 + h_2 = h_o \qquad (4.3)$$

In the derivation of (4.3) a division by (4.1) has been carried out. h is specific enthalpy i.e. enthalpy per unit mass. p_1, T_1 and u_1 are measured experimentally. If we know the temperature dependence of the enthalpy

$$h = f(T) \qquad (4.4)$$

and introduce the ideal gas law

$$p = \rho RT \qquad (4.5)$$

(R in $Jkg^{-1}K^{-1}$)

we have 5 equations with 5 unknowns, p_2, ρ_2, T_2, h_2, and u_2, and can solve for the post-shock conditions. The ideal gas-law is a very good approximation at the pressures used.

The dependence of enthalpy upon temperature is complex when vibrational relaxation or chemical reaction occurs, so the equations must be solved iteratively. We shall consider firstly the case of vibrational relaxation only and then extend the method to encompass chemical reactions.

4.2 Solution for Vibrational Relaxation

The iterative method used is that given by Lapworth [98]. The enthalpy h_2 is expressed as the sum of two terms. The first term is due to the n translational and rotational degrees of freedom, which are making their full contribution to the heat capacity, and the second due to the vibrational degrees of freedom, which are not:

$$h_2 = (1 + n/2)RT_2 + \mathscr{D}(T_2) \qquad (4.6)$$

If $\mathscr{D} = 0$ (i.e. when negligible vibrational relaxation has occurred) iteration is not necessary as algebraic manipulation of equations (4.1), (4.2), (4.3), (4.5) and (4.6) yields direct expressions for the post-shock variables. This is the case for a monatomic gas. Otherwise T_2 and u_2 are expressed in terms of each other:

$$T_2 = u_2(i/m - u_2)/R \qquad (4.7)$$

$$u_2 = \frac{\theta i/m - [(\theta i/m)^2 - 2(n+1)(h_o - \mathscr{D}(T_2))]^{1/2}}{n+1} \qquad (4.8)$$

(with $\theta = 1+n/2$) in an iterative procedure. To obtain values of $\mathscr{D}$, h_2 is expressed as a polynomial function of temperature (the polynomial is obtained by fitting to the J.A.N.A.F. thermochemical tables [99]) and substituted into equation (4.6). Initially h_2 is calculated at room temperature T_1. The resultant value of $\mathscr{D}$ is substituted into equation (4.8) to give u_2, and hence T_2 is obtained from equation (4.7). h_2 is now recalculated at T_2 and the process repeated until T_2 has converged. ρ_2 and p_2 are now obtained from equations (4.1) and (4.5).

For mixtures, (1+n/2) is mole-fraction-averaged and R is calculated from the mole-fraction-averaged molecular weight. The whole procedure

is included in subroutine CONDITS of program SHOCKIT on the North Star Advantage computer.

4.3 Solution for Chemical Reaction

When a chemical reaction occurs, an additional cycle of iterations is necessary. From T_2 and p_2 calculated as above for no reaction, the position of equilibrium is deduced using the J.A.N.A.F. tables. The enthalpy of the post-reaction mixture is now calculated (all enthalpies are calculated relative to 298 K, and the enthalpy of reaction at 298 K included) and hence new values of T_2 and p_2 deduced as in section (4.2). A new position of equilibrium is calculated, and the process continued until T_2 and p_2 have converged. The procedure is carried out using program DECOCS, for instance, on the LSI-11 computer.

4.4 Calculation of Laser Gain

We have seen how the temperature and density of the heated gas are calculated. To obtain information on the kinetics, the laser absorption method is used to monitor the population of a species involved in the chemical events.

The absorption of the laser beam in the shock tube is given by:

$$\log \frac{I_o - \Delta I}{I_o} \propto \frac{n_l}{g_l} - \frac{n_u}{g_u} \qquad (4.9)$$

where n_l, g_l, n_u, g_u are the populations and degeneracies of the lower and upper levels of the test gas, linked by the laser transition. I_o is the laser power, measured with the shock tube evacuated, and ΔI the absorption i.e the decrease in laser power caused by the presence of the test gas. The proportionality constant need not be calculated for the

analysis of results detailed in this thesis, but its estimation is useful in the planning of experiments and will be described in the next section.

The quantity $\log[(I_o - \Delta I)/I_o)]$ is called the 'gain'. In all experiments to date it has been negative; positive gain would imply potential for lasing in the heated test gas. The numbers passed from the transient recorder, after the baseline has been deducted, correspond to ΔI for each point. Each is converted to a gain; what happens next is described in the chapters on individual experiments.

4.5 Absorption Coefficients. The Voigt Profile

It is useful to calculate the absorption coefficient for absorption by molecules in thermodynamic equilibrium i.e. with vibrational relaxation complete. The relationship between n_l and n_u in equation (4.9) is then known and indeed the population terms are included in the absorption coefficient, $k(\nu_o)$, at laser frequency ν_o, as defined by Weisbach and Chackerian [25]:

$$(I_o - \Delta I)/I_o = \exp[-k(\nu_o)l] \qquad (4.10)$$

Here l is the path-length of absorbing gas, 7.64 cm in our case. The spectral width of the laser line is very small, so $k(\nu_o)$ is the value of the absorption coefficient at the line-centre of the shock-heated CO.

The value of the integral of the absorption coefficient over the whole line, $\int k(\nu)d\nu$, is given by theory, as shown below. To relate $k(\nu_o)$ to $\int k(\nu)d\nu$ we need to know the line-shape function. At the temperatures and pressures used in this work, Doppler-broadening and

pressure-broadening are both significant. In this situation there is no analytical function to describe the line-shape. The line-shape is then given by the Voigt profile which is found in tables e.g. that given by Davies and Vaughan [100].

The Voigt profile is a function of the ratio of the pure Doppler-width $\Delta\nu_D$ to the pure pressure-(Lorentz-)width, $\Delta\nu P$. Here 'width' refers to the full-width of the line at half the maximum intensity (FWHM). A purely Doppler-broadened line has a Gaussian shape and a purely pressure-broadened line a Lorentzian shape. Mathematically, the Voigt profile is a folding integral of the Lorentzian and Gaussian distributions.

Davies and Vaughan's table gives ψ, the ratio (height of line : pure Lorentz height) as a function of η where

$$\eta = \frac{\Delta\nu_D}{\Delta\nu_P(1n2)^{1/2}} \qquad (4.11)$$

$\Delta\nu_D$ and $\Delta\nu_P$ are given in cm^{-1} by:

$$\Delta\nu_D = 1.356x10^{-7}\nu_o T^{1/2} \quad \text{(for CO)} \qquad (4.12)$$

and:

$$\Delta\nu_P = \frac{3.57x10^{10}\sigma_1\sigma_2}{\pi c} \cdot \left[\frac{M_1+M_2}{M_1M_2}\right]^{1/2} \cdot p/T^{1/2} \qquad (4.13)$$

Here σ_1 and σ_2 are optical collision diameters, in Angstroms, for CO and its collision-partner, M_1 and M_2 are the molecular weights in grams, and p is in atmospheres [101].

The Voigt function H(a) used by Weisbach and Chackerian [25] ($a=1/\eta$) is given by:

$$H(a) = \psi \eta \pi^{-1/2} \tag{4.14}$$

H(a) is then the fraction of the pure Doppler height.

We obtain $k(\nu_o)$ from $\int k(\nu)d\nu$ by [25]:

$$k(\nu_o) = \frac{H(a)}{(\Delta\nu_D/2)(\pi/1n2)^{1/2}} \cdot \int k(\nu)d\nu \tag{4.15}$$

For the (v+1)->vP(J) line of CO in thermodynamic equilibrium [25],

$$\int k(\nu)d\nu = \frac{8\pi^3 \nu J p_{CO} |R_{v+1,v}|^2 e^{-E_v/kT} [1 - e^{-h\nu/kT}]}{3hckTZ(T)} \tag{4.16}$$

Combining equations (4.14) and (4.15), the equation used to calculate the absorption coefficient for equilibrium CO is:

$$k(\nu_o) = \frac{H(a) J p_{CO} |R_{v+1,v}|^2 2.12x10^{10} e^{-E_v/kT} [1-e^{-h\nu/kT}]}{T^{3/2} Z(T)} \tag{4.17}$$

Then the gain is given by:

$$\text{Gain} = 1\log[(I_o - \Delta I)/I_o)] = -k(\nu_o)1 \tag{4.18}$$

Here J is the rotational quantum number of the lower level, p is the (partial) pressure of CO in atm., $|R_{v+1,v}|$ is the electric dipole matrix element in Debye, Z(T) is the vibrational-rotational partition function and E_v is the energy of the lower level (not including zero-point energy). 1 is in cm.

There is a number of conclusions that can be drawn from equation (4.17).

(i) Effect of increasing vibrational quantum number at constant temperature and pressure: The gain falls as $e^{-E_v/kT}$ falls and this outweighs the increase in $|R_{v+1,v}|$ except at extremely high temperatures.

(ii) Effect of increasing rotational quantum number at constant temperature and pressure: The change in $e^{-E_v/kT}$ is much less here, so generally will be outweighed by the increase in J. For large J the energy gap between successive rotational levels increases and this will no longer be the case.

(iii) Effect of increasing pressure at constant temperature, for the same laser line. This depends on the relative magnitude of $\Delta\nu_D$ and $\Delta\nu_p$. At sufficiently low pressures for Doppler-broadening to dominate, the gain will be proportional to pressure. As pressure increases, the dependence is reduced until when presure-broadening dominates, further increase in pressure has no effect on the signal, as for each doubling of p, H(a) is halved.

(iv) Effect of increasing temperature at constant pressure and for the same laser line: $e^{-E_v/kT}$ rises but the denominator of the expression rises. For low v i.e. low E_v the increase in the numerator will cease to prevail over the increase in the denominator at a lower temperature. For constant density rather than pressure, the $T^{3/2}$ in the denominator is in effect replaced by $T^{1/2}$, so the dependence of the denominator on temperature is reduced.

4.6 Absorption Coefficients. Comparison of Experiment and Theory

In order to use equation (4.17) to predict gains for future experiments, it is necessary to see whether it can agree with past experimental measurements. The calculation is carried out as follows:

Z(T) is calculated for a simple harmonic oscillator - rigid rotator model i.e.

$$Z(T) = \frac{kT}{B} \cdot \left[\frac{1}{1-\exp(-h\omega/kT)}\right] \qquad (4.19)$$

where B is the rotational constant and ω the vibrational frequency. The experiments of Weisbach and Chackerian determined values of $|R_{v+1,v}|$ for $v \geq 4$, and of the optical collision diameter for pure CO, $\sigma = 3.79$ A ($2500 < T < 5000$ K). For values of $|R_{v+1,v}|$ for $0 \leq v \leq 3$, the data given by Werner [102] are used. To a very good approximation, $|R_{v+1,v}|^2$ is proportional to the vibrational quantum number, v+1. Most of our experiments use argon as a diluent gas, so we need a value for the optical collision diameter for argon. No measurement has been made of this at high temperatures, but it can be estimated as described in the following paragraph:

σ_{CO-CO} and σ_{CO-Ar} have been measured for a wide range of laser lines at room temperature [103]. At room temperature each decreases as rotational quantum number J rises, tending towards an asymptotic value. Weisbach and Chackerian found σ to be independent of J at high temperatures, and, at 3.79 A, close to the room temperature asymptotic value of 3.70 A. Thus, for a high temperature value for σ_{CO-Ar}, we take the room temperature asymptotic value, $\sigma_{CO-Ar} = 2.76$ A.

So, substituting in equation (4.12), we use, for CO-CO:

$$\Delta\nu_p = 1.38p/T^{1/2} \qquad (4.20)$$

and for CO–Ar:

$$\Delta\nu_p = 0.92p/T^{1/2} \qquad (4.21)$$

Using these values of $\Delta\nu_p$, and calculating H(a) from the tables of Davies and Vaughan, we deduce theoretical values of the gain from equations (4.17) and (4.18). Agreement is obtained with experimental values for the gain at equilibrium to within 25% which is an adequate estimate. This calculation has only been made for a small sample of shocks.

4.7 Line-Widths

Tabulations of the Voigt profile give the absorption coefficient not only at the line-centre, but also elsewhere in the line-profile. This is useful for calculating line-widths, and evaluating the absorption of a CO laser-line by a transition other than its own, but to which it is very close in frequency (an 'accidental coincidence'). Such coincidences can be useful for monitoring non-lasing $^{12}C^{16}O$ lines, lines of other CO isotopes or lines from the vibrotational spectrum of other species e.g. DCl, NO. However, when a CO laser line is being used to monitor that same transition in hot CO, any accidental absorption is a disadvantage. Contribution to absorption from adjacent lines must be allowed for.

From a value of η from equation (4.11), the table of Davies and Vaughan yields δ, the FWHM of the Voigt profile, relative to $\Delta\nu_p$. It also gives the height of the line, relative to the height at line-centre, as a function of distance from the centre, relative to δ. This

enables the contribution to the net gain from coincidental absorption to be calculated.

A typical value for δ is 0.02 cm^{-1}. As an example, for CO in Ar at 4400 K and 0.45 atm, $\Delta\nu_D$ = 0.018 cm^{-1}, $\Delta\nu_P$ = 0.009 cm^{-1}, and δ = 0.023 cm^{-1}. $\Delta\nu_D$ rises with $T^{1/2}$; $\Delta\nu_P$ falls with $T^{1/2}$ and rises with p. δ = 0.02 cm^{-1} is a rough estimate for most experiments.

4.8 Coincidences between CO Laser Lines and other CO Absorption Lines

Coincidences between $^{12}C^{16}O$ laser lines and other species will be described in the chapters detailing the experiments on those species; $^{12}C^{16}O$ and $^{13}C^{16}O$ will be considered here. 1 % of natural CO is $^{13}C^{16}O$, so absorption by both these species must be considered for all experiments for which the test gas contains isotopically unenriched CO.

It is useful to describe the spectrum of CO. Successive P-branch lines (v+1)->vP(J) and (v+1)->vP(J+1) are ~4 cm^{-1} apart, a spacing much greater than the line-width in the heated gas of ~0.02 cm^{-1}. However the different vibrational bands overlap such that, for instance, (v+1)->vP(J) and (v+2)->(v+1)P(J-6) are generally within 1 cm^{-1}, so there is a chance of close coincidences.

The frequencies of CO laser lines may be generated from the Dunham coefficients of Todd et al [104], to within 0.001 cm^{-1}. The Dunham coefficients are the Y_{ij} in Dunham's formula for the energy of level v,J:

$$E(v,J) = \sum_{ij} Y_{ij}(v+1/2)^i[J(J+1)]^j \qquad (4.22)$$

By this method a computer search has been carried out to establish which laser lines are liable to absorption by neighbouring lines, and

experiments have been run to check this. For instance, the generated frequencies show that 9->8P(7) of $^{12}C^{16}O$ is within 0.008 cm^{-1} of 2->1P(46) of $^{12}C^{16}O$. At around 2000 K, the population of molecules of equilibrium CO in (v=8) is negligible and 9->8 generally show no absorption, but 9->8P(7) is absorbed ~80 %. This is a good validation of the Dunham coefficients, as the experimental measurements on which they were based did not extend beyond a rotational quantum number of 34. It is also a test for the calibration of the monochromator as it provides a way to unambiguously assign 9->8P(7). This example is the most spectacular, as it shows very large absorption where none would be expected. Other examples show absorption greater than expected e.g. 6->5P(8) which is within 0.06 cm^{-1} of 3->2P(26) of $^{12}C^{16}O$ and 5->4P(10) which is within 0.028 cm-1 of 1->0P(24) of $^{13}C^{16}O$. Laser lines, such as these, which it is wise not to use because of accidental coincidences, have been tabulated and are avoided in normal work.

4.9 Boundary Layer Effects

The calculation of post-shock conditions outlined in section (4.2) takes no account of the interaction of the heated test gas with the boundary layer, which grows behind the shock front as noted in section (2.6). Apart from the deceleration of the shock wave itself, the mainstream flow behind the shock is also decelerated. Temperature, density, and the ratio of laboratory time to real time are increased. The effects accentuate as the boundary layer grows. Simplified formulae for making estimates are given by Belford and Strehlow [23]. They are expressed in terms of the ratio of laboratory time to 'maximum hot flow transit time', t_m, that is, the asymptotic maximum value for the time between the arrival of the shock front and the arrival of the contact surface. t_m is large for high p_1 and low shock-speed. It is thus at low pressures and high temperatures that it is most important to take

account of non-ideal effects.

The early work in this shock tube, using the interferometry and laser schlieren techniques, was done very close behind the shock front where $t_{lab}/t_m < 0.001$ and non-ideal effects could be safely neglected [36,40]. Experiments using the laser absorption technique have been over longer timescales (t_{lab}/t_m approaching 0.1 in some cases). However, no account of non-ideal effects has been taken in calculating any of the temperatures, pressures and rate constants quoted in this thesis. Much of the work has been concerned with obtaining mechanistic information rather than 'hard data' so this is not important. Using the equations given by Belford and Strehlow, for a typical OCS decomposition experiment, the final equilibrium T_2, ρ_2 and t_{real}/t_{lab} have been underestimated by 2.5 %, 4 % and 10 % respectively. The values immediately behind the shock front are unaltered, so the average value will be underestimated by 1.25 %, 2 % and 5 % respectively. The overall effect is estimated to be a systematic overestimation of the rate constant by ~10 %. Account could be taken of non-ideal effects in future work. The necessary equations can easily be built into computer programs. However the theory only allows for the non-ideal effects due to shock deceleration, and not due to finite diaphragm opening-time, and should be applied with caution. The latter effects have been investigated at length in this shock tube (see section 3.11).

In the vast majority of cases, after the reaction or relaxation region, laser absorption does not significantly change, so we conclude that that non-idealities do not cause us serious problems.

4.10 Choice of Experimental Conditions

Certain criteria apply to the choice of conditions for any experiment, although in any particular case they may be overridden by other criteria. These are maximisation of signal-to-noise and optimisation of the timescale over which the chemical events take place.

The signal-to-noise is limited by the laser power, since ΔI cannot be greater than I_o. The InSb detector saturates at about 6 mW and is non-linear just below this point. Thus the maximum usable laser power is 2 mW which gives a signal of 2 V. (Using a 1->0 laser transition it is rarely possible to produce a laser power of greater than 1 mW.) By considering the number of photons produced by the laser per second ($\sim 10^{16}$), and the number of test gas molecules passing through the beam per second ($\sim 10^{20}$), it is easy to show that at these powers the laser is acting as a probe, not a pump, exciting a negligible quantity of the species which it is probing.

Absorption of over 70 % of the laser power is undesirable. For $\Delta I/I_o = 0.7$, the gain, $\log[(I_o - \Delta I)/I_o]$, varies by 2 % for each 1 % change in $\Delta I/I_o$, so experimental error has a greater effect.

The minimum useful value for the signal-to- noise ratio is about 10, as signal-averaging is not possible. Experimental experience, where necessary supplemented by calculation of the absorption coefficient as outlined in section 4.5, enables suitable conditions to achieve a high signal-to-noise to be estimated.

The time resolution for our apparatus is ~1 μs (limited by the rise-time of the detector/preamplifier). Also, the passage of the shock front brings an enormous density gradient which deflects the laser beam. This results in a 'blip', called a schlieren spike, at the beginning of every laser absorption trace. This is useful as it marks the time

origin, but it is about 2 μs wide, so obscures a significant portion of the trace for very rapid events. The transit time of the test gas across the laser beam also limits the time resolution and is of the order of 1 μs. The process under observation should not be so fast as to reach completion in less than 20 μs lab. time.

On the other hand, the process should not be so slow as to run into flow problems before completion. The time at which this becomes a problem varies with conditions as shown in section 4.9. Experience shows that noise increases as the contact surface approaches.

Knowledge of the dependence of the rate process on temperature and pressure, built up as an experiment proceeds, enable conditions to be estimated under which the desired timescale of events is achieved. A compromise must be reached between signal-to noise and timescale.

Where a diluent gas is used, and is actively involved in the rate process, varying its identity can affect the rate and so provide an additional variable. The choice of CO/He/Ar mixtures in the CO vibrational 'ladder-climbing' experiment is outlined in chapter 6. Use of a diluent is always beneficial in that it reduces the temperature change caused by the rate process i.e. it acts as a heat-bath. This prevents rate constants changing significantly during one experiment and is especially important for reactions where the enthalpy of reaction, and thus the resultant change of temperature, are unknown.

An estimate of the effects of changing one experimental variable, temperature, pressure or mixture composition, must be made carefully. Past experimental experience should be used where available, otherwise only small changes should be made.

4.11 Attainment of Experimental Conditions: Choice of Diaphragms and Driver Gas

Having decided the temperature T_2 and pressure p_2 we wish to attain, we can deduce what pressure p_1 and shock-speed u_1 we require from the mathematics of sections 4.1,4.2 and 4.3. Past experience can frequently suggest the driver-gas/diaphragm combination to be used to produce the desired shock-speed. In its absence, there is a theoretical relationship linking (p_4/p_1) with u_1, assuming ideal shock tube flow [22]:

$$p_{41} = p_{21}\left[1-\frac{a_1(\gamma_4-1)(p_{21}-1)}{a_4(\gamma_1-1)\left[\frac{2\gamma_1 p_{21}}{\gamma_1-1}\,\frac{\gamma_1+1}{\gamma_1-1}+\frac{1}{p_{21}}\right]^{1/2}}\right]^{-2\gamma_4/(\gamma_4-1)} \qquad (4.23)$$

Here p_{21} is shorthand for p_2/p_1 etc. Subscript 4 refers to conditions in the driver gas before the diaphragm bursts. (Subscript 3, never used in this thesis, refers to the driver gas after the diaphragm has burst.) a is the speed of sound, given by $a = (\gamma RT/M)^{1/2}$, where R is the molar gas constant, M the molecular weight and γ the ratio of heat capacities, C_p/C_v. p_{21} is given by:

$$p_{21} = \frac{2\gamma_1(u_1/a_1)^2 - (\gamma_1-1)}{\gamma_1+1} \qquad (4.24)$$

(For this purpose, we are interested in conditions immediately behind the shock front before vibrational relaxation so the Rankine-Hugoniot equations can be solved analytically.)

Because of non-ideal effects, in particular finite diaphragm opening time, the equations underestimate the p_{41} required for a given u_1 by as much as 20 % but are a useful guide. A gauge connected to the

driver section measures p_4 for each experiment and so establishes the link between diaphragm choice and p_4 - this varies for different batches of aluminium sheet. For one batch, carefully made diaphragms allow the achievement of conditions reproducible to within 2 %. p_4 is recorded after the shock but does not enter into the data analysis. Calibration of the p_4 gauge against the Wallace and Tiernan 1500 torr pressure gauge reveals that it reads about 8.5 P.S.I. too high.

It can be seen that the u_1 achievable for a given p_{41} depends on the heat capacities and velocities of sound of the driver and test gases. For a given test gas the shock speed (and hence temperature) achievable increases in the driver gas order $SF_6 < CO_2 < N_2 < CH_4 < He < H_2$;these are the driver gases used in this work. For a given combination of test gas and driver gas, a graph of u_1 against p_{41} decreases in slope as p_{41} rises and reaches a limiting value. For a given driver gas and diaphragm, lowering the velocity of sound in the test gas (e.g. by replacing He by Ar) leads to a higher T_2. This does not break the law of conservation of energy. He and Ar have identical heat capacities but the energy difference is taken up by the driver gas. A heavier diluent in the test gas lowers the p_4 required for a given T_2.

PART TWO

EXPERIMENTS ON ENERGY TRANSFER

CHAPTER FIVE. VIBRATIONAL RELAXATION FOLLOWING SHOCK-HEATING.

5.1 Introduction

Energy is imparted to the test gas by the shock front as translational energy. Rotational-translational (RT) energy transfer is extremely rapid [105] (except for the special case of hydrogen, which is not used as a test gas component in the work described here) and occurs on a timescale faster than our time resolution. The transfer of energy to vibration by vibration-translation (VT) and vibration-rotation (VR) processes is much slower and occurs on a suitable timescale for experimental measurements by the present technique.

We shall be concerned with the evolution of the populations in the individual levels of a diatomic gas following shock-heating. In this chapter emphasis shall be placed on the theoretical estimate of the relative values of the different rate constants - rather than the evaluation of their absolute values - and the consequent predictions for the shape of the population/time curves. Previous experimental work will also be considered.

We shall consider (VT), (VV) and (VR) processes in turn for a simple harmonic oscillator, and then bring in complicating factors such as anharmonicity.

5.2 The Magnitude of (VT) Rate Constants

Energy is transferred from translation to vibration by processes such as:

$$CO(v=0) + M \underset{k_{10}}{\overset{k_{01}}{\rightleftharpoons}} CO(v=1) + M \qquad (5.1)$$

$$CO(v=1) + M \underset{k_{21}}{\overset{k_{12}}{\rightleftharpoons}} CO(v=2) + M \qquad (5.2)$$

$$CO(v=0) + M \underset{k_{20}}{\overset{k_{02}}{\rightleftharpoons}} CO(v=2) + M \qquad (5.3)$$

M is the collision partner which may be a molecule of CO or of any other species present. A multiquantum process such as equation (5.3) requires approximately twice as much translational energy as single-quantum processes such as equations (5.1) and (5.2). For a single quantum process in CO the energy required is ~2100 cm^{-1}. Only the most energetic collisions can provide this.

Traditional theories determine rate constants by calculating probabilities per collision and multiplying these by the collision number. This involves the definition of a 'collision' by means of an arbitrary collision diameter, and is avoided in modern theories. Today cross-sections are calculated at different velocities and an average over the velocity distribution is carried out.

Historically, the theory of (VT) energy transfer is dominated by the classical theory of Landau and Teller [106] and the quantum-mechanical theory of Schwartz, Slawsky and Herzfeld [107]. Both theories regard the vibrational motion of the molecules quantum mechanically. Both make use of perturbation theory. The wavefunctions of a simple harmonic oscillator are orthogonal so a transition between them is impossible unless some perturbation occurs. The perturbing force for collisional energy transfer is provided by the intermolecular potential. As only very energetic collisions are successful, the repulsive part of the potential is important for (VT) transfer.

The two theories differ in their treatment of the collision-partner M. Classical theory views it as particulate, quantum theory as an incoming wave-pattern. The two strands of theory reach the same conclusions on the temperature dependence of the rate constants, and the ratios of the rate constants $k_{01}:k_{12}:k_{23}$ etc which particularly interests us here.

SSH theory was a clear improvement on Landau-Teller theory for predicting the absolute magnitude of rate constants. For instance, the shock tube results of Matthews [108] and of Hooker and Millikan [50] for the vibrational relaxation of CO fit well to an early version of SSH theory. The improvements brought by subsequent theoretical developments are largely at temperatures lower than those attainable in shock tube experiments and for special cases, e.g. the presence of strong attractive intermolecular forces, which need not concern us here. Such developments are reviewed in the standard texts [105,109-111] on energy transfer. An example of a recent theoretical paper, by-passing the need for collision diameters, is provided by the Simpson group [65].

5.3 The Relative Values of (VT) Rate Constants

The Landau-Teller theory is rewritten in English, with some new material incorporated, by Bethe and Teller [112]. Its starting point is Ehrenfast's adiabatic principle. Applied to this situation, it states that there will be efficient energy transfer (non-adiabatic) if the duration of the collision τ_c is short compared to a period of vibration τ_o, but very little energy transfer (adiabatic) if the duration of the collision is long compared to a period of vibration. The latter is the case since the effective range of the intermolecular potential is large compared to the vibrational amplitude.

A rotational period is much longer than a vibrational period. Rotation-translation energy transfer is orders of magnitude more efficient for this reason as well as because a smaller quantity of energy is transferred.

Landau and Teller assume the energy transfer probability is proportional to $e^{-\tau_c/\tau_o}$, calculate this factor as a function of velocity, and integrate over the thermal distribution of velocities analytically using the saddle-point method. The result for the temperature dependence is that the logarithm of the probability varies as $T^{1/3}$. This temperature dependence is confirmed by subsequent theories and experimental results at high temperatures.

Other important conclusions arise from the adiabaticity considerations above. Efficient (VT) energy transfer is favoured by:

1) Low frequency of vibration (increases period of oscillation)

2) Low mass of collision partner (increases relative velocity and so reduces time of collision)

3) Steep intermolecular potential (reduces time of collision)

The assumptions made by Landau and Teller in the calculation of the ratio $k_{01}:k_{12}:k_{23}$ are as follows:

1) First order perturbation theory may be applied. This is justified if the probability of excitation/de-excitation is low, as we have seen is the case.

2) The intermolecular potential is linear in the normal co-ordinate of the vibration. This is justified as long as the vibrational amplitude is small compared to the distance over which the potential acts.

3) The molecule may be regarded as a simple harmonic oscillator. This is a good approximation for the low levels of a strongly-bound molecule.

The effects of anharmonicity will be accounted for later.

These assumptions lead to the results that multiquantum transfer ($\Delta v \neq 1$ e.g. equation (5.3)) has zero probability, and that the matrix element for the collision-induced transition from level v to level v+1 is proportional to $(v+1)^{1/2}$. The transition probability P is proportional to the matrix element squared i.e.

$$P_{01}:P_{12}:P_{23} = k_{01}:k_{12}:k_{23} = 1:2:3 \qquad (5.4)$$

This is a very important result as section 5.4 will make apparent.

SSH theory reaches the same conclusions for the dependence of the (VT) rate constants on temperature, vibrational frequency, mass, steepness of potential and vibrational quantum number. The conclusions are reached by considering the criteria for good overlap between the initial and final wave functions. The quantum mechanical approach is summarised well by Pilling [113]. To deduce the dependence on vibrational quantum number, it is necessary to assume that the wave function can be separated into parts due to the relative translational motion of the colliding species, and the vibration of the oscillator. The same integral occurs in the latter part as in the consideration of radiative transitions between vibrational levels. This is why the 'selection rules' and vibrational quantum number dependence are the same for radiatively and collisionally induced transitions.

5.4 Consequences for Evolution of Population of Vibrational Levels

For the Landau-Teller model, the relative values of the (VT) rate constants are given by:

$$k_{v,v+1} = (v+1)k_{01} \qquad (5.5)$$

$$k_{v+1,v} = (v+1)k_{10} \tag{5.6}$$

$$k_{01} = k_{10}e^{-h\nu/kT} \tag{5.7}$$

where ν is the frequency of the simple harmonic oscillator and T is the translational temperature. Equation (5.7) is a consequence of detailed balancing.

Initially, the molecules are in equilibrium at room temperature, T_1. Passage of the shock-front causes the translational (and rotational) temperature to rise almost instantaneously to final temperature T_f, but the vibrational levels are left in a Boltzmann distribution appropriate to T_1. When vibrational relaxation is complete, the translational and vibrational degrees of freedom will be in full thermodynamic equilibrium. For the moment we shall assume that this is at temperature T_f. This assumes the oscillator molecule is infinitely diluted in an inert gas, otherwise as energy is transferred from translation to vibration, the translational temperature falls. The problem we are concerned with, then, is the relaxation of a system of simple harmonic oscillators from an initial Boltzmann distribution to a final equilibrium Boltzmann distribution, at constant translational temperature. We wish to determine the populations of individual vibrational levels at interim times.

To solve this problem we must write down the master equation for the rate of change with time of the population density n_v in vibrational level v.

As we are considering only (VT) processes with $\Delta v = \pm 1$ i.e. the processes exemplified by equations (5.1) and (5.2), the rates of change for the zeroth and first levels and the generalised master equation are:

$$\frac{dn_0}{dt} = n_M(k_{10}n_1 - k_{01}n_0) \tag{5.8}$$

$$\frac{dn_1}{dt} = n_M(k_{01}n_0 - k_{10}n_1 + k_{21}n_2 - k_{12}n_1) \tag{5.9}$$

$$\frac{dn_v}{dt} = n_M(k_{v-1,v}n_{v-1} - k_{v,v-1}n_v + k_{v+1,v}n_{v+1} - k_{v,v+1}n_v) \tag{5.10}$$

where n_M is the number density of diluent species M.

At t=0,

$$n_v = ne^{-v\theta_1}(1 - e^{-\theta_1}) \tag{5.11}$$

and at t=∞,

$$n_v = ne^{-v\theta_f}(1 - e^{-\theta_f}) \tag{5.12}$$

where $n=\Sigma n_v$ is the total number density of the oscillator species, $\theta_1 = h\nu/kT_1$ and $\theta_f = h\nu/kT_f$. Equations (5.11) and (5.12) describe Boltzmann distributions of harmonic oscillators.

To solve for n_v at interim times, the master equation must be integrated. This can be done analytically, or numerically using a suitable computer program, and these methods will be described in sections 5.5 and 5.6. Initially, a consideration of integration over short periods of time by simple algebra will be set out. This approach shows clearly how the ratios of rate constants described in equations (5.4)-(5.6) lead to the final result.

Defining $F = -1/n_M(dn_0/dt)$, and $r = n_{v+1}/n_v$, and substituting equations (5.5)-(5.7) into (5.8)-(5.10), gives:

$$\frac{dn_0}{dt} = -F \tag{5.13}$$

$$\frac{dn_1}{dt} = F-2Fr \tag{5.14}$$

$$\frac{dn_2}{dt} = 2Fr-3Fr^2 \tag{5.15}$$

$$\frac{dn_3}{dt} = 3Fr^2-4Fr^3 \tag{5.16}$$

$$\frac{dn_v}{dt} = vFr^{v-1}-(v+1)Fr^v \tag{5.17}$$

At time t=0, let $n_0 = a$. Then $n_1 = ar^1$, $n_2 = ar^2$ etc, and:

$$n_v(t=0) = ar^v \tag{5.18}$$

This defines the initial Boltzmann distribution.

Then at time $t+\delta t$, where $f = F\delta t$,

$$n_0 = a-f \tag{5.19}$$

$$n_1 = ar+f-2fr \tag{5.20}$$

$$n_2 = ar^2+2fr-3fr^2 \tag{5.21}$$

$$n_v = ar^v+vfr^{v-1}-(v+1)fr^v \tag{5.22}$$

Rearranging,

$$n_0 = a-f \tag{5.23}$$

$$n_1 = r(a-f)+f(1-r) \tag{5.24}$$

$$n_2 = r^2(a-f)+2fr(1-r) \tag{5.25}$$

$$n_v = r^v(a-f)+vfr^{v-1}(1-r) \tag{5.26}$$

If f is sufficiently small that terms in f squared and higher can be neglected this is equivalent to:

$$n_0 = a-f \tag{5.27}$$

$$n_1 = (a-f)\left[r+f\frac{(1-r)}{(a-f)}\right] \tag{5.28}$$

$$n_2 = (a-f)\left[r+f\frac{(1-r)}{(a-f)}\right]^2 \tag{5.29}$$

$$n_v = (a-f)\left[r+f\frac{(1-r)}{(a-f)}\right]^v \tag{5.30}$$

If we substitute A = a-f and R = r+f(1-r)/(a-f), it is clear that the vibrational levels are still in a Boltzmann distribution at time t+δt. The new Boltzmann distribution is defined by slightly decreased n_0 and slightly increased n_{v+1}/n_v. The transformation of (5.26) to (5.30) is valid if $(a-f) \gg f(1-r)$ i.e. $f \ll a/(2-r)$. As relaxation proceeds r rises (from 3.4×10^{-5} at 300 K to 0.21 at, say, 2000 K for CO), and a/(2-r) rises, thus the required values for f and hence δt for the inequality to be true rise slightly. We can repeat the integration over δt for an indefinite number of times, as successive values of δt do not approach zero, so our conclusion is the following statement:

Relaxation of a system of simple harmonic oscillators from an initial Boltzmann distribution to a final Boltzmann distribution

proceeds via a continuous series of Boltzmann distributions. That is, at all times during the relaxation, the number densities in different vibrational levels are given by:

$$n_v = ne^{-v\theta}(1-e^{-\theta}) \tag{5.31}$$

where:

$$\theta = h\nu/kT_{vib} \tag{5.32}$$

The vibrational temperature T_{vib} is equal to T_1 at t=0 and T_f at t=∞ and gradually rises at intermediate times. Meanwhile θ falls from θ_1 to θ_f. At any time, the population of every level may be described in terms of one parameter T_{vib}. This is only true for relaxation via a continuous series of Boltzmann distributions.

These conclusions are a direct consequence of the adoption of the Landau-Teller collisional transition probabilities.

We shall postpone the consideration of the resultant shape of a n_v/time profile until section 5.12 after the effects of (VV) and (VR) processes have been considered. In the following two sections we consider the rigorous solution of the master equation (5.10) (i) numerically using a computer, and (ii) analytically. The first of the sections also serves as an introduction to the numerical integration program used several times in this work.

5.5 Computer Program for Numerical Integration

The numerical integration of the master equations for vibrational relaxation following shock-heating has been done before. Amongst the work that will be referred to in the subsequent sections is that of

Borrell and Millward [47] and of Kewley [114]. The possession of such a program is an important aid to comprehension of the mechanism of vibrational relaxation, and the program has been extended for the kinetics experiments described in Part Three of this thesis.

The numerical integration itself is carried out by the D02EBF subroutine supplied by the National Algorithm Group. This makes use of Gear's method to integrate a system of stiff differential equations i.e. equations with widely varying time constants. Gear's method is a variable step-size predictor-corrector method. The user provides the differential equations (kinetic equations in this case) and initial values (initial concentrations) in separate subroutines. In our case, the rate constants are calculated in another subroutine. This is convenient for rate constants which are related to each other. The program is written so that the variables which are changed from one run to the next are fed in as data, to avoid time-consuming editing. The program runs on the University of Oxford ICL 2988 mainframe computer.

In the present case, the relaxation of simple harmonic oscillators, only a finite number of vibrational levels can be considered. In most runs it has been assumed that levels above v=7 do not exist. This leads to deviations away from a continuous series of Boltzmann distributions for the higher levels. That this is a 'finite-level effect' can be proved by extending the model to include levels up to v=10 when the deviations in the populations of v=6 and v=7 disappear.

5.6 Analytical Solution of the Master Equation

This was achieved by Montroll and Shuler [3] for several initial distributions including an initial Boltzmann distribution, with the same conclusion as from the numerical methods for this case: relaxation via a continuous series of Boltzmann distributions. They too used the

Landau-Teller transition probabilities and assume heavy dilution in an inert gas.

As well as deducing the time-dependence of the number densities in individual vibrational levels, they also considered the time-dependence of the total vibrational energy. It is the relaxation of the vibrational energy which defines the vibrational relaxation time, τ, and which is discussed in the next section.

5.7 The Vibrational Relaxation Time. Relaxation of Total Vibrational Energy

The total energy in vibration is given by: $E = \sum_v E_v n_v$. For a simple harmonic oscillator, $E_v = vE_1$ where E_1 is the energy of the first vibrational level. Thus we can write, for simple harmonic oscillators,

$$E = E_1 \sum_v v n_v \tag{5.33}$$

The change of energy with time is then:

$$\frac{dE}{dt} = E_1 \sum_v v \frac{dn_v}{dt} \tag{5.34}$$

dn_v/dt is given by equation (5.10). From equations (5.5),(5.6),(5.10) and (5.34) we deduce:

$$\frac{1}{n_M}\frac{dE}{dt} = E_1 \sum_v (v^2 k_{01} n_{v-1} - v^2 k_{10} n_v + v(v+1) k_{10} n_{v+1} - v(v+1) k_{01} n_v) \tag{5.35}$$

The sum can be rearranged by collecting together terms in n_v from different dn_v/dt to give:

$$\frac{1}{n_M}\cdot\frac{dE}{dt} = E_1\Sigma_v(n_v(v+1)k_{01} - n_v v k_{10}) \tag{5.36}$$

Since $\Sigma v n_v = E/E_1$ and $\Sigma n_v = n$,

$$\frac{1}{n_M}\cdot\frac{dE}{dt} = E(k_{01}-k_{10}) + nk_{01}E_1 \tag{5.37}$$

As at $t=\infty$, $dE/dt = 0$, it must be that:

$$nk_{01}E_1 = -E_\infty(k_{01}-k_{10}) \tag{5.38}$$

where E_∞ is the total vibrational energy at final equilibrium. (This equation also follows from equation (5.45) below.) Thus:

$$\frac{1}{n_M}\cdot\frac{dE}{dt} = (k_{10}-k_{01})(E_\infty-E) \tag{5.39}$$

This is the energy relaxation equation, first obtained by Bethe and Teller. Its integral form is:

$$\frac{E_\infty - E_t}{E_\infty - E_0} = e^{-(k_{10}-k_{01})n_M t} \tag{5.40}$$

We define the vibrational relaxation time, τ by:

$$\tau = \frac{1}{(k_{10} - k_{01})n_M} \tag{5.41}$$

Thus:

$$\frac{E_\infty - E_t}{E_\infty - E_0} = e^{-t/\tau} \tag{5.42}$$

For a shock tube experiment on a gas without very low frequency vibrational modes, $E_0 = 0$, to a very good approximation, thus:

$$E_t = E_\infty(1 - e^{-t/\tau}) \qquad (5.43)$$

Note that the derivation of (5.39) does not depend on the distribution of the molecules between the vibrational levels. It applies for any initial distribution.

Many shock tube techniques obtain the vibrational relaxation time directly via equation (5.42) and thus can obtain no information on the behaviour of individual levels. For instance, the changing density measured by the interferometry and laser schlieren techniques is a direct consequence of the change of vibrational energy and hence enthalpy of the test gas. The intensity of emission observed in an infrared emission experiment is directly proportional to the vibrational energy (provided that the gas is optically thin for all levels). This is because the emission intensity is proportional to $\Sigma v n_v$, as a result of the harmonic oscillator transition probabilities.

The simple dependence of the total vibrational energy on relaxation time was originally derived by Bethe and Teller [112]. Once again, it depends on the Landau-Teller transition probabilities. Note the difference between a simple harmonic oscillator and a two-level system (v=0 and v=1), for which $(k_{10} - k_{01})$ in equation (5.41) must be replaced by $(k_{10} + k_{01})$.

Conventionally the vibrational relaxation time is written as $(p\tau)$, having been corrected to 1 atm, i.e.

$$(p\tau) = 1/(k_{10} - k_{01}) \qquad (5.44)$$

where k_{10} and k_{01} are in pressure units e.g. $atm^{-1}s^{-1}$. As a result of the conclusions of Landau and Teller on the temperature dependence, experimentally obtained values of $(p\tau)$ are displayed as plots of $\log(p\tau)$ against $T^{-1/3}$. It is interesting to recall, however, that it is the probability of energy transfer that should depend on $T^{1/3}$. The probability is related to the rate constant via a collision number, $k_{10} = P_{10}Z$, and the collision number Z at constant pressure is proportional to $T^{-1/2}$, so it would be more logical to plot $\log[(p\tau).T^{-1/2}]$ against $T^{-1/3}$. The conventional plot is simpler, and serves the purpose of producing an empirical formula for the dependence of $(p\tau)$ on temperature. The plot is only used to determine empirical constants. From $(p\tau)$, the value of individual (VT) rate constants may be deduced via (5.44) and (5.5)-(5.7).

5.8 Expression for the Variation of Vibrational Temperature

If we combine our two major results, that (i) relaxation occurs through a continuous series of Boltzmann distributions and (ii) the total vibrational energy evolves exponentially as in equation (5.39), we can deduce an expression for the variation of vibrational temperature with time. The combination of (i) and (ii) shall henceforth be referred to as the LBTMS (Landau-Bethe-Teller-Montroll-Shuler) model. Landau and Teller derived the relative collisional transition probabilities, Bethe and Teller used them to prove (ii), and Montroll and Shuler used them to prove (i), which Landau and Teller had assumed. (i) determines that such a parameter as the vibrational temperature, in terms of which the population of every level can be described, exists at all times. Using (ii) we substitute (5.33) into (5.42). For a Boltzmann distribution

$$\sum_v vn_v = \sum_v nv(1 - e^{-\theta})e^{-v\theta} = ne^{-\theta}/(1-e^{-\theta}) \qquad (5.45)$$

(via some algebraic manipulation) and thus equation (5.42) becomes:

$$\frac{e^{-\theta_f}}{1 - e^{-\theta_f}} - \frac{e^{-\theta}}{1 - e^{-\theta}} = \left[\frac{e^{-\theta_f}}{1 - e^{-\theta_f}} - \frac{e^{-\theta_1}}{1 - e^{-\theta_1}}\right] e^{-t/\tau} \qquad (5.46)$$

Much algebraic manipulation yields:

$$\frac{h\nu}{kT_{vib}} = \theta = \log\left[\frac{e^{-t/\tau}(1 - e^{\theta_f - \theta_1}) - e^{\theta_f}(1 - e^{-\theta_1})}{e^{-t/\tau}(1 - e^{\theta_f - \theta_1}) - (1 - e^{-\theta_1})}\right] \qquad (5.47)$$

This result was first given by Montroll and Shuler [3]. Note that in their notation τ is a dimensionless time and is equal to t/τ in our notation. At $t=0$, $\theta = \theta_1$ and at $t=\infty$, $\theta = \theta_f$.

This expression is used in the treatment of experimental results in chapter 6.

5.9 (VV) Rate Constants

The conclusions of this chapter have followed from a master equation, (5.10), containing only (VT) energy transfer terms. However (VV) processes will also occur e.g.

$$CO(v=1) + CO(v=1) \underset{k_r}{\overset{k_f}{\rightleftharpoons}} CO(v=0) + CO(v=2) \qquad (5.48)$$

$$CO(v=2) + CO(v=3) \rightleftharpoons CO(v=1) + CO(v=4) \qquad (5.49)$$

For a simple harmonic oscillators such processes are exactly resonant i.e. no energy is exchanged between vibration and translation. Landau and Teller did not extend their theory to (VV) processes, but

SSH theory has been extended to cover them. Integration over the thermal velocity distribution must be numerical rather than via the saddle-point method. The processes are predicted to be orders of magnitude faster than (VT) processes because they are resonant. For extremely high probabilities, the first-order perturbation treatment of SSH theory breaks down.

Sharma and Brau [115] developed an alternative theory for near resonant energy transfer based on long-range forces rather than the short-range forces which dominate SSH theory. They considered (VV) energy transfer brought about by the long-range dipole-dipole (or higher multipole) coupling between the transition dipoles of the two molecules. In reality both long-range and short-range forces must be considered.

The important point for simple harmonic oscillators is that (VV) rate constants are much greater than (VT) rate constants.

(VV) rate constants in CO have been determined experimentally by Hancock and Smith [116], using a fluorescence quenching method, and Powell [117], using a continuous wave CO laser to monitor CO excited by an electric discharge. It is not possible to usefully discuss the dependence on temperature and vibrational quantum number until anharmonic effects have been discussed, in section 5.15, as such effects become significant for near-resonant energy transfer processes. For the moment we note that (VV) rate constants are found to be of the order of 10^{-12} $cm^3 molecule^{-1} s^{-1}$ [117] which is ~1,000 times greater than the CO-CO (VT) rate constant k_{10} at 2000 K [50].

5.10 Inclusion of (VV) Processes in Master Equation

It might be thought that the conclusions for the model containing only (VT) rate processes would be radically altered upon the inclusion of (VV) processes as these latter have rate constants ~10^3 times higher. For simple harmonic oscillators, taking equation (5.48) as an example, the forward and reverse rate constants will be equal as there is no energy defect, $k_f = k_r$. Since the process is so much faster than (VT) processes, at any instant in time, it leads to the existence of a quasi-equilibrium governed by: $k_f n_1^2 = k_r n_0 n_2$. This implies $n_2/n_1 = n_1/n_0$ i.e. a Boltzmann distribution.

Yet for the model under consideration (VT) processes themselves ensure relaxation via a continuous series of Boltzmann distributions so the inclusion of (VV) processes has no effect, whatever the magnitude of the (VV) rate constants.

This is confirmed by the numerical integration. The only effect of inclusion of (VV) rate constants in the computer model described in section 5.5 is to greatly reduce the 'finite-level effects' discussed there.

It is only because the initial vibrational distribution is a Boltzmann distribution that (VV) processes have no effect. If the initial vibrational distribution were non-Boltzmann, the early dynamics of the relaxation would be dominated by the (VV) processes which would tend to bring about a Boltzmann distribution. For instance, if a molecule is formed in a chemical reaction with a vibrational distribution peaking at a high level (e.g. CO from O+CS->CO+S), (VV) processes will establish a Boltzmann distribution characterised by a vibrational temperature higher than the translational one. Relaxation will subsequently proceed via a continuous series of Boltzmann

distributions until the translational and vibrational temperatures are equal.

5.11 (VR) Processes

For HCl [48,118] the relaxation time is found to be two to three orders of magnitude faster than SSH theory predicts and, furthermore, HCl relaxes faster than DCl despite having a greater vibrational frequency. This can be explained by invoking vibration-rotation energy transfer on the grounds that in such molecules with low moments of inertia, the rotational velocity of the H atom will be greater than the translational velocity.

Moore [119] developed a pure (VR) theory which was a great improvement on SSH theory. The hydride/deuteride ratio is predicted correctly, but absolute rates are generally under estimated because of the complete neglect of concurrent (VT) energy transfer. Improved theories include (VT) and (VR) processes e.g. [120] for CD_4.

The ratio of rate constants $k_{v,v+1}:k_{01}$ remains as according to Landau and Teller as the consideration of the vibrational matrix elements is unchanged. The only change is in the treatment of the motion of the collision partner. The LBTMS model is thus still applicable if (VR) processes are more important than (VT) processes. Therefore henceforth when (VT) processes are referred to, it is to be understood that a (VR) component is included.

5.12 Summary on Evolution of Population of Vibrational Levels of Simple Harmonic Oscillators

In sections 5.14 et seq. we shall discuss the effects of anharmonicity. It will be seen that the approximation of simple

harmonic oscillators is a good one for the lowest vibrational levels, so it is worth pausing to summarise the theory for simple harmonic oscillators.

The vibrational levels are predicted to relax via a continuous series of Boltzmann distributions, as defined by (5.31), characterised by temperature T_{vib}. T_{vib} rises from initial temperature T_1 to final temperature T_f during the relaxation in the manner given by (5.47).

The population of (v=1) rises approximately exponentially behind the shock front. The population of (v=2) has an initial slope of zero and an 'S' shape. This follows from the fact that the ratio n_{v+1}/n_v rises throughout the relaxation (e.g. from 3.4×10^{-5} at 300 K to 0.21 at 2000 K for CO). For each higher level, the rise in population is delayed to a longer time. The predicted curves for the rise in population of (v=1) and (v=4) for T_f = 2100 K are shown in figure 5.1. They have been normalised to unity at final equilibrium. Also shown, by the dashed lines, are the differences in population $n_1 - n_2$ and $n_4 - n_5$, as these are a closer approximation to the experimental laser gains.

The rate of increase of vibrational energy is controlled by the (VT) processes. As a result of the Landau-Teller collisional transition probabilities, the (VT) processes ensure relaxation via a continuous series of Boltzmann distributions. If this were not the case, the (VV) processes, which are three orders of magnitude faster for CO at 2000 K, would control the vibrational distribution which would still be a Boltzmann distribution. The (VV) processes make no contribution to the overall relaxation of vibration into equilibrium with translation, but merely distribute vibrational energy between different levels. Thus the computer model, described in section 5.5, shows that setting all of the (VV) rate constants to zero has no effect on the relaxation of a system of simple harmonic oscillators. Setting all the (VT) rate constants to

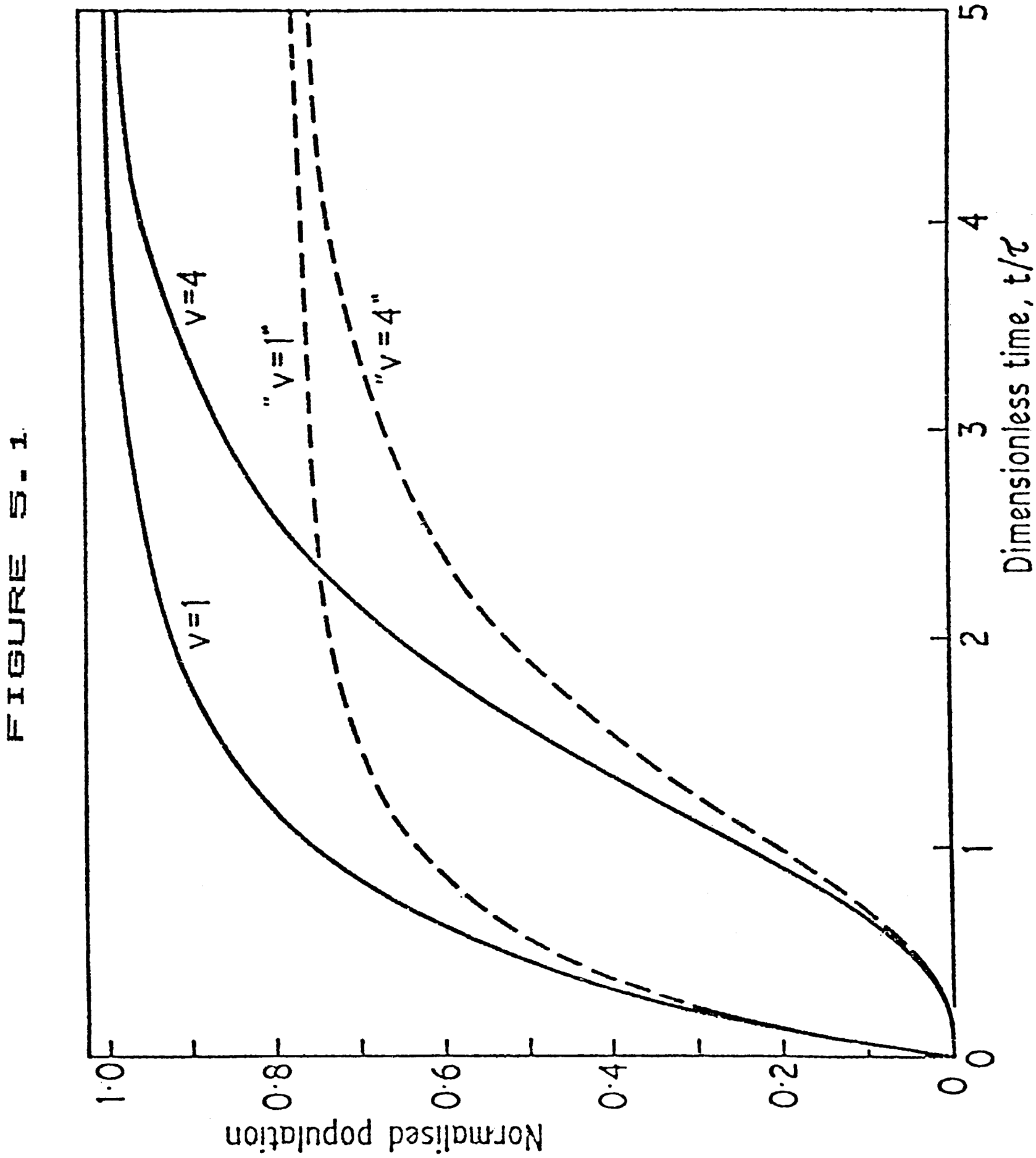

Normalised population
1·0
0·8
0·6
0·4
0·2
0
0
1
2
3
4
5
Dimensionless time, t/τ
V=4
"V=1"
"V=4"
V=1

FIGURE 5.1

zero except k_{01} and k_{10} preserves a continuous series of Boltzmann distributions but slows down the overall rate, to which higher $k_{v,v+1}$ also contribute.

5.13 Effect of Changing Temperature

So far we have assumed that the relaxing gas is in a heat-bath at constant temperature. However in reality as energy flows from translation into vibration in a shock tube experiment, the translational temperature falls. By solving the Rankine-Hugoniot equations (chapter 4) before and after vibrational relaxation, we can calculate the magnitude of this fall. Examples are 2214 K to 1985 K for 100 % CO and 2136 K to 2129 K for 2 % CO diluted with a rare gas. Herman and Rubin [121], and Rankin and Light [4], extended the work of Montroll and Shuler [3] to show that relaxation still occurs via a continuous series of Boltzmann distributions under these conditions. The analytical treatment of the master equation was carried out once again for simple harmonic oscillators with rate constants assuming the Landau-Teller transition probabilities. The only effect of a changing translational temperature on the algebraic treatment of section 5.4 is to change the value of F; all dn_v/dt are proportional to F so all are changed equally and the treatment still applies.

The rate of relaxation of the total vibrational energy is now given by:

$$\frac{1}{p}.\frac{dE}{dt} = \frac{1}{(p\tau)}(E_T - E) \qquad (5.50)$$

where E_T is the energy that would be in vibration at equilibrium at the current translational temperature T_T. T_T is approximately given by:

$$T_T = T_f - (T_f - T_a)e^{-t/\tau} \qquad (5.51)$$

where T_a is the value of the translational temperature immediately behind the shock and T_f is the value after vibrational relaxation is complete. In equation (5.50) E_T and $1/(p\tau)$ both change with time. The shock tube work of this group using the interferometry and laser schlieren techniques [36,40] used equation (5.50) to analyse the data. For each shock, $(p\tau)$ was determined as a function of temperature between T_a and T_f.

In the expression for the dependence of the vibrational temperature on time, (5.47), θ_f must be replaced by θ_T where $\theta_T = e^{-h\nu/kT_T}$.

As our laser absorption experiments do not probe the energy in vibration directly, an analysis taking account of the change in translational temperature has not been attempted for the energy transfer results reported in this thesis. In most cases dilution has made the temperature change low.

It is common practice in shock tube work on energy transfer to obtain a single relaxation time per experiment and assume it applies to the mean translational temperature, $(T_f - T_a)/2$. This convention will be followed here. However, Borrell and Millward [47], by numerically integrating the master equation, allowing for the changing temperature, came to the conclusion that a relaxation time obtained in this way applies more closely to T_a. This is because as time progresses $(p\tau)$ increases, so the relaxation gets slower, but E_T falls, so the system is closer to final equilibrium. The two effects tend to cancel each other out.

5.14 Effects of Anharmonicity. (i) (VT) Rate Constants

Real gases are composed of molecules which are not simple harmonic oscillators. The extent of any deviation away from the LBTMS model caused by anharmonicity is not a simple matter to discuss. It is not clear (i) how to allow for anharmonicity in the master equation and (ii) how to measure the extent of deviation away from the LBTMS model.

Bearing in mind that (VV) processes are much faster than (VT) processes, the vibrational distribution will be determined by the former. Nevertheless, it is interesting to discuss the effects for the master equation with (VT) processes alone.

Whereas for a simple harmonic oscillators the energy levels are given by $E_v = vE_1$, for an anharmonic oscillator:

$$E_v = \omega_e v - x_e\omega_e(v^2+v) \qquad (5.52)$$

(unusual form, not including zero point energy).

The energy difference between successive levels decreases for higher v:

$$E_{v+1} - E_v = \omega_e - 2x_e\omega_e(v+1) \qquad (5.53)$$

and thus transitions between higher levels are more probable than for simple harmonic oscillators. The Landau-Teller collisional transition probabilities are no longer applicable, and $k_{v+1,v} > (v+1)k_{10}$. Also, multiquantum (VT) energy transfer no longer has zero probability. Discussion of this last point will be postponed until section 5.17.

The second effect of anharmonicity is a consequence of microscopic reversibility. If, for simplicity, the Landau-Teller probabilities are

still assumed to apply such that $k_{v+1,v} = (v+1)k_{10}$ then it cannot be that $k_{v,v+1} = (v+1)k_{01}$ if $k_{v,v+1} = k_{v+1,v}e^{-h\nu/kT}$ is to be kept since ν is now a function of v. Probably the best solution is to 'symmetrise' the (VT) rate constants such that, assuming the Landau-Teller transition probabilities,

$$k_{v+1,v}=(v+1)k_1e^{+h\nu/2kT} \; ; \; k_{v,v+1}=(v+1)k_1e^{-h\nu/2kT} \qquad (5.54)$$

where k_1 is the geometric mean of k_{01} and k_{10}.

Many papers have been written about the effects of anharmonic (VT) rate constants on vibrational relaxation dynamics [114,122-125]. Some authors symmetrise the (VT) rate constants and some do not. The Landau-Teller transition probabilities may be assumed or, alternatively, the expressions given by Bray [124] from a fit to SSH theory may be used. There is agreement that for the case of relaxation from an initial Boltzmann distribution, and for low v, the effects are small.

5.15 Effects of Anharmonicity. (ii) (VV) Rate Constants

For simple harmonic oscillators, the (VV) rate constant for a process such as:

$$CO(v) + CO(u) \rightleftharpoons CO(v+1) + CO(u-1) \qquad (5.55)$$

is given by:

$$k^{u,u-1}_{v,v+1} = u(v+1)k^{10}_{01} \qquad (5.56)$$

and the forward and reverse rates are equal. For anharmonic oscillators the process has an energy defect and when v and u are far apart this

will be significant compared to kT. Small defects can be cancelled out by simultaneous rotational transitions and thus, at room temperature, an energy defect of $\leq 100\ cm^{-1}$ is found not to reduce the probability [116]. Bearing in mind that, below T_{vib} =4000 K, half the molecules are in v=0, the dominant (VV) process will be

$$CO(v) + CO(1) \rightleftharpoons CO(v+1) + CO(0) \qquad (5.57)$$

and thus for anharmonic oscillators (VV) rates decline for high levels. Powell [117] measured CO (VV) rate constants at 100 K, 300 K and 500 K and fitted his results to the empirical expression

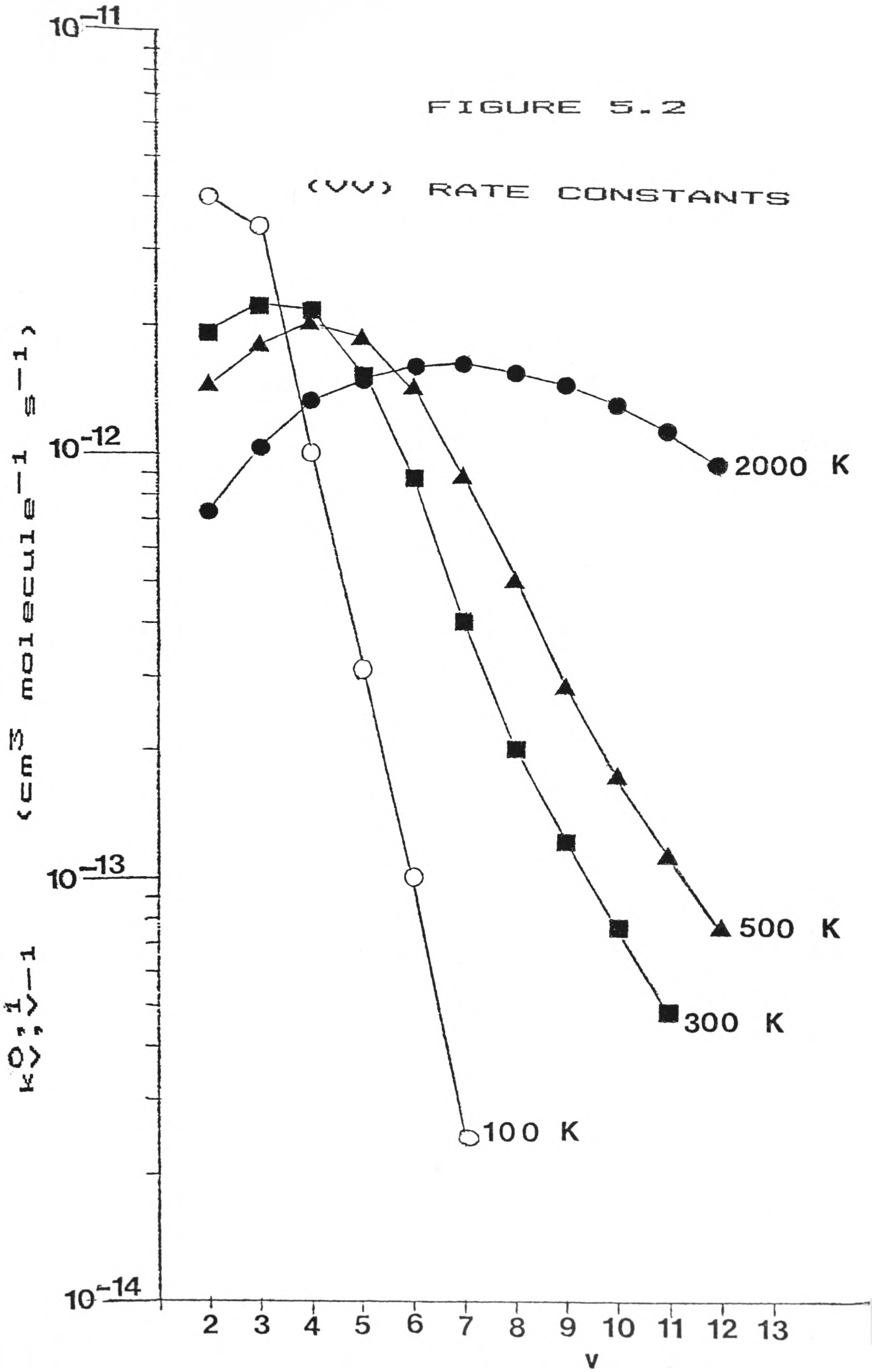
$$k^{0,1}_{v+1,v} = (v+1)Z(0.919T^{-1} + 61.9T^{-2})\exp[-(0.188\Delta E_v/T^{1/2})^2] \qquad (5.58)$$

where Z is the gas kinetic collision number, given by $Z = 1.73 \times 10^{-11} T^{1/2}\ cm^3 molecule^{-1} s^{-1}$. In figure (5.2) the results of this expression at 2000 K are sketched, along with the experimental results at 100, 300 and 500 K. The fall in $k^{0,1}_{2,1}$ with increase in temperature is in accord with Sharma-Brau theory. The extrapolation to 2000 K is made here in the absence of any experimental data at higher temperatures. In fact the same expression is unlikely to apply as well at 2000 K, as short-range forces are expected to become more important in determining the value of the rate constant at higher temperatures. The important result is that the fall in rate constant is postponed to very high vibrational quantum number v, and to a good approximation, $k^{0,1}_{v+1,v} = 10^{-12}\ cm^3 molecule^{-1} s^{-1}$ for v = 2 to 13.

This is three orders of magnitude greater than the values of the (VT) rate constants for CO [50] so (VV) rate constants will determine the vibrational distribution at any time. Following the treatment of section 5.10, we will look at the position of equilibrium of the process

FIGURE 5.2

(VV) RATE CONSTANTS



$$CO(v=1) + CO(v=1) \underset{k_r}{\overset{k_f}{\rightleftharpoons}} CO(v=0) + CO(v=2) \qquad (5.48)$$

Now, $k_f/k_r = n_0 n_2/n_1^2 = e^{\Delta E/KT_T}$ where T_T is the translational temperature. Defining T_1^* by $n_1 = n_0 e^{-E_1/kT_1^*}$, it follows that:

$$n_2 = n_0 e^{-2E_1/kT_1^*} e^{\Delta E/kT_T} \qquad (5.59)$$

where ΔE is the energy change for the process. For a simple harmonic oscillator, $\Delta E = 0$ and so this expresses a Boltzmann distribution. Otherwise, $\Delta E = 2E_1 - E_2$, and generalizing for all v,

$$n_v = n_0 e^{-vE_1/kT_1^*} e^{(vE_1 - E_v)/kT_T} \qquad (5.60)$$

This expression defines a Treanor distribution. It was originally derived by Treanor, Rich and Rehm [79]. They derived it in two ways, by solving the master equation with (VV) processes dominant and from the statistical mechanics of a system in which the number of quanta is conserved.

Treanor et al. pointed out that, where (VV) processes dominate, relaxation will proceed via a continuous series of such distributions. There are a number of features of Treanor distributions to be emphasised:

(i) When $T_1^* = T_T$, equation (5.60) reduces to $n_v = n_0 e^{-E_v/kT_T}$, which defines a Boltzmann distribution of anharmonic oscillators. Otherwise the distribution is non-Boltzmann and there is no longer a common vibrational temperature in terms of which the population of each level

can be expressed. T_1^* could be taken as the vibrational 'temperature' of level v=1, in which case successive vibrational levels would have vibrational 'temperatures' defined by either:

$$n_v = n_0 e^{-E_v/kT_v^*} \tag{5.61}$$

or:

$$n_v = n_{v-1} e^{-(E_v - E_{v-1})/kT_v^*} \tag{5.62}$$

The two sets of T_v^* will be different. We shall adopt the latter definition in the treatment of results in chapters 6 and 7 as it is more convenient in the analysis adopted there.

(ii) If $vE_1 = E_v$ the expression reduces to the expression for a Boltzmann distribution of simple harmonic oscillators.

(iii) If $T_T > T_1^*$, the first exponential term in equation (5.60) dominates, and the distribution is close to a Boltzmann distribution of simple harmonic oscillators. This is the case in our experiment for which, typically, T_T is 2100 K and T_1^* rises from 300 K to 2100 K during the experiment.

(iv) If $T_1^* >> T_T$, as in the CO laser (section 3.6) such that the second exponential term dominates, a population inversion results, $n_v > n_0$. The ratios n_{v+1}/n_v grow as v rises i.e. there are more pronounced inversions for higher levels.

It is instructive to compare the form of (i) a Boltzmann distribution of simple harmonic oscillators (SHOs), (ii) a Boltzmann distribution of anharmonic oscillators (AHOs), and (iii) a Treanor

distribution, for a typical experimental situation of $T_1^* = 1500$ K, $T_T = 2100$ K, for CO:

n_{v-1}/n_v	v=1	v=2	v=3	v=4	v=5
Boltzmann (SHO)	7.81	7.81	7.81	7.81	7.81
Boltzmann (AHO)	7.81	7.61	7.41	7.22	7.04
Treanor	7.81	7.66	7.52	7.39	7.25

In a Treanor distribution, upper levels are populated less than for a Boltzmann distribution of anharmonic oscillators but more than for a Boltzmann distribution of simple harmonic oscillators, and are closer to the former, for a given n_1/n_0. The value of 7.25 for n_4/n_5 corresponds to an individual vibrational 'temperature', as defined by equation (5.62) for level v=5 of 1480 K, only 20 K less than for v=1. The vibrational 'temperature' of level v=5 according to equation (5.61) is 1490 K.

In fact, the difference between relaxation via a continuous series of Boltzmann distributions and relaxation via a continuous series of Treanor distributions for anharmonic oscillators is too small for us to observe experimentally. It was thus that Teitelbaum [123], in his recent extension of the Shuler-type analytical integration of the master equation, felt justified in making approximations that led to the result that relaxation proceeds via a continuous series of Boltzmann distributions for anharmonic oscillators as well as for simple harmonic oscillators.

5.16 Conclusions on Effects of Anharmonicity

In practice (VT) processes will play some role in determining the vibrational distribution at any time. Three orders of magnitude are not infinity, and dilution in an inert gas will decrease the relative importance of the (VV) processes. Treatments considering (VT) and (VV)

processes [114,123-125], by numerical or analytical integration of the master equation, nevertheless conclude that for low levels relaxing from an initial Boltzmann distribution, deviations from a continuous series of Boltzmann distributions are small. This is confirmed by the computer model of section 5.5, even with all (VV) rate constants set to zero.

The Bethe-Teller energy relaxation equation ((5.50) allowing for change in T_T) is not strictly applicable for anharmonic oscillators, as its derivation depends on the Landau-Teller transition probabilities. It is found to remain a good approximation [123,125].

It is likely that relaxation via a continuous series of Boltzmann distributions is kept to more closely than exponential relaxation of the vibrational energy. The fast (VV) processes ensure that the former is a good approximation, whatever the extent of the deviation of the (VT) rate constants from the Landau-Teller ratios. However the latter depends almost entirely on the (VT) processes.

5.17 Effects of large variations from Landau-Teller (VT) Rate Constants

Three possibilities will be considered here: firstly (VT) rate constants rising very steeply with v e.g. $k_{v+1,v} = (v+1)^2 k_{10}$, secondly multiquantum (VT) processes, e.g equation (5.3), with large rate constants, and thirdly all (VT) constants except k_{01} and k_{10} having a value of zero. Consideration of the first is necessary following the discovery of a $v^{2.7}$ dependence for rates of relaxation of vibrational levels of laser-excited HF at 300 K [126], and the second must be considered as a limiting case given that multiquantum processes have non-zero probabilities for real molecules. Borrell and Millward [47] considered both these cases and concluded that, given realistic values of the (VV) rate constants, they caused negligible deviation away from relaxation via a continuous series of Boltzmann distributions. The

overall process is made faster, however. Calculations using the program described in section 5.5 support these conclusions. With biquantum processes included, with $k_{20} = 5k_{10}$ and a translational temperature of 2100 K (then $k_{01} \sim k_{02}$) in pure CO, (VT) processes would have to have rate constants of the same order of magnitude as the (VV) processes to make a significant deviation away from a continuous series of Boltzmann distributions occur.

Since the estimate of the biquantum (VT) rate constants is ridiculously large, we conclude that multiquantum (VT) energy transfer will not cause observable deviations away from relaxation via a continuous series of Boltzmann distributions. A similar (VT)/(VV) ratio is required to make the (VT) rate constants varying as v^2 have an effect. Again, this is an unrealistic choice of (VT) rate constants. The $v^{2.7}$ dependence for HF was found at low temperatures, where energy transfer in HF is dominated by long-range forces and the probability falls as the temperature rises.

The third possibility is considered as a response to Glanzer's surprising conclusion (see section 5.22) that $k_{01} >>$ higher $k_{v,v+1}$ for NO. The computer model showed that relaxation via a continuous series of Boltzmann distributions is preserved but the whole process is slowed down.

The computer model also shows that the relaxation of the total vibrational energy remains exponential to a very close approximation, with biquantum processes included. With rate constants varying as v^2, there is some acceleration as the relaxation proceeds and higher levels come into play, but the effect does not seem large enough to be observable experimentally. With ~~all~~ (VT) rate constants set to zero there is a similar small retardation as relaxation proceeds, again unlikely to be large enough to be observed.

No realistic choice of (VT) rate constants will cause a significant deviation away from a continuous series of Boltzmann distributions. It is generally stated, for low levels in a shock tube experiment, that relaxation proceeds via a continuous series of Boltzmann distributions to a very good approximation. It is not necessary to be more precise and mention Treanor distributions. The continuous series of Boltzmann distributions model has the great advantage of the population of all levels being described analytically in terms of one parameter, the vibrational temperature.

In the next two sections we will briefly consider the cases of high levels relaxing from a Boltzmann distribution, and all levels from other initial distributions.

5.18 High Vibrational Levels

For very high vibrational levels, higher than those with which we are concerned experimentally, close to the dissociation limit, the above considerations break down. It is no longer true that (VV) processes are much faster than (VT) ones, since (i) the (VT) rate constants rise as v rises and ΔE decreases and (ii) the (VV) rate constants $k^{10}_{v,v+1}$ fall as their ΔE increases. The Treanor distribution is no longer appropriate, but is now more different from a Boltzmann distribution anyway. Also multiquantum (VT) processes will become more important as ΔE falls. The occurrence of dissociation causes further distortions, so large deviations away from a continuous series of Boltzmann distributions are likely in this region.

As relaxation proceeds, higher levels are populated and processes that are only highly probable for high v become more important. Thus some decrease in the apparent relaxation time as equilibrium is

approached is to be expected. An equivalent statement is that the instantaneous relaxation time will not depend only on the translational temperature, as in equation (5.50), but also on the vibrational temperature, getting shorter for large T_{vib}. The experimental evidence as to whether this is an observable effect is divided. No evidence has been found for it in this shock tube during careful studies on N_2 [94], CO_2 [40], or N_2O [19]. Kewley [114] numerically integrated the master equation for the specific case of relaxation behind a shock front and predicted the occurrence of 'hooks' i.e. the $\log(p\tau)$ v. $T^{-1/3}$ plot obtained from one shock using equation (5.50) - see section 5.13 - will have a 'hook' on the end instead of being part of one line from all the shocks. He included only single quantum transitions in his model, and concluded that the hooks are caused by the fact that for high levels (VV) processes have high enough energy defects to accelerate the relaxation towards vibration-translation equilibrium. Inclusion of multiquantum (VT) will presumably accentuate this effect, as these will become significant for high levels. Hooks will be more prominent at higher temperatures, when higher levels are more populated .

5.19 Initial non-Boltzmann Distributions

The case of relaxation of low vibrational levels from an initial Boltzmann distribution is the simplest to analyse, and fortunately the one we are concerned with experimentally. For other initial distributions there are no such simple results for the relaxation of the individual level populations or the total vibrational energy. For simple harmonic oscillators the relaxation of the total vibrational energy is independent of the initial distribution, but anharmonicity will cause much greater deviations for non-Boltzmann initial distributions. Teitelbaum [123,127] has considered the form of the relaxation of the total energy in different circumstances.

When the vibrational temperature is greater than the translational, as in laser fluorescence or nozzle expansion experiments or in the relaxation of molecules formed highly excited in a chemical reaction, a Treanor distribution is very different from a Boltzmann distribution, but is itself less likely to hold because of the occurrence of such effects as multiquantum (VT) energy transfer. These cases do not directly concern us in detail here, and have been dealt with elsewhere [3,4,114,123,127,128].

Generally, for an arbitrary initial distribution, there is an initial phase in which (VV) processes dominate, and bring the system into a Treanor-like distribution, followed by relaxation via a continuous series of Treanor distributions controlled by the slower (VT) processes.

5.20 Experimental Work on HI

It is clear from theory that within experimental error diatomic molecules are expected to vibrationally relax through a continuous series of Boltzmann distributions following shock-heating. The first experimental work on the relaxation of individual vibrational levels was carried out by Chow and Greene [5] and published in 1965. They followed the population of levels v=0,1,2 and 3 of HI, 10 % in Ar using an ultra-violet absorption technique (section 2.17).

All the light from a mercury-arc lamp was collimated and passed across the shock tube perpendicularly. After passage of the light beam through the shock tube, small frequency ranges, corresponding to excitation to an excited electronic state of molecules in the v=0, 1, 2 and 3 levels, were separated out using filters or a monochromator with multiple exit slits. In this way absorption signals due to all four levels were recorded for each shock. The time resolution of the

experiment was poor. The relaxation times measured were all less than 10 μs, but their schlieren signal was 1.4 μs wide, and the rise-time for their v=0 signal was 1.8 μs when it should have been instantaneous compared with the subsequent vibrational relaxation. Both the width of the schlieren signal and the v=0 rise-time were larger than expected and left unexplained.

The beginning of the absorption signal was hidden by the schlieren signal but Chow and Greene, allowing for the latter, felt able to state that v=1, v=2 and v=3 all reach equilibrium exponentially with the same time constant, and that it was unlikely that there was a delay as great as expected by the LBTMS model of relaxation via a continuous series of Boltzmann distributions.

The results thus directly contradict the theoretical expectations. The theory predicts relaxation via a continuous series of Boltzmann distributions with a common vibrational temperature, which describes the population of each level, rising during the relaxation from T_1 to T_f. Chow and Greene's result that all levels rise exponentially with the same rate implies level v=1 having a vibrational 'temperature' rising in that manner but all other levels having a vibrational 'temperature', as described by equation (5.62), which rises instantaneously to T_f and remains there.

The data were not of the highest quality, and if Chow and Greene had emphasised their utter disagreement with theory, might not have been given much weight. However Chow and Greene gave a false, but persuasive, explanation that appeared to show that their results were what was expected. They considered relaxation via:

$$HI(v=0) + M \rightleftharpoons HI(v=1) + M \qquad (5.63)$$

followed by:

$$HI(v=1) + HI(v=1) \rightleftharpoons HI(v=0) + HI(v=2) \qquad (5.64)$$

and subsequent (VV) processes to populate higher levels.

They believed (5.63) to be rate-limiting, and the (VV) processes to be much faster so that (v=2) and above are populated at the same rate as (v=1). This explanation neglects the quasi-equilibrium that process (5.64) inevitably produces - a Boltzmann distribution (or Treanor distribution, considering anharmonicity) as we have seen. Chow and Greene noted that the forward process in equation (5.64) is very fast but failed to realise that the reverse process is equally fast.

They did not comment on reasons for their disagreement with the LBTMS model. Montroll and Shuler's historic paper [3], published in 1957, did not consider (VT) and (VV) processes occurring together but the extension to their work by Herman and Rubin [121] considered this case in 1959, specifically for relaxation behind shock waves, and concluded relaxation via a continuous series of Boltzmann distributions was expected.

5.21 Impact of Results on HI

There appears to be no comment on the falsity of Chow and Greene's explanation of their results prior to the publication of reference [1]. Breshears [129] points out, correctly, that at times longer than two relaxation times, $t/\tau > 2$, all levels relax exponentially with the same time constant for relaxation via a continuous series of Boltzmann distributions, but neglects to say that, at earlier times, an increasingly long delay should be observed prior to the rise in population for v=2, and v=3. Breshears' own figure 2 shows that, at

$t = 2\tau$, the population of v=1, v=2, and v=3 have reached 91 %, 80 % and 71 % of their final equilibrium values. Chow and Greene ought to have seen non-exponential behaviour at earlier times. Thus Breshears' paper fails to reconcile Chow and Greene's results with the established theory.

Since Chow and Greene had been able to explain their results, it was not universally realised that their interpretation of the results and the conventional LBTMS theory were incompatible. Thus Lambert [105], in his standard text on energy transfer, published in 1977, outlines Chow and Greene's results and repeats their explanation, but two pages later states that an initial Boltzmann distribution relaxes via a continuous series of Boltzmann distributions. The natural conclusion from reading Lambert's book is that relaxation via a continuous series of Boltzmann distributions involves all levels relaxing exponentially at the same rate, and indeed this erroneous conclusion was initially made by us before consideration of the output of the computer program of section 5.5 revealed the truth. It is ironic that Herzfeld and Litovitz, in 1959, in their standard text on energy transfer [109], had written: 'It is often said that, for the simple harmonic oscillator, all transitions have the same relaxation time. This is quite wrong.'

5.22 Previous Work on NO

Glanzer and Troe [130] used ultra-violet absorption to study v=0, v=1 and v=2 of NO in Ar. They observed that v=2 rose more slowly than v=1, and, apparently unaware of the work of Montroll and Shuler (and Chow and Greene), expressed surprise at this result.

In a curious paper, Glanzer [131] extended the work to very dilute NO in Ar mixtures, and encompassed v=3. He found that $k_{12}, k_{23} \ll k_{01}$. He

reached this conclusion by fitting a theoretical model to his experimental rate constants. The experimental rate constants were calculated assuming single exponential growth for v=2 and v=3, which is not consistent with the LBTMS model. Glanzer's results are closer to the theoretical expectations than Chow and Greene's in that the populations of upper levels are seen to rise more slowly, but his failure to observe a zero initial slope remains a puzzle. Glanzer's results need reevaluation in the light of the LBTMS model, of which Glanzer apparently remained unaware.

5.23 Previous Work on CO

Windsor, Davidson and Taylor [132] observed the overtone ($\Delta v = 2$) emission from CO heated by the reflected shock. Hooker and Millikan [50] looked at overtone and fundamental emission behind the incident shock. Both sets of workers found that the overtone signal rose with initial slope of zero behind the shock-front. Only vibrational levels v=2 and higher contribute to the overtone emission, so this shows that (v=2) is not populated directly but via a two-step process, where the second step is not very much faster than the first. The results of Hooker and Millikan clearly show the difference between the fundamental emission (which rises exponentially) and the overtone emission. The results are as expected from LBTMS theory.

Chackerian and Weisbach [59] studied shock-heated CO by infrared absorption using a continuous wave CO laser. Since they used undiluted CO they were unable to observe levels below v=4 as the populations in lower levels are large enough to absorb the laser beam almost totally. They compared their experimental profiles to theoretical ones calculated assuming relaxation via a continuous series of Boltzmann distributions and obtained good agreement. They did not comment on the different

behaviour observed by Chow and Greene. Their time resolution was superior to Chow and Greene's but inferior to ours.

The experimental evidence so far on CO is thus at variance with the results of Chow and Greene. The results of the conclusive investigation of the mechanism of the vibrational relaxation of CO following shock-heating are presented in the next chapter.

CHAPTER 6 - EXPERIMENTAL WORK ON CARBON MONOXIDE

6.1 Introduction

In order to interpret the results of any experiment in which individual vibrational levels of CO are monitored, it is essential to understand the vibrational relaxation of those levels. Therefore the first experiments to be undertaken during this work were investigations of the evolution of the population of those levels following shock-heating, in the absence of chemical reaction.

The comprehension of vibrational energy transfer is essential for kinetic studies generally, regardless of whether vibrational levels are being directly monitored in an experiment. Vibrational relaxation of both reactants and products may be important.

Many reactions are necessarily preceded by the acquisition of vibrational energy by the reactants, an obvious case being the dissociation of diatomic molecules. The 'ladder-climbing' models discussed in chapter 5 may be extended to include dissociation from high levels and thus calculate dissociation rate constants from theory [114,133]. The vibrational energy transfer behaviour must be understood in order that the such rate constants might match those obtained from experiment e.g. [134] for N_2.

The distribution of a product amongst its vibrational energy levels can be a useful guide to its reaction dynamics, as will be shown in part three of this thesis. Rapid vibrational energy transfer will prevent the determination of the initial distribution. Thus energy transfer rates must be known in order that suitable experimental conditions might be chosen for this measurement.

The mechanism of vibrational relaxation following shock-heating is of theoretical interest in itself, of course. The discussions of chapter 5 have shown that the theoretical predictions are clear, but the contrary results of Chow and Greene show that the matter had not been entirely resolved, and the results of our experiments were not a foregone conclusion.

6.2 Choice of Experimental Conditions

Conditions were sought under which relaxation via a continuous series of Boltzmann distributions could be clearly verified or negated. It is desirable to observe several vibrational levels. It is particularly useful for one of those levels to be v=1, as its population should rise approximately exponentially, in clear contrast to the populations of higher levels which should evolve with zero initial slope (recall figure 5.1).

The higher the value of post-shock temperature T_2, the more vibrational levels have populations large enough to be monitored. However this also means stimulated emission from the upper level becomes more important relative to absorption by the lower level. While this creates no great mathematical problem in the data analysis, it makes the physical understanding of the data analysis less clear-cut. A temperature in the region of 2000 K was selected, where $n_v/n_{v+1} \sim 5$.

Use of undiluted CO renders the observation of the relaxation of levels v=1 and v=2 impossible as 100 % absorption of the laser beam occurs before relaxation is complete. The pressure cannot be lowered indefinitely as the relaxation is not then complete before the arrival of the contact surface; the limit is about $p_1 = 5$ torr for undiluted CO. Therefore a mixture of CO and inert gas was employed. A CO/He/Ar mixture was used, as varying the He/Ar ratio allowed the vibrational

relaxation time to be varied independently of pressure and dilution. The vibrational relaxation times of CO in one atmosphere of Ar, CO and He respectively are given by Millikan [135] as $\ln(p\tau) = 182T^{-1/3}-22.4$, $160T^{-1/3}-22.2$ and $87T^{-1/3}-19.1$ respectively. Here τ is in seconds. At 2100 K this corresponds to 278 μs, 60.9 μs and 4.52 μs respectively for $(p\tau)$. The relaxation of the CO is therefore dominated by helium in most mixtures.

The ideal mixture composition may be chosen as follows:

i) A partial pressure of CO sufficient to give the desired absorption signal (i.e. ~50 % for a 2->1 laser line) is selected. The signal depends only slightly on pressure-broadening at our pressures.

ii) The partial pressure of He sufficient to make the relaxation occur in the desired timescale - < 100 μs lab. time - is calculated.

iii) A partial pressure of Ar is chosen so that the mixture requires readily-obtainable driver conditions. The size of the schlieren spike depends on the total pressure. To make the schlieren spike small compared to the absorption signal, the minimum possible argon pressure should be used, but an increase in the concentration of CO makes the process less isothermal so a compromise is necessary.

In this way optimum signal-height and optimum time resolution are achievable.

In practice, the first mixture to be selected was one containing 1.99 % CO, 5.71 % He and 92.3 % Ar, using p_1 ~ 10 torr. This was superseded by a mixture containing 10.04 % CO, 35.45 % He and 45.51 % Ar using p_1 ~ 2 torr. With the latter mixture the same absorption signal but 1/5 the schlieren signal were obtained. This made the trace easier to analyse, at the crucial early times.

It should be noted that the radiative decay time of CO is 33 ms [136] (at room temperature for the 1->0 transition), and so radiative decay is insignificant on our timescale. If this were not so, it would result in an irreversible loss of energy from the test gas and a rapid decrease in temperature.

The gases used were as follows: B.O.C. c.p. grade CO with 99.9 % purity, B.O.C. A grade He with 99.995 % purity, and B.O.C. zero grade Ar with 99.998 % purity. The stated CH_4 and H_2 impurities in the CO are sufficient to decrease the apparent CO-CO relaxation time by 3 %, using the data of references [97,135].

6.3 Results - Qualitative

The traces obtained for the 10 % CO mixture are shown in figure 6.1 (a)-(d). 6->5 and higher laser lines were insufficiently absorbed. As expected from theory, the 2->1 trace rises immediately behind the shock front (the trace does not return to the baseline immediately after the schlieren spike) and traces for higher lines exhibit increasingly large delays before the rise in absorption. The horizontal scale is 10 μs/div in each case; the vertical scale becomes less coarse as the signal goes down in line with the population of higher levels. Details of the experiments carried out on the two CO/He/Ar mixtures are given below:

10 % mixture. In each case 10/5.5 diaphragms (section 3.2) and He driver gas were used. All traces 10μs/div lab. time.

FIGURE 6.1 - 106 -

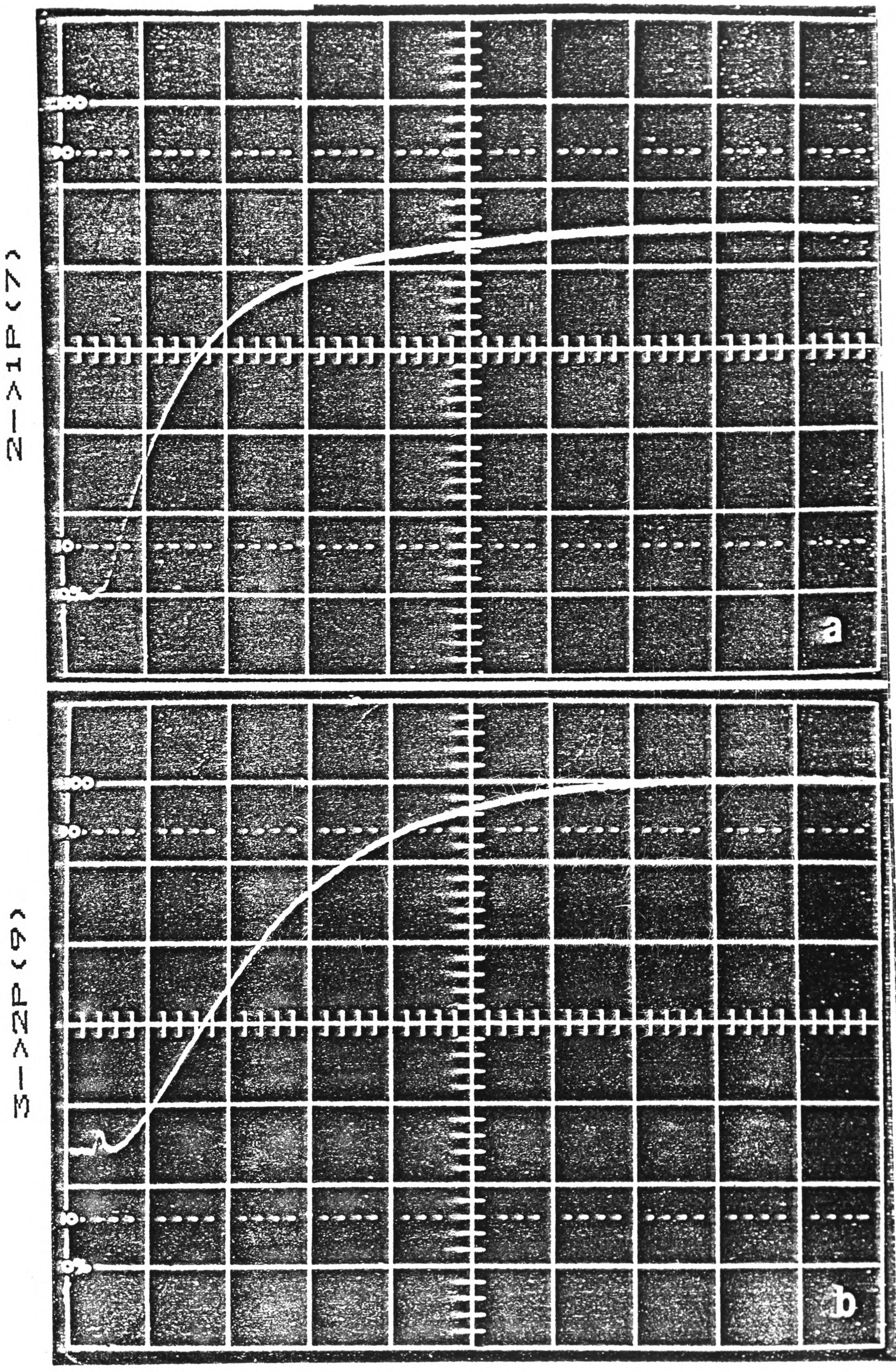
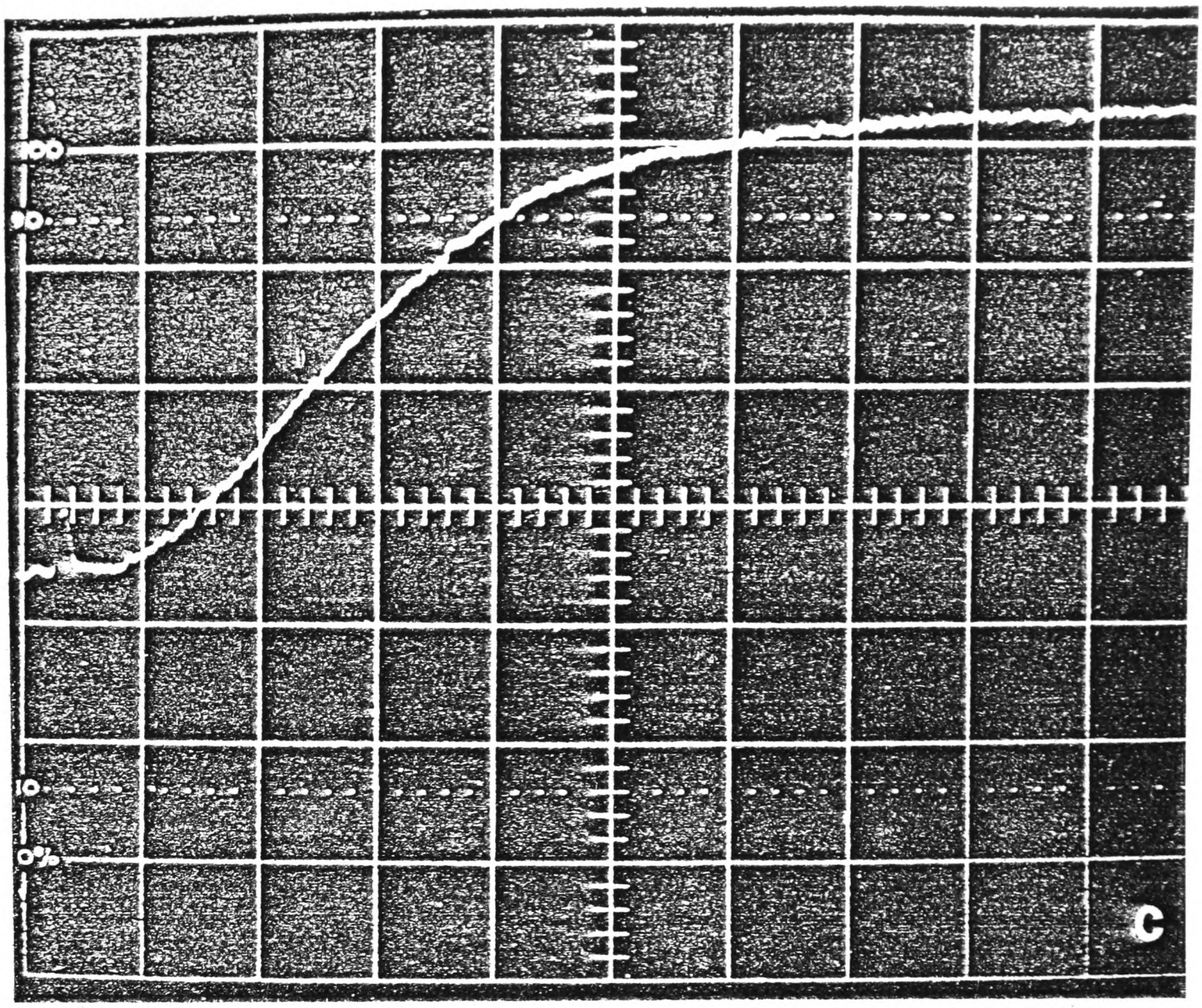


FIGURE 6-1



laser line	p_1/torr	T_1/^oC	u_1/mm.μs^{-1}	mv.div^{-1}	I_o/V
2->1P(7)	2.07	17.2	1.82	100	1.49
3->2P(9)	2.06	18.7	1.83	50	1.75
4->3P(8)	2.06	18.9	1.84	20	1.85
5->4P(8)	2.08	18.0	1.81	5	1.86

The resultant post-shock conditions were:

laser line	T_a/K	T_f/K	p_a/torr	p_f/torr	ρ_{21a}	ρ_{21f}
2->1P(7)	2136	2105	55.8	56.3	3.67	3.75
3->2P(9)	2151	2119	55.6	56.1	3.67	3.75
4->3P(8)	2142	2111	55.2	55.7	3.66	3.75
5->4P(8)	2123	2092	55.5	56.0	3.66	3.75

2 % mixture. 18/6.5 diaphragms and He driver were used.

laser line	p_1/torr	T_1/^oC	u_1/mm.μs^{-1}
2->1P(7)	11.27	19.3	1.49
3->2P(8)	11.23	18.9	1.50
4->3P(9)	11.25	17.3	1.50

The resultant post-shock conditions were:

laser line	T_a/K	T_f/K	p_a/torr	p_f/torr	ρ_{21a}	ρ_{21f}
2->1P(7)	2138	2131	290	291	3.53	3.54
3->2P(8)	2148	2142	291	292	3.53	3.55
4->3P(9)	2159	2152	295	296	3.53	3.55

Subscripts a and f refer to post-shock conditions before and after vibrational relaxation respectively.

From a comparison of figures 6.1(a) and 6.1(d) with figure 5.1, it is clear that the results are close to what is expected according to the LBTMS model. The 2 % mixture gave similar results. Therefore the development of a data analysis technique to test this more closely was necessary. This is described in the next section.

6.4 Data Analysis

The experiments described in this, and the next, chapter were carried out before the installation of the transient recorder and North Star Advantage computer. Analysis therefore proceeded via photography of the oscilloscope trace, expansion onto graph paper using an epidiascope, and reading off values of the absorption ΔI at equal time intervals. Noise was smoothed out by eye. These values were converted into gain values, $G_v = \log[(I_o-\Delta I)/I_o]$.

The post-shock conditions before (subscript a) and after (subscript f) relaxation were calculated as described in section 4.2. Laboratory time must be converted into real time, as discussed in section 2.4. This is achieved by multiplying by $u_1/u_2 = \rho_2/\rho_1 = \rho_{21}$, but ρ_{21} rises as the relaxation proceeds. This is a very small effect (2 % for the 10 % mixture) but was fully taken account of as follows: ρ_t, the density at time t, is assumed to be given by:

$$\rho_t = \rho_f[1-(1-\rho_a/\rho_f)e^{-t/\tau}] \qquad (6.1)$$

using a value of τ calculated from the results of Millikan (see section 6.2). Different time intervals Δt_{lab} are multiplied by the appropriate ρ_t to give Δt_{real}. An iterative procedure is necessary. Since ρ_a/ρ_f is

very close to unity, the exact value of τ chosen has very little effect. The gain values are also corrected for changing density by multiplying by ρ_a/ρ_t to refer them to the initial density.

For both the 10 % and 2 % mixture result sets, a gain versus real time plot was obtained for each laser line. Within each set, post-shock conditions were assumed to be identical and equal to the average values. The procedure carried out to test for a continuous series of Boltzmann distributions was as follows:

Pairs of traces were taken for adjacent vibrational transitions (i.e. 2->1 and 3->2, 3->2 and 4->3, 4->3 and 5->4). By carrying out a point-to-point comparison of the absorption for a given pair, a vibrational temperature was deduced at each time.

The details are now set out. At any given time, for a v+1->vP(J) laser line, the gain G_v depends on the populations and degeneracies of the upper and lower levels of the test gas:

$$G_v \alpha n_1/g_1 - n_u/g_u \tag{6.2}$$

Rearranging,

$$G_v \alpha \frac{n_1}{g_1}\left[1 - \frac{n_u}{n_1} \cdot \frac{g_1}{g_u}\right] \tag{6.3}$$

Assuming the rotational partition function is independent of v,

$$\frac{n_u}{n_1} = \frac{n_{v+1}}{n_v} \cdot \frac{n_{J-1}}{n_J} \tag{6.4}$$

Now,

$$n_{v+1}/n_v = e^{-\Delta E_{v+1->v}/kT_{vib}} \qquad (6.5)$$

and

$$n_{J-1}/n_J = (g_u/g_1)e^{-\Delta E_{J-1->J}/kT_{rot}} \qquad (6.6)$$

(All vibrational levels have degeneracies of unity and rotational degeneracies are given by $g_u = 2J+1$, $g_1 = 2J-1$.)

From equations (6.3)-(6.6),

$$G_v \propto (n_1/g_1)(1-e^{-\Delta E_{v+1->v}/kT_{vib}} \cdot e^{-\Delta E_{J-1->J}/kT_{rot}}) \qquad (6.7)$$

Note that the degeneracies have cancelled out. There is a similar expression for G_{v+1}, the gain of the other trace in the pair, $v+2->v+1P(J^{\#})$. Dividing G_{v+1} by G_v, at any time:

$$\frac{G_{v+1}}{G_v} \propto \frac{g_J}{g_{J^{\#}}} \cdot AB\left[\frac{1-CD}{1-AE}\right] \qquad (6.8)$$

where: $A = e^{-\Delta E_{v+1->v}/kT_{vib}}$,

$B = e^{-\Delta E_{J^{\#}->J}/kT_{rot}}$,

$C = e^{-\Delta E_{v+2->v+1}/kT_{vib}}$,

$D = e^{-\Delta E_{J^{\#}-1->J^{\#}}/kT_{rot}}$,

and $E = e^{-\Delta E_{J-1->J}/kT_{rot}}$.

T_{rot} is assumed to be equal to $(T_a+T_f)/2$ throughout. The vibrational and rotational energy differences may be calculated either from the Dunham coefficient formula for levels' energies (equation 4.22) or from the constants ω_e, $x_e\omega_e$, B and D given by Huber and Herzberg [137]. The

former procedure is more exact but the difference is negligible for our purposes. T_{vib} rises from T_1 to T_f during the relaxation. The value of the right hand side of equation (6.8) is calculated as a function of T_{vib} between T_1 and T_f. The proportionality constant is calculated from the experimental final equilibrium gain when $T_{vib} = T_f$, and hence the vibrational 'temperature' T_{vib} corresponding to each individual gain ratio is determined. T_{vib} is thus strictly a function of the population of 3 levels, n_v, n_{v+1} and n_{v+2} although under our conditions it is dominated by n_v and n_{v+1}. So strictly we are deriving vibrational 'temperatures' for trios of levels, not pairs. Nevertheless if we find that the vibrational temperatures are the same for two or more trios, we are still proving relaxation via a continuous series of Boltzmann distributions. Thus an experimental vibrational 'temperature' versus time plot is obtained.

If the vibrational 'temperature' is common to each pair at any one time, there is a Boltzmann distribution at that time, characterised by a true vibrational temperature. If this is the case at all times, relaxation proceeds via a continuous series of Boltzmann distributions. This does not necessarily imply that the common vibrational temperature evolves in the manner of section 5.8; this will only be the case if the relaxation of the total vibrational energy is exponential. In order to investigate this point, we firstly rearrange equation (5.46) to give:

$$F(T_{vib}) = -\ln\left[\frac{e^{\theta-\theta_1}-e^{\theta_f-\theta_1}+e^{\theta_f-\theta}}{1-e^{\theta_f-\theta_1}+e^{\theta_f+\theta-\theta_1}-e^{\theta}}\right] = \frac{t}{\tau} \qquad (6.9)$$

It can be seen that at t=0, $\theta = \theta_1$, so the numerator and denominator are equal, and at $t=\infty$, $\theta = \theta_f$, so the numerator equals zero. Equation (6.9) is no more than the exponential relaxation of total vibrational energy expressed for harmonic oscillators, relaxing through a continuous series

of Boltzmann distributions. If the relaxation of the vibrational energy is exponential, a graph of $F(T_{vib})$ against time will be a straight line passing through the origin and the slope will be equal to the reciprocal of the relaxation time τ. τ is multiplied by the pressure p_2 in atmospheres to give $(p\tau)$. For a mixture, $(p\tau)$ is broken down into its components using the linear mixture rule, e.g. for CO/He/Ar:

$$\frac{1}{(p\tau)_{mix}} = \frac{x_{CO}}{(p\tau)_{CO-CO}} + \frac{x_{Ar}}{(p\tau)_{CO-Ar}} + \frac{x_{He}}{(p\tau)_{CO-He}} \qquad (6.10)$$

where x_i is the mole-fraction of species i in the mixture. Our value for the relaxation time can thus be compared with the previous experimental data of Millikan [135]. Carruthers and Teitelbaum [138] have shown that the linear mixture rule, though generally not strictly true, is perfectly valid for diatomic molecules following shock-heating.

Our measurement of $(p\tau)$ from two laser absorption traces is in principle similar to the method suggested by Shuler [139] of monitoring two vibrational levels. The difference is that we have had to allow for the fact that each trace measures the difference in population of two levels. Moreover these are not entire vibrational levels but just the fraction in a particular rotational level, and the rotational level is different for the upper and lower vibrational levels. This too is allowed for as described above.

6.5 Detailed Results and Discussion

The analysis above was carried out for both 10 % and 2 % mixtures. The plots of T_{vib} against time and $F(T_{vib})$ against time that resulted are shown in figures 6.2 to 6.5. Details are tabulated below (T_{vib} is abbreviated to T_v in the figures):

FIGURE 6.2 Time variation of vibrational temperature T_v as defined by the ratio of populations in adjacent levels during relaxation for the 10 % CO mixture. The results are obtained from the oscilloscope traces of figure 6.1.

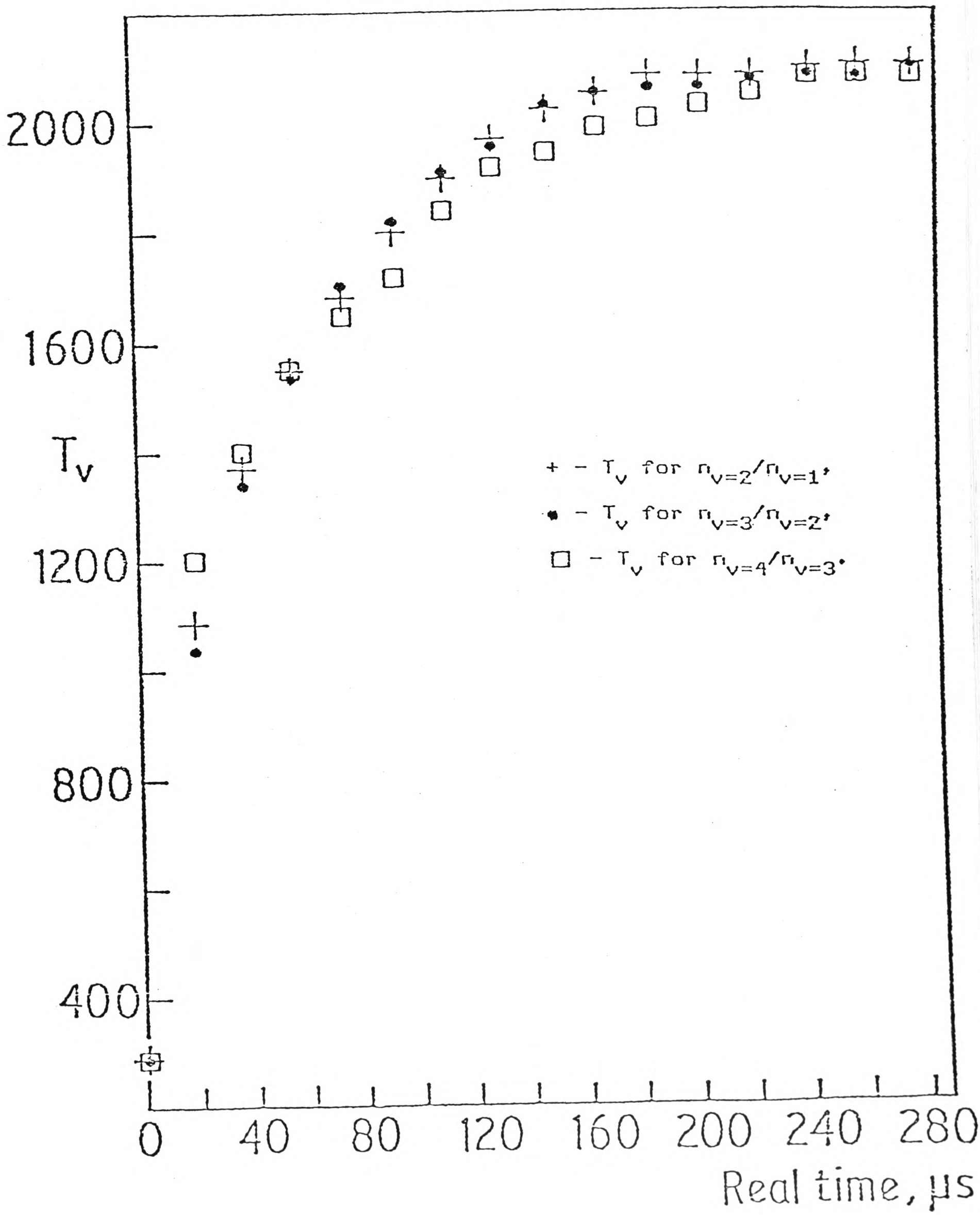
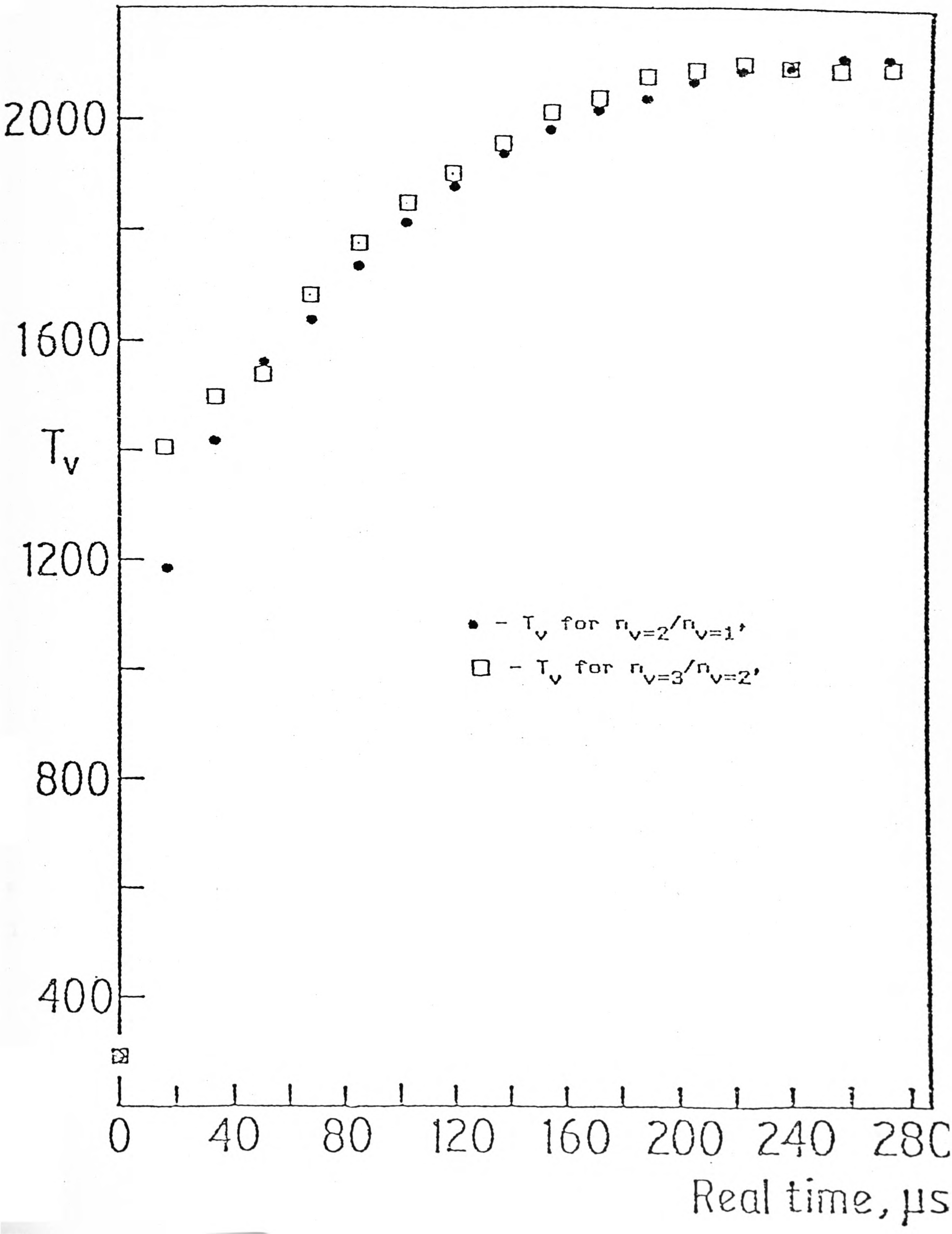


FIGURE 6-3 Time variation of vibrational temperature T_v as defined by the ratio of populations in adjacent levels during relaxation for the 2 % CO mixture.



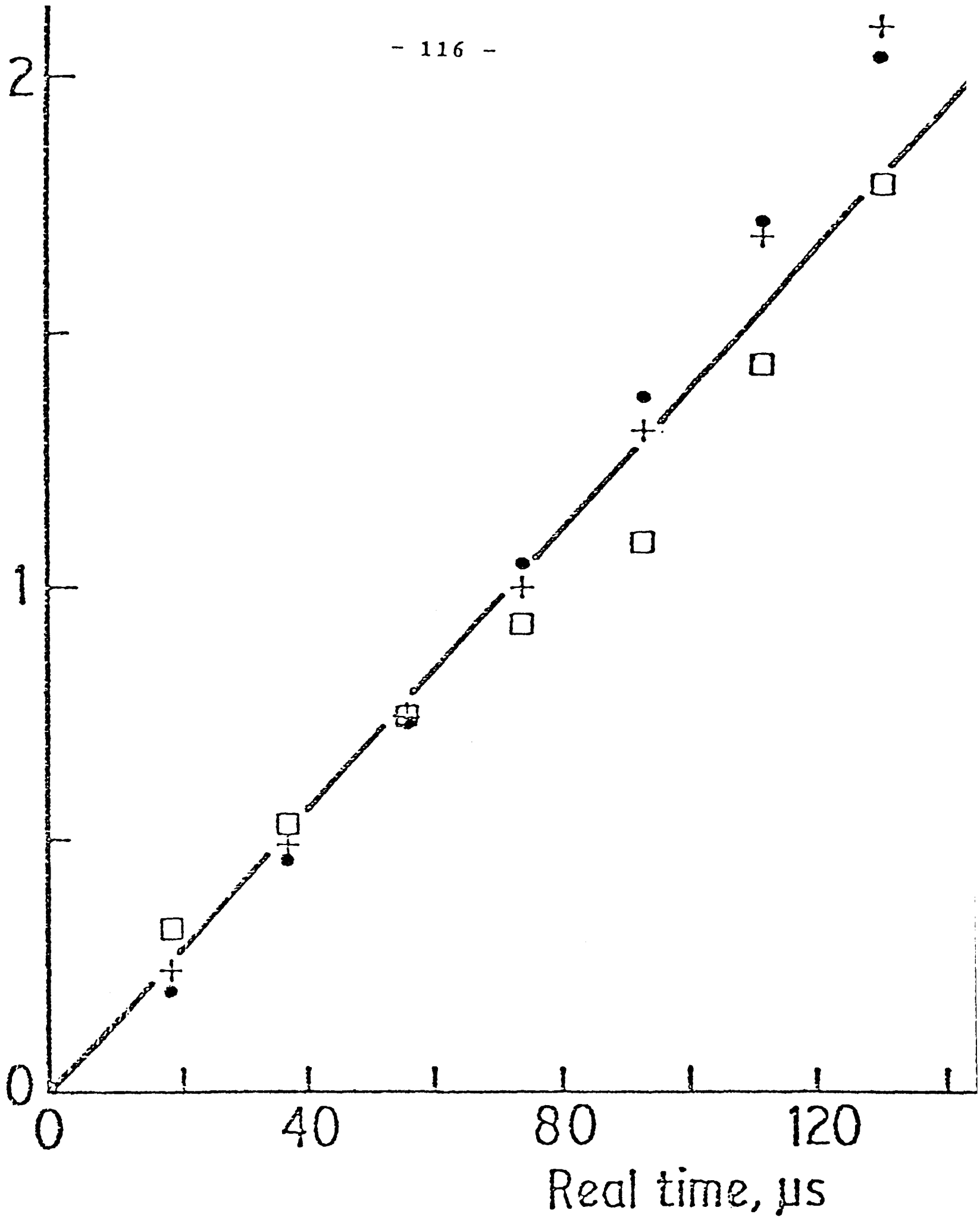


FIGURE 6-4 Time variation of $F(T_v)$ for the 10 % CO mixture using the T_v points of figure 6.2.

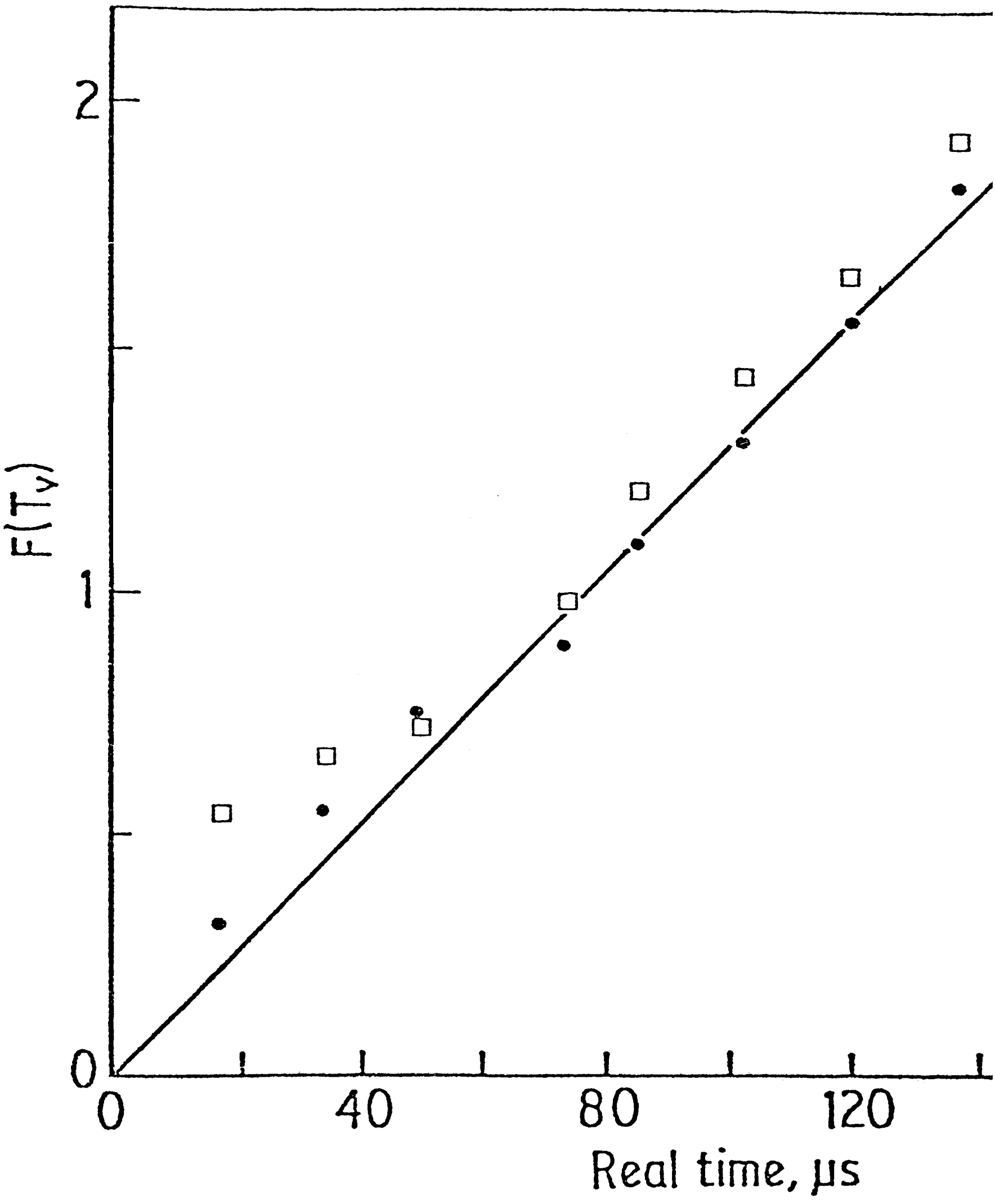


FIGURE 6.5 Time variation of $F(T_v)$ for the 2 % CO mixture using the T_v points of figure 6.3.

Mixture	T_f	T_{rot}	$(p\tau)_{mix}$
10 % CO	2107	2123	5.2
2 % CO	2142	2146	29

T_f is the average of T_f for each shock in the set and T_{rot} the average of $(T_f+T_a)/2$. T_{rot}, as well as being the assumed rotational temperature throughout the relaxation, is also the temperature to which the calculated relaxation time is assumed to apply.

We conclude that, within experimental error, (i) relaxation does proceed through a continuous series of Boltzmann distributions, and (ii) the vibrational energy does relax exponentially. The scatter in the graph of $F(T_{vib})$ against time is inevitable for a technique which obtains vibrational temperatures by dividing one noisy signal by another. The scatter is greater at early times, when, with the exception of the 2->1 trace, the signal is comparable to the noise.

$F(T_{vib})$ becomes more sensitive to T_{vib} as time proceeds. For this reason, only points at times less than $t=2\tau$ were used in calculating the relaxation times. The straight-line was fitted by eye. Since the absolute values of the relaxation times does not concern us greatly in this experiment, a more elaborate procedure was deemed unnecessary.

The calculation of vibrational temperature is made using precise values for the energies of different levels, taking account of anharmonicity. The calculation of $F(T_{vib})$ and hence τ by equation (6.9) assumes CO is a harmonic oscillator with $\nu = 2143\ cm^{-1}$. This is not inconsistent - as we saw in chapter 5, strictly speaking for anharmonic oscillators the Bethe-Teller vibrational energy equation does not apply, and there is no such thing as a vibrational relaxation time. Thus the simple harmonic oscillators approximation is absolutely necessary to

calculate a value for τ.

The major source of scatter is in the inherent signal-to-noise. Other errors lie in assuming all shocks in a set had exactly the same conditions, and that T_2 and p_2 are constant throughout the relaxation (and hence the proportionality constant in equation (6.8) is constant). The change in T_2 from T_a to T_f leads to a change in τ of only about 3 % for the 10 % mixture. Strictly, θ_f in equation (6.9) should be replaced by θ_T as described in section 5.13 but θ_T is itself dependent on τ and the resultant complications in the data analysis are not justified by the smallness of the effect.

The values for $(p\tau)_{mix}$ calculated from equation (6.10) using the data of Millikan are more than double the experimental values obtained by us. In order to investigate the reasons for this discrepancy, experiments were carried out on undiluted CO and on a CO/Ar mixture to measure values of $(p\tau)_{CO-CO}$ and $(p\tau)_{CO-Ar}$. The details of the experiments are set out below:

Undiluted CO. 18/10 diaphragm and H_2 driver

laser line	p_1/torr	$T_1/^oC$	u_1/mm.μs^{-1}
4->3P(8)	11.26	19.6	2.04
5->4P(8)	11.25	17.3	2.01
6->5P(9)	11.26	17.6	2.02

which give rise to post-shock conditions:

laser line	T_a/K	T_f/K	p_a/torr	p_f/torr	ρ_{21a}	ρ_{21f}
4->3P(8)	2214	1985	445.4	458.6	5.23	6.01
5->4P(8)	2170	1950	439.0	451.8	5.22	5.98
6->5P(9)	2186	1963	442.4	455.4	5.23	5.99

CO/Ar 30/12 diaphragm and H_2 driver

laser line	p_1/torr	T_1/^oC	u_1/mm.μs^{-1}
3->2P(7)	42.21	17.9	1.53
4->3P(8)	42.06	16.9	1.52

which give rise to post-shock conditions:

laser line	T_a/K	T_f/K	p_a/torr	p_f/torr	ρ_{21a}	ρ_{21f}
3->2P(7)	2108	2050	1172	1188	3.83	4.00
4->3P(8)	2100	2042	1167	1183	3.83	4.00

For undiluted CO, a relaxation time of 61±6 μs.atm was obtained c.f. Millikan's 64±6 μs at 2078 K. For CO/Ar, a relaxation time of 250±70 μs.atm was obtained c.f. Millikan's 290±30 μs.atm at 2075 K.

For the CO shocks, two sets of vibrational temperatures were obtained. The variation of $F(T_{vib})$ is shown in figure 6.6 There is more scatter because the laser lines monitored were 4->3, 5->4 and 6->5 (lower lines being absorbed 100 %). Since, as the vibrational quantum number v increases, the curves for n_v and n_{v+1} become less dissimilar this is an inevitable result of using higher laser lines. For the CO/Ar mixture, the data were inferior. Only 3->2 and 4->3 lines were monitored. A 20.19 % CO 79.81 % Ar mixture was used. A large pressure

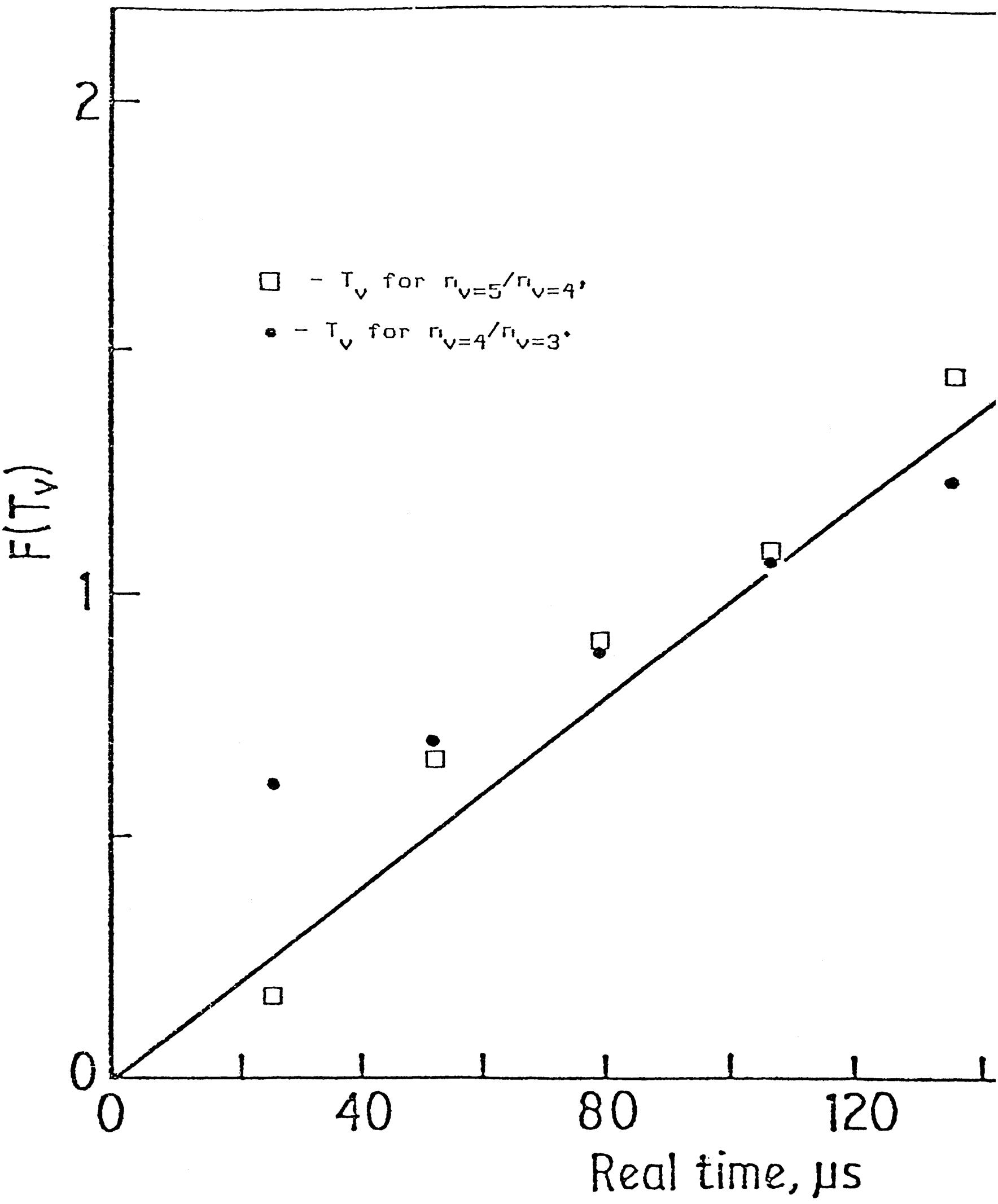


FIGURE 6.6 Time variation of F(T_v) for pure CO.

was necessary to ensure the relaxation was complete on our timescale and this caused a noisier trace. Nevertheless, the relaxation times obtained for CO–CO and CO–Ar are in agreement with Millikan within experimental error, so the discrepancy in our CO/He/Ar relaxation times can be put down to a lower result being obtained by us for $(p\tau)_{CO-He}$. In assuming that τ is constant throughout the relaxation and applicable to $(T_a+T_f)/2$ we follow Millikan.

We carried out further experiments on CO/He/Ar at about 1500 K and obtained data of similar quality to that for the mixture at 2100 K. Assuming the CO–CO and CO–Ar relaxation times are as given by Millikan, our result for $(p\tau)_{CO-He}$ (5.0 ± 0.5 μs.atm) is 1.9 times as fast as Millikan (9.5 ± 1) at 1540 K, and 2.3 times as fast at 2123 and 2145 K (4.4 ± 0.4 c.f. 1.9 ± 0.2. This rules out impurities in the helium as a cause, as the relaxation times due to different species diverge as the temperature is lowered. Repeating the experiments with research-grade He produced results which agreed within 10 %.

The cause of the disagreement between Millikan and this work over the CO–He relaxation time is unknown. Measurements of CO–He rate constants over a wider temperature range are described in chapter 8.

The important conclusions of this chapter are that CO does relax via a continuous series of Boltzmann distributions and that the relaxation of the total vibrational energy is exponential, within experimental error. This is as predicted by theory. It is not possible to make precise estimates of specific vibrational energy transfer rate constants in a shock tube experiment as it would require rate constants drastically different from those expected for the conclusions not to be the case. We can say that it cannot be true both that (VV) rate constants are orders of magnitude lower than expected, and that ratios

of (VT) rate constants differ greatly from the Landau-Teller values.

Chackerian and Weisbach [59] also concluded that the results for v=4-7 of CO implied that relaxation proceeds via a continuous series of Boltzmann distributions. Their approach was to calculate theoretical gain curves assuming the exponential relaxation of vibrational energy, relaxation via a continuous series of Boltzmann distributions, and relaxation times as given by Millikan, and compare them to experimental curves. They found the theoretical and experimental curves to be the same shape. Our work improved on theirs by monitoring levels v=1->3, the differences between which are greater. (Chackerian and Weisbach could not even monitor the v=3 level as they used a shock tube 12" in diameter, wide enough to completely absorb 4->3 lines.) Our method is more direct, by comparing curves for different levels and plotting $F(T_{vib})$ in order to calculate values for relaxation times.

CHAPTER SEVEN - EXPERIMENTAL WORK ON DEUTERIUM CHLORIDE

7.1 Introduction

The experimental results obtained in the previous chapter for CO are completely different to those of Chow and Greene [5] on HI. In some respects CO and HI are very different molecules. HI is much more polar, and it has a hydrogen atom which may have special effects on energy transfer rates. Certainly (VR) processes are a lot more important than for CO but this does not account for deviations away from the LBTMS model (see section 5.11). Also HI is approximately three times as anharmonic as CO ($x_e\omega_e/\omega_e$ = 0.172 and 0.061 respectively [137]). There seems to be no reason why these differences should result in relaxation not in accordance with the LBTMS model , but clearly an investigation of a molecule more similar to HI is desirable.

DCl has its fundamental vibrational frequency similar to that of CO (2145 cm^{-1} as opposed to 2170 cm^{-1}) and so there is a chance of frequency coincidences between CO laser lines and DCl absorption lines (c.f. section 4.7). DCl is a hydrogen halide, and has $x_e\omega_e/x_e$ = 0.127 [137]. Thus an experimental investigation on DCl was begun.

7.2 Experimental Conditions

The self-relaxation of DCl is much faster than that of CO (as explained in section 5.11) and so we were unable to perform experiments with as good a time resolution. The relaxation could have been made to occur on a longer timescale by reducing the partial pressure of DCl, but this would have reduced the signal-to-noise too much. A 10 % DCl in Ar mixture was used. This matched the mixture for which Seery [48] had obtained relaxation times with a shock-tube / infrared-emission technique. The DCl used was obtained from Merck, Sharp and Dohme (99

atom %) and the Ar from B.O.C. (99.995 % pure).

Since chlorine has two isotopes occurring in significant abundances, ^{35}Cl and ^{37}Cl, the chance of finding a close CO/DCl coincidence is doubled. DCl frequencies were obtained from the Dunham coefficients given by Coxon and Ogilvie [140] and CO frequencies from those given by Todd et al [104]. A computer search was carried out, but experiments showed that the closest coincidences between $^{12}C^{16}O$ laser lines and either isotope of DCl were not close enough to give satisfactory absorption by 2->1 or 3->2 lines of DCl. The computer search was repeated for laser lines of $^{13}C^{16}O$, again with frequencies from the Dunham coefficients of Todd et al. Closer coincidences did exist, and experiments were undertaken using the 9->8P(7) line of $^{13}C^{16}O$ to monitor 2->1P(14) of $D^{35}Cl$ (coincidence to within 0.021 cm^{-1}) and the 8->7P(7) line of $^{13}C^{16}O$ to monitor 3->2P(8) of $D^{35}Cl$ (coincidence to within 0.010 cm^{-1}). 90 atom % $^{13}C^{16}O$ from Prochem was used in the laser.

7.3 Results and Discussion

Details of the experiments are shown below:

10/7 diaphragm, He driver, 5 mV/div, 2 $\mu s.div^{-1}$

CO line	DCl line	p_1/Torr	T_1/°C	u_1/mm.μs^{-1}	I_o/V
9->8P(7)	2->1P(14)	5.11	16.4	1.51	0.9
8->7P(7)	3->2P(8)	5.17	16.3	1.53	0.9

giving rise to post-shock conditions:

Line	T_a	T_f	P_a	p_f	ρ_{21a}	ρ_{21f}
2->1P(14)	2223	2190	144.7	145.9	3.69	3.78
3->2P(8)	2243	2210	146.6	147.9	3.69	3.78

The results obtained are shown on figure 7.1. It is clear that the 3->2 trace shows a slower rise to equilibrium than the 2->1 trace, in accordance with the CO results. The 3->2 trace shows a larger absorption because the coincidence is closer. The schlieren spike is much larger with respect to the signal than on the CO work, both vertically and horizontally, because signal-to-noise was low (absorption away from line centre) and we were forced to work on $2\mu s.div^{-1}$ instead of $10\mu s.div^{-1}$.

An analysis was made in the same manner as for CO in chapter 6. The plot of $F(T_{vib})$, as defined in equation (6.9), against time is shown in figure 7.2. From such apparently poor experimental data, a remarkably good straight line is produced. Since the derivation of equation (6.9) depends on (i) relaxation via a continuous series of Boltzmann distributions and (ii) exponential relaxation of total vibrational energy, this gives strong support for these two assumptions. It is better to examine more than one pair of traces, but that was not possible here.

The behaviour is quite different to that seen by Chow and Greene for HI. They saw the levels (v=1) and (v=2) rising exponentially at the same rate. In our data analysis this would give $F(T_{vib})$ equal to infinity at all times.

The relaxation time obtained from figure 7.2 is $3.1\pm0.8\mu s.atm.$ for 10 % DCl in Ar at 2230 K. Seery's data gives $2.6\pm0.7\ \mu s.atm.$ at this

FIGURE 7.1

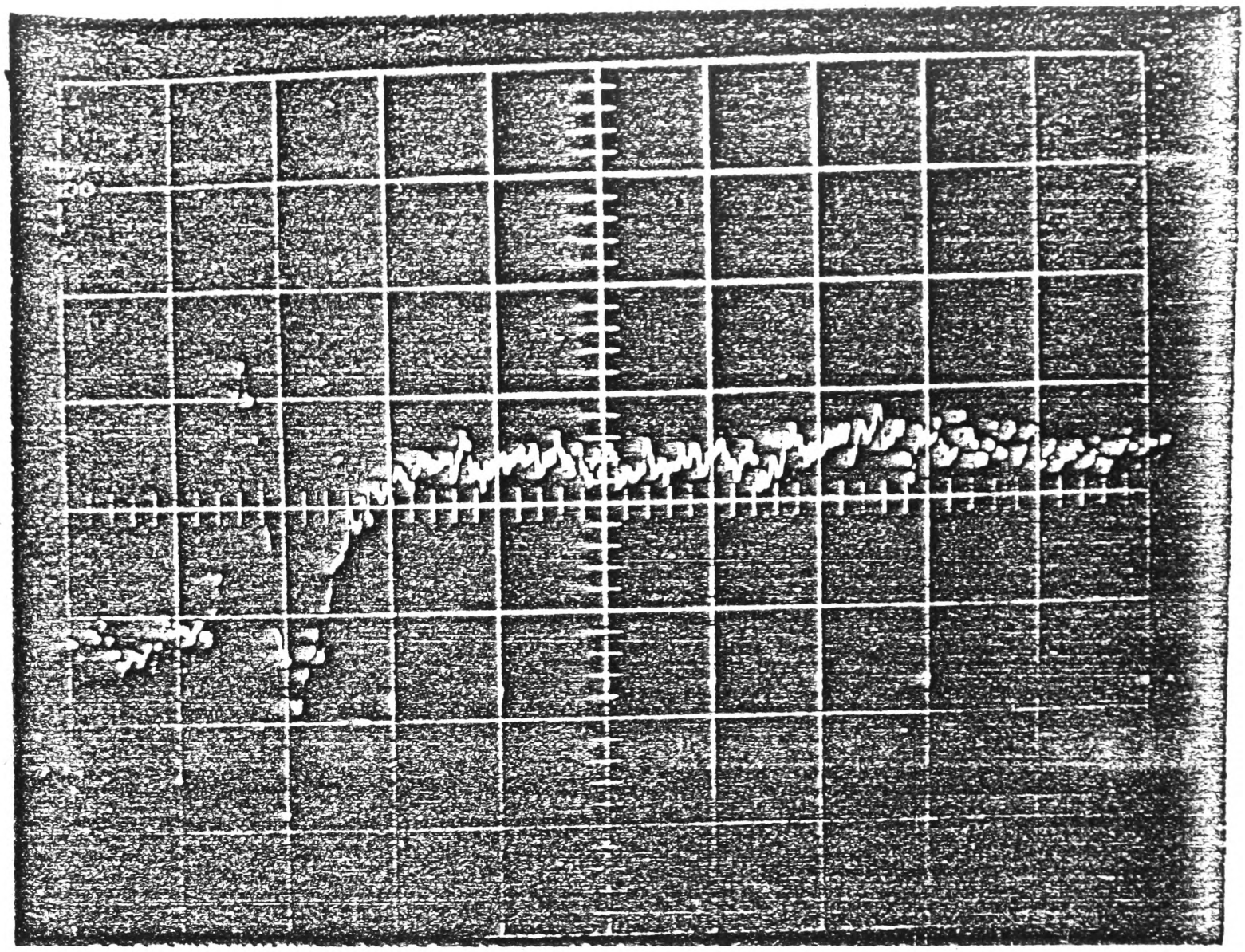
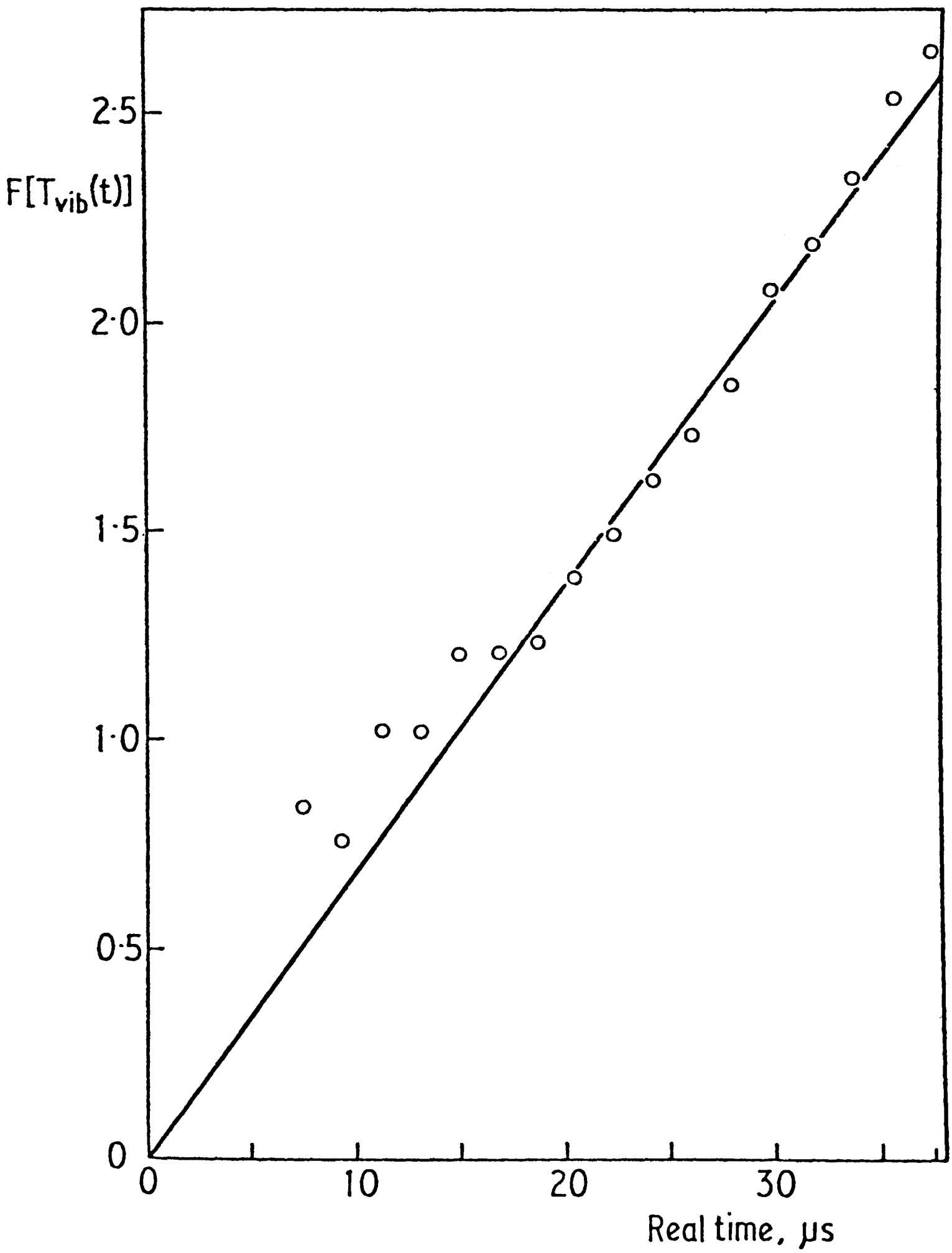


FIGURE 7.2



temperature which is in good agreement.

We suggest that it is generally true that, following shock-heating, and within experimental error, the vibrational levels of all diatomic molecules relax via a continuous series of Boltzmann distributions, and that the total vibrational energy relaxes exponentially. The experimental results of Chow and Greene are unlikely to be correct.

Greene [141] agrees that there is no explanation for these results. It is difficult to find an error in the experiment 19 years on. A tentative suggestion is that the power of the beam from their mercury-arc lamp might have been sufficient to affect the vibrational relaxation that they were monitoring by pumping the HI molecule rather than probing them. It is more likely that their time resolution was not good enough, or that they were not monitoring the different vibrational levels cleanly.

CHAPTER 8 - DETERMINATION OF RELAXATION TIMES FROM SINGLE LASER ABSORPTION TRACES

8.1 Theory

Once it has been established that it is a good approximation that relaxation proceeds via a continuous series of Boltzmann distributions, and that the total vibrational energy relaxes exponentially, then a relaxation time may be obtained from a single laser absorption trace.

The procedure begins with equation (6.7). In chapter 6 vibrational 'temperatures' were calculated by comparing the populations of adjacent levels, using two laser absorption traces. No assumptions were made about the populations of these levels relative to all the other levels. Having established that the populations are given by a Boltzmann distribution, we need no longer proceed from equation (6.7) to equation (6.8) but can go straight from a measurement of gain to a vibrational temperature. The relaxation time can then be found from equation (6.9).

Energy levels are assumed to be as for a simple harmonic oscillator, thus $\Delta E_{v+1->v}/kT_{vib} = \Theta$. Rewriting (6.7),

$$G_v \propto (n_1/g_1)(1-e^{-\Theta}e^{-\Delta E_{J-1->J}/kT_{rot}}) \qquad (8.1)$$

Now, where q_{vib} and q_{rot} are the vibrational and rotational partition functions,

$$n_1 = (n_v g_1 e^{-\Delta E_{J->J=0}/kT_{rot}})/q_{rot} \qquad (8.2)$$

and

$$n_v = (ne^{-v\theta})/q_{vib} = ne^{-v\theta}(1-e^{-\theta}) \qquad (8.3)$$

The change in gain G_v during the experiment is caused solely by the change in vibrational temperature. The rotational temperature remains constant. Including n and $e^{-\Delta E_{J->J=0}/kT_{rot}}/q_{rot}$ in the proportionality constant, A, and writing $C = e^{-\Delta E_{J-1->J}/kT_{rot}}$, we deduce:

$$G_v = Ae^{-v\theta}(1-e^{-\theta})(1-e^{-C\theta}) \qquad (8.4)$$

As Θ cannot be factorised out, an iterative procedure is necessary to get Θ from an experimental G_v. (This is not because the absorption technique looks at the difference in population of two levels; it would still be the case if the $(1-Ce^{-\theta})$ term were not there.) The iterative procedure is detailed in the next section.

8.2 Details of Analysis

The analysis is carried out in subroutine 'CONDITS' of program 'SHOCKIT'. The points which have been fetched from the transient recorder are numbers in the range 0-255. Those making up the baseline are averaged, and the result is subtracted from those to be analysed. These then correspond to values of ΔI. The gain is given by $\log[(I_o-\Delta I)/I_o)]$. The laser power I_o is converted into the same units, given that the transient recorder voltage fullscale setting corresponds to 256 units. The final points, corresponding to equilibrium, are averaged, and from this average a value for the final equilibrium gain is produced. T_f is calculated by solving the Rankine-Hugoniot equations as in section 4.2, and hence A may be calculated from equation (8.4), with $\Theta = \theta_f$ and G_v the final equilibrium value. C is calculated from the rotational energies of levels J and J+1, and rotational temperature

T_f. Values used for rotational constants B and D are those taken from Huber and Herzberg [136] for v=1, 1.905 and 6.120×10^{-6} cm^{-1} respectively. C has a value of 1.06 for a P(10) line at 940 K and is closer to unity at higher temperatures.

The first point to be analysed is the first one for which ΔI is 5 units greater than the baseline. By not analysing earlier, points whose values are affected by the occurrence of the schlieren spike are avoided.

The iterative procedure used to obtain θ from G_v is outlined in this paragraph. θ is set to θ_1 and the function

$$\theta_g = -\frac{1}{v} \ln \left[\frac{G_v}{A(1-e^{-\theta})(1-e^{-C\theta})} \right] \qquad (8.5)$$

is calculated. This equation is a rearrangement of equation (8.4). If the true value of θ has been guessed, $\theta_g = \theta$. The initial guess of $\theta = \theta_1$ is too high. The resultant θ_g is lower. θ is reset to the value of θ_g and hence successively lower values of θ are generated until θ has converged to within 0.001. This procedure is carried out for each point to be analysed, and, for each point, θ is converted into the function $F(T_{vib})$ of equation (6.9).

As T_{vib} approaches T_f, $F(T_{vib})$ becomes increasingly sensitive to small changes in T_{vib} so a cut-off is necessary. The cut-off is at, or just before, two relaxation times have elapsed. In order to achieve this, the last point to be analysed is the one before the first for which $F(T_{vib})$ has a value greater than 2. The analysis is never carried out over more than 2000 points owing to constraints in computer memory.

A least-squares fit is carried out to calculate the slope of the $F(T_{vib})$ versus time graph. The slope is equal to $1/\tau$. τ is multiplied

by the pressure in atmospheres to give ($p\tau$).

The program has facilities to put the results in an output file, and plot either the experimental $F(T_{vib})$ values together with the fitted straight-line, or the experimental ΔI values together with a theoretical fit calculated back from the fitted straight-line. The plot may be either on the screen or the lineprinter.

An alternative approach is to calculate a relaxation time from the first set of θ_g, without iteration, use this value of the relaxation time to calculate a new set of θ, and then obtain another set of θ_g from equation (8.5). These are used to calculate a new relaxation time until the relaxation time has converged. This method is no longer used as it is more unwieldy, and the result depends on the choice of the point corresponding to t=0. In the favoured method t=0 is not fixed by the operator.

8.3 Experimental Results for CO/He/Ar Mixtures.

The procedure outlined above has been applied to measuring relaxation times of CO/He/Ar mixtures. These experiments have been carried out to test the data analysis technique and to obtain further measurements of CO/He/Ar rate constants, following the disagreement between those of Millikan [136] and those obtained by the two-trace technique of chapter 6.

The results are tabulated below:

Shock no.	laser line	T_2 /K	p_2 /torr	$(p\tau)_{CO-He}$ /μs.atm	2σ ±	$10^2 T^{-1/3}$ $K^{-1/3}$
002	4->3P(10)	2326	60.9	1.48	0.005	7.547
003	2->1P(10)	1972	49.3	2.17	0.011	7.974
004	2->1P(10)	2235	28.8	1.89	0.014	7.648
005	2->1P(10)	1711	83.8	3.95	0.006	8.361
006	2->1P(10)	1754	170.6	4.46	0.012	8.292
008	2->1P(10)	1310	194.9	10.08	0.017	9.139
009	2->1P(10)	1027	179.1	22.36	0.049	9.912
010	2->1P(10)	939	243.4	29.23	0.076	10.212

The mixtures used were for shocks 002-006, 10.08 % CO, 34.95 % He, 54.98% Ar, for shock 008 10.01 % CO, 34.88 % He and 55.11 % Ar, and for 009-010 a dilution of 008 with CO and He to 9.98 % CO, 85.45 % He and 4.57 % Ar. The values for $(p\tau)_{CO-CO}$ and $(p\tau)_{CO-Ar}$ given by Millikan [136] were used to calculate the values of $(p\tau)_{CO-He}$. T_2 and p_2 are the mean of the values before and after relaxation.

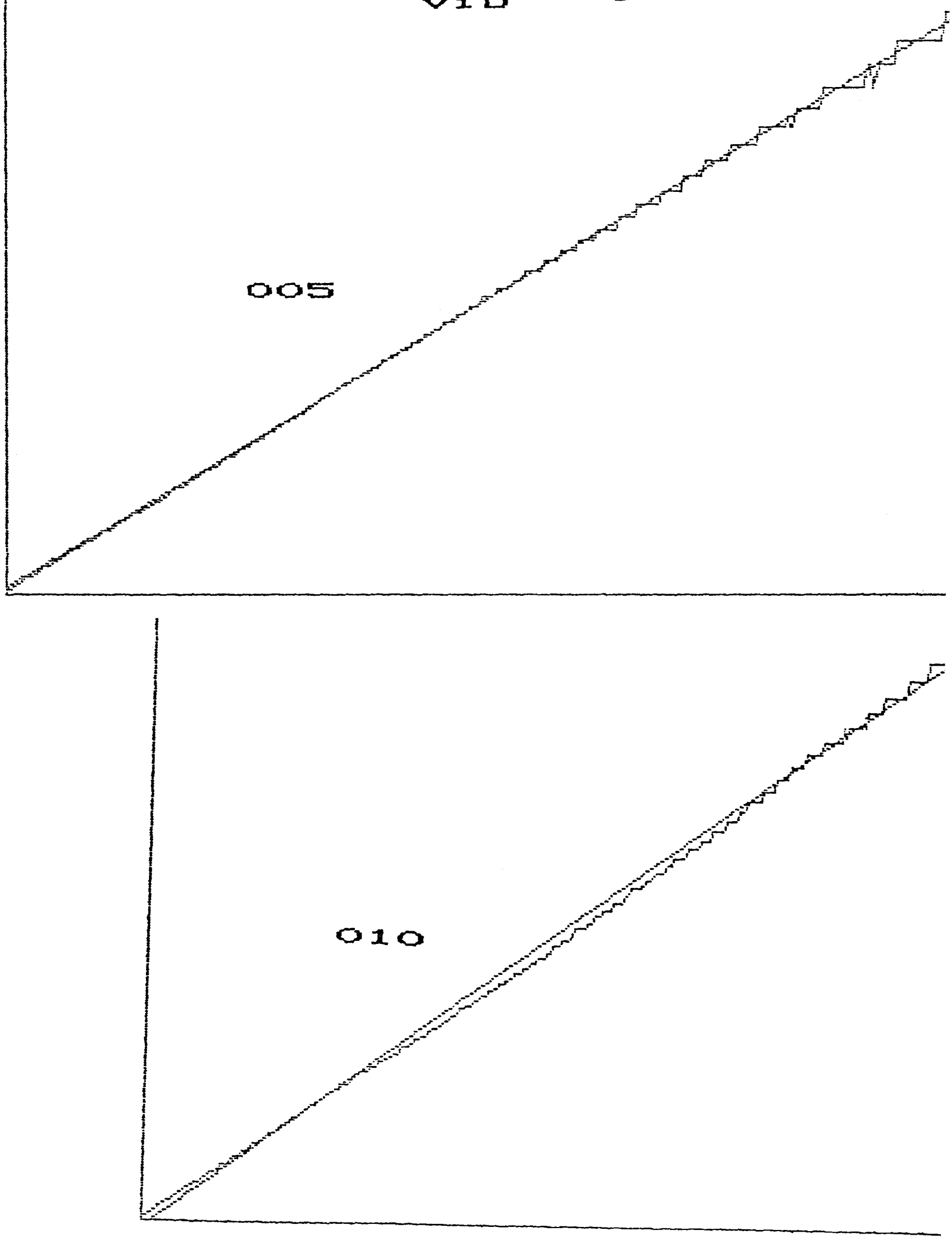
A 2->1 line was used for most runs, as it provides optimum signal-to-noise for a given percentage of CO. The percentage of CO is kept low to make the relaxation more isothermal. The change in temperature is 38 K for shock 002, and 4 K for shock 010.

The He is responsible for 97 % of the relaxation for shock 002 and 99.7 % for 010. Thus the values of $(p\tau)_{CO-CO}$ and $(p\tau)_{CO-Ar}$ have little effect on the final result.

In figure 8.1, typical plots of $F(T_{vib})$ against time, together with the fitted straight-line, are shown. That for shock 010 is a typical plot and that for 005 a very good straight line.

FIGURE 8.1

Plots of $F(T_{vib})$ against time



Curvature, though slight, is always upwards. This may be thought to be evidence for the 'hook' effect mentioned in section 5.18. If this effect were the cause, the curvature would be expected to become more pronounced with increased T_2, as then higher levels become more populated. There is no clear evidence for this. It is significant that the result with the worst curvature, 004, is one for which the relaxation is only just complete before the arrival of the contact surface. The relaxation time for the mixture, at the pressure of the experiment, was between 50 and 150 μs (real time) for each shock. However the maximum hot flow transit time (section 4.9) falls as the temperature rises, and this fall is greater because of the necessity for higher temperature shocks to employ lower pressures to lengthen the relaxation time. Flow non-idealities are a more likely cause of the curvature than a real dependence of the relaxation time on vibrational as well as translational temperature.

The analysis typically extends over 1000 points, so for each shock twice the standard deviation is less than 1 % of the slope. The stepped nature of the plots is due to the digitised nature of the input data. It becomes more pronounced as equilibrium approaches and $F(T_{vib})$ rises more steeply with ΔI.

A plot of log ($p\tau$) against $T^{-1/3}$ is shown in figure 8.2. As well as the results of this chapter, the results from chapter 6 are included. A straight-line fit to the results of this chapter gives $\ln(p\tau) = 112T^{-1/3}-7.95$. Error limits on the slope and intercept, calculated as two standard deviations, are ± 9 and ± 0.77 respectively. Millikan's equivalent was $\ln(p\tau) = 87T^{-1/3}-19.1$. Millikan's results are shown in the figure by the dashed line. His measurements extended over the range 580-1500 K. The disagreement between Millikan's results [136] and our results obtained by the two-trace technique (chapter 6) is

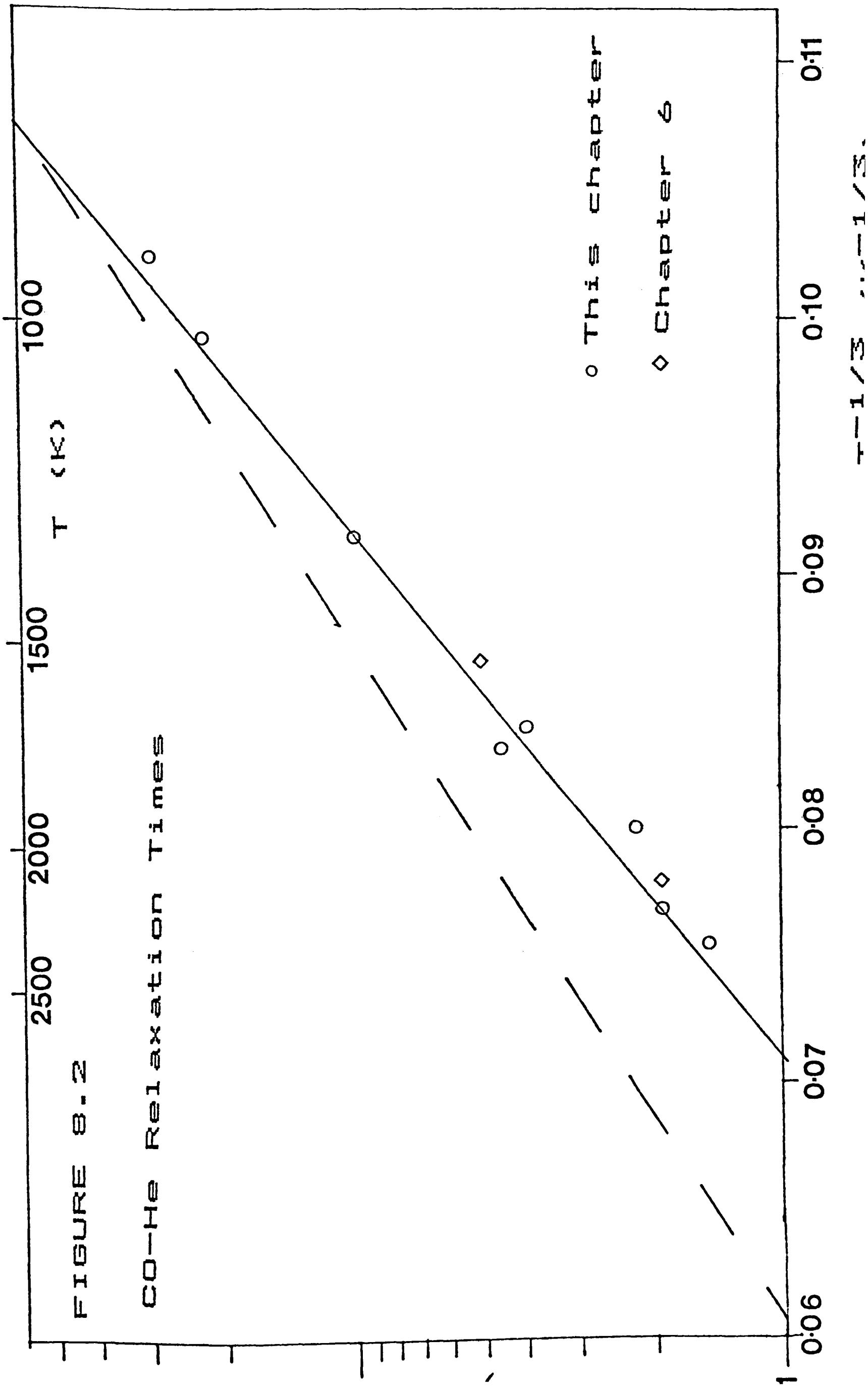


FIGURE 8.2

CO—He Relaxation Times

confirmed. Our results of chapters 6 and this chapter fall neatly on the same straight line. The reason for the disagreement is unknown.

It should be possible for us to obtain results at lower temperatures. The limiting-factor is not signal height but rate. As the temperature is reduced, increasingly large pressures of test gas are required, for the relaxation to be fast enough, giving data of poorer quality (noise greater) at greater cost.

8.4 Accuracy

Computer runs have been carried out to test the sensitivity of the calculated value of the relaxation time to the various experimentally measured quantities. The least precisely determined quantity is the laser power I_o. This is determined by measuring the height of the chopped laser power signal on an oscilloscope screen. The determination is made before the shock and immediately afterwards, but the power may have varied in between times. Short-term fluctuations will be visible on the laser absorption trace which can be discarded, but not longer ones of the order of seconds. The sensitivity of the relaxation time to I_o is greater when the final $\Delta I/I_o$ is greater. As ΔI approaches I_o, the gain is no longer proportional to ΔI and hence a change in I_o has an unequal effect on gain values at different times, in particular affecting those at early times less than the final equilibrium value. In the majority of cases I_o measured before and after the shock has the same value, and it is very likely that in these cases it has the same value at the time of the shock. In the rare cases where it is found to have changed, and if $\Delta I/I_o$ is large i.e. ~50 %, an error of not greater than 20 % in the relaxation time is possible.

Other errors have much less effect. The monochromator does not have sufficient resolution for there to be absolute certainty of the

identity of the operational laser line. Only when an accidental coincidence is successfully utilised is there such certainty. If the line used is in fact out by one rotational quantum number, an error of less than 1 % is caused.

The transient recorder has guaranteed accuracy of ± 1 % of the vertical height of the signal, but the resolution will be worse than this if the signal is less than 100 units high. Care must be taken to set the voltage fullscale and offset controls of the transient recorder so that the signal stretches over as wide a range as possible between 0 and 255. The accuracy of the timebase of the transient recorder is to within 1 %.

A 1 % error in the shock-speed causes an approximately 2 % error in T_2. When two timers are used together, they invariably agree to within 0.1 μs. Their stated accuracy is ± 0.1 μs.

The accuracy of the Baratron pressure meter is also to within 1 %. An error in p_1 will cause an equal percentage error in the relaxation time. An error in the T_1 measurement of 1 K would cause an error in T_2 of 1 K which is negligible.

8.5 Conclusions

The results are preliminary. Test gases were not the purest possible. The results form a self-consistent set and are also consistent with the results of chapter 6, where the $F(T_{vib})$ plot is obtained from two traces. The method of data analysis is established as sound, and so vibrational relaxation time measurements can now be readily made as desired.

PART THREE

EXPERIMENTS ON REACTION KINETICS

CHAPTER 9 - THE DECOMPOSITION OF CARBONYL SULPHIDE

9.1 Introduction

The first experiment carried out on reaction kinetics with this shock tube is reported in this chapter. The subject of the experiment was the reaction, OCS->CO+S.

This is a comparatively simple reaction, but one on which our shock-tube / CO-laser combination could be used to cast new light. The new information was the initial vibrational distribution of the CO product. The activation energy was also obtained to compare with that of other workers.

The success of the experiment depended on an understanding of the energy transfer processes which occur between the newly born CO and other species present, so a brief account of energy transfer in polyatomic molecules will be given in the next section. Before outlining the results, previous work on (i) vibrational product distributions from unimolecular reactions, and (ii) the kinetics of the OCS decomposition, will be discussed.

9.2 Vibrational Energy Transfer in Polyatomic Molecules

In the discussion of the theory of vibrational energy transfer in chapter 5, only diatomic molecules were alluded to. Polyatomic molecules (including triatomic molecules under this heading) have more than one vibrational mode, so the question arises of whether all the modes relax with the same relaxation time.

As an example, in OCS there is the bend (ν_2) at 520 cm^{-1}, the mainly C-S stretch (ν_1) at 859 cm^{-1} and the mainly C-O stretch (ν_3) at 2062 cm^{-1}. The first point to notice is the small value of the

frequency of the lowest vibrational mode, compared to CO whose 2143 cm^{-1} is a large value for a vibrational frequency. The mechanism of the vibrational excitation of OCS following shock-heating is (VT) excitation of the lowest level, (010), followed by inter- and intra-molecular (VV) exchange to populate the levels of other modes (including levels with vibrational quanta in more than one mode). The (VV) exchange is fast compared to the first step so only one relaxation time is observed [91] i.e. the total vibrational energy relaxes exponentially. (For molecules where the frequency of the second lowest mode is more than double that of the lowest mode, e.g. SO_2, two relaxation times are observed [105].) The overall rate is controlled by the (VT) excitation of the ν_2 mode. This is itself fast compared to the (VT) excitation of CO because of the smaller vibrational frequency. At 2000 K, the CO_2-Ar relaxation time is 200 times as fast as the CO-Ar one. Larger molecules relax faster still in general, as they have lower frequency vibrations. The levels in each mode will have populations described by a Boltzmann distribution at all times.

It is because the (VT) process is slow compared to all (VV) processes that different rates amongst the (VV) processes do not lead to different vibrational modes behaving differently following shock-heating. However, if energy is placed directly in an upper level, the different modes can behave differently, and an excellent example of this is provided by the N_2O/N_2 system studied by Demin et al. [142] and discussed in the next section.

9.3 Previous Work on Vibrational Distribution Analyses of Products of Unimolecular Reactions

Vibrational product distributions have been carried out for unimolecular decomposition reactions brought about thermally,

photolytically, and following chemical activation i.e. dissociation of an energy-rich molecule formed in a chemical reaction. In the photolytic case, the initial step is excitation to an upper electronic state by absorption of a photon. It does not necessarily follow that the pyrolysis and photolysis of a particular species occur from different electronic states, as curve-crossing may occur.

We only know of one previous study where information on the vibrational energy content of a product has been obtained following thermal excitation. That study is the shock tube work of Demin et al. on the dissociation of N_2O. They employed conditions such that the N_2O was only partially dissociated (1600-2000 K, 9-28 atm, which for this unimolecular reaction is in the transition region between the high and low pressure limits [143]) behind a reflected shock wave. The reaction was probed with an N_2O laser working on the 100->001 transition, and amplification - i.e. positive gain - of the laser beam was observed for a period of 20-30μs behind the reflected shock. A population inversion had been produced in the N_2O, and must have been caused by fast (VV) transfer with N_2 produced in the decomposition:

$$N_2O(000) + N_2(v+1) \rightleftharpoons N_2O(100) + N_2(v) \qquad (9.1)$$

(this is near resonant as the fundamental frequencies of N_2O (ν_1) and N_2 are 2224 cm^{-1} and 2359 cm^{-1} respectively). If the experimental results are correct, the full explanation must be as follows:

The population inversion produced is between the $N_2O(100)$ level (at 2224cm^{-1}) and the $N_2O(001)$ level (at 1285 cm^{-1}). The results imply N_2 with a vibrational temperature greater than the translational one, i.e. 'vibrationally hot' N_2. We can calculate a lower limit for this temperature as follows. We assume that the distribution of levels in the

ν_3 mode is governed by a Boltzmann distribution at 2000 K, the translational temperature. (This implies that there is no fast (VV) pathway between the ν_3 mode and the ν_1/N_2 coupled system.) The fractional population relative to level (000) of level (001) is then 0.4. The fractional population of level (100) relative to the groundstate must be greater than 0.4, despite its higher energy, for inversion to occur, which implies that the vibrational temperature of the ν_1 mode must be greater than 3500 K, allowing for its higher energy. Treanor et al. [79] showed that for a mixture of two molecules A and B in (VV) quasi-equilibrium, in our notation ($\Theta = h\nu/kT$)

$$\Theta_A - \Theta_B = \Delta E_{AB}/kT_T \qquad (9.2)$$

where ΔE_{AB} is the energy difference between the fundamental vibrational frequencies of A and B, and T_T is the translational temperature. At T_T = 2000 K, this gives the vibrational temperature of N_2 as greater than 3350 K. Thus in the thermal decomposition of N_2O, the N_2 is born vibrationally hot i.e. there is more energy in vibration than there would be at equilibrium at the translational temperature.

This is an unusual example of a use of a 'collisional pumping' scheme to put energy into a specific mode of a polyatomic molecule. The population inversion in the N_2O is said to be maintained because (VV) transfer between the ν_1 and ν_3 modes is not fast enough to equilibrate the populations at a common vibrational temperature. It must be said that this is surprising as at 2000 K many levels are significantly populated and relatively large energy defects will be 'near resonant' because of the population of high rotational levels.

It is not possible to determine the population of individual vibrational levels of N_2 at the moment of its birth because, as noted in

section 5.19, very rapid (VV) energy transfer will bring about a Boltzmann distribution at some vibrational temperature almost immediately. (In the concentrated mixtures used by Demin et al, (VV) transfer will certainly be that rapid.)

The results of Demin et al. show N_2 born with a vibrational temperature greater than 3350 K (although they did not take the analysis that far themselves). As a guide, if all the N_2 molecules were born in v=1, rapid (VV) transfer would create a Boltzmann distribution at vibrational temperature 4400 K before a measurement could be made. All molecules in (v=2) would lead to a vibrational temperature of 7600 K. There is of course no reason why one would expect all the molecules to be born in the same level.

The reasons why N_2O might give vibrationally hot N_2 will be disussed along with the OCS vibrational product distribution in section 9.7.

Although that is the only experiment carried out on a vibrational product distribution following thermal excitation of the parent compound, a great deal of work has been done on unimolecular reactions following excitation by absorption of radiation. The latter type of experiment is perhaps easier because signal-averaging is possible.

Lin [7] studied the photodissociation of OCS using a vacuum ultraviolet flash to excite the CO. The CO was born extremely vibrationally excited, and laser action was observed on the 13->12 to 7->6 vibrational bands of CO. The OCS dissociated from an excited electronic (singlet) state, so there is no direct comparison with thermal experiments.

Two further examples are the work of Houston and Moore [8] on formaldehyde decomposition and of Sonobe et al. [9] on cyclopentenone

decomposition. In each case CO is born vibrationally hot. In photochemical experiments, the dissociating molecules are given energy in excess of the minimum required for dissociation, so it is no surprise that the products are born vibrationally excited. In thermal experiments, there is no such excess and the additional possibility of the products being born vibrationally cold (i.e with the vibrational temperature less than the translational temperature) arises.

We shall return to the subject of energy disposal in sections 9.7 and 11.1. General accounts of energy disposal following chemical reaction, including unimolecular decomposition following chemical activation, are given by Holmes and Setser [144], and Smith [145].

9.4 Previous Work on the Thermal Decomposition of OCS

There have been two earlier shock tube studies, by Hay and Belford [146] and by Schecker and Wagner [147]. Hay and Belford used time-of-flight mass spectrometry to follow the concentrations of OCS, CO, S, S_2 and SO. Schecker and Wagner used infrared emission to follow OCS and ultraviolet absorption to follow S_2 behind the reflected shock. After these experiments the kinetics were well understood. Hay and Belford's experiments were in the low pressure region of unimolecular decay like ours, but Schecker and Wagner were able to get results in both low ($<1.3\times10^{-4}$ mol.cm^{-3}) and high ($>1.2\times10^{-3}$ mol.cm^{-3}) pressure regions.

The experiments reported in this chapter produce a new piece of information on the OCS decomposition, the vibrational distribution of the CO product, as well as corroborating the earlier work.

9.5 Choice of Experimental Conditions

The experiments carried out fall into two categories:
(i) Those to measure rate constants over a wide range of temperatures and hence calculate an activation energy. These were largely carried out by Asghar Fakhr and Malcolm Wood, and details are not listed here.
(ii) Those to measure the initial vibrational distribution of the CO product, which are presented here.

Different conditions were required for each. The criteria for (i) are basically as discussed in section 4.10. Data over a wide range of temperatures are required. A high dilution of OCS in Ar is especially important, as the reaction is very endothermic. For 2 % OCS at 3000 K, the temperature falls by about 200 K as the reaction proceeds. Either 2 % or 0.5 % OCS in Ar was used [6].

Since the population of a vibrational level of CO would depend on both the dissociation rate and the vibrational relaxation rate, the parent OCS was monitored instead, for the determination of dissociation rate constants. To avoid interference from absorption by CO product, $O^{13}CS$ was used. Coincidences between ^{12}CO and ^{13}CO are rare. However the infrared absorption of triatomics is more continuous than that of diatomics. Triatomics have more vibrational bands and smaller rotational constants, so many $^{12}C^{16}O$ laser lines can be used to monitor $O^{13}CS$. 5->4P(9) was used in fact.

For the product vibrational distribution experiments, the dissociation must be fast compared to subsequent vibrational relaxation processes. These processes are: (i) (VT) relaxation of CO by Ar, OCS, CO and S, (ii) (VV) relaxation of CO by itself and (iii) (VV) relaxation by OCS. Processes (ii) and (iii) can be reduced in importance by increasing the dilution in Ar. All the vibrational relaxation processes

can be reduced in importance by increasing the temperature. The temperature dependence of (VV) rates is negative at low temperatures (section 5.9) and whereas at high temperatures it may well be positive, as short range forces are more important, it will be a small positive temperature dependence compared to that of the decomposition. The CO-X (VT) rate constants also have less steep rate constants than the decomposition. This can be verified by comparing the previous data on OCS-Ar decomposition [146,147] with the Millikan CO-CO and CO-Ar relaxation times [135]. CO-S (VT) rate constants are unmeasured, but since they are likely to be higher than CO-CO ones they are expected to rise less steeply with temperature.

Thus the vibrational product distribution experiments were carried out at high temperatures and low OCS concentrations. The temperature was higher than the range over which the activation energy was determined, as it was necessary for the dissociation to be very fast, too fast to measure its rate. $O^{12}CS$ could be used for monitoring (v=0) and (v=1) as 1->0 and 2->1 ^{12}CO laser lines were not absorbed by the OCS parent.

The gases used were B.O.C. zero grade argon (99.9985% pure), Matheson OCS (97.5 %) and Prochem $O^{13}CS$ (90 atom %). The OCS samples were purified before mixtures were made. This was done by repeatedly freezing and pumping in a bath of liquid nitrogen to remove light gases, and then distilling from a dry-ice/acetone bath which froze out CO_2, the major impurity, and H_2O.

9.6 Results

Fourteen shocks were fired to find the activation energy of the reaction [6]. Temperatures and pressures were calculated as outlined in sections 4.2 and 4.3 for (i) vibrationally relaxed reactant, no

reaction, and (ii) complete equilibrium between OCS, CO, S, S_2, C, O, and O_2. The rate constants obtained were taken to refer to the average of the temperature and pressure for these two conditions. The temperature range over which the experiments were carried out was 2400-3500 K, and the total density range was $8x10^{-7}$-$2x10^{-6}$ $mol.cm^{-3}$, well within the low pressure region of unimolecular decay.

Rate constants were obtained using the rate law $[OCS]_t = [OCS]_0 e^{-k[Ar]t}$. The experimentally-determined gain G(t) is proportional to $[OCS]_t$ as in this case both the upper and lower levels of OCS, connected by the laser transition, are proportional to the total OCS population. The OCS vibrational relaxation is complete and all OCS levels are in Boltzmann equilibrium at the translational temperature. Thus the the slope of a graph of ln[-G(t)] against time is divided by the argon concentration to give the rate constant.

To identify the experimental rate constant with the rate constant for the elementary step

$$OCS + Ar \xrightarrow{k_1} CO + S + Ar \qquad (9.3)$$

cannot be done without careful thought. This is because of the abstraction process:

$$OCS + S \xrightarrow{k_2} CO + S_2 \qquad (9.4)$$

If $k_2[S] >> k_1[Ar]$, then half the CO is produced by the second process, and the apparent rate constant is equal to $2k_1$. Hay and Belford [146] were able to show that their measured rate constant was equal to k_1 under some conditions and $2k_1$ under others, by monitoring all species

including S atoms. Their experimental rate constant was always equal to k_1 above 2800 K, because k_1 rises more steeply with temperature than k_2. Our results agree very well with the k_1 values of Hay and Belford so our measurement is a direct measurement of k_1.

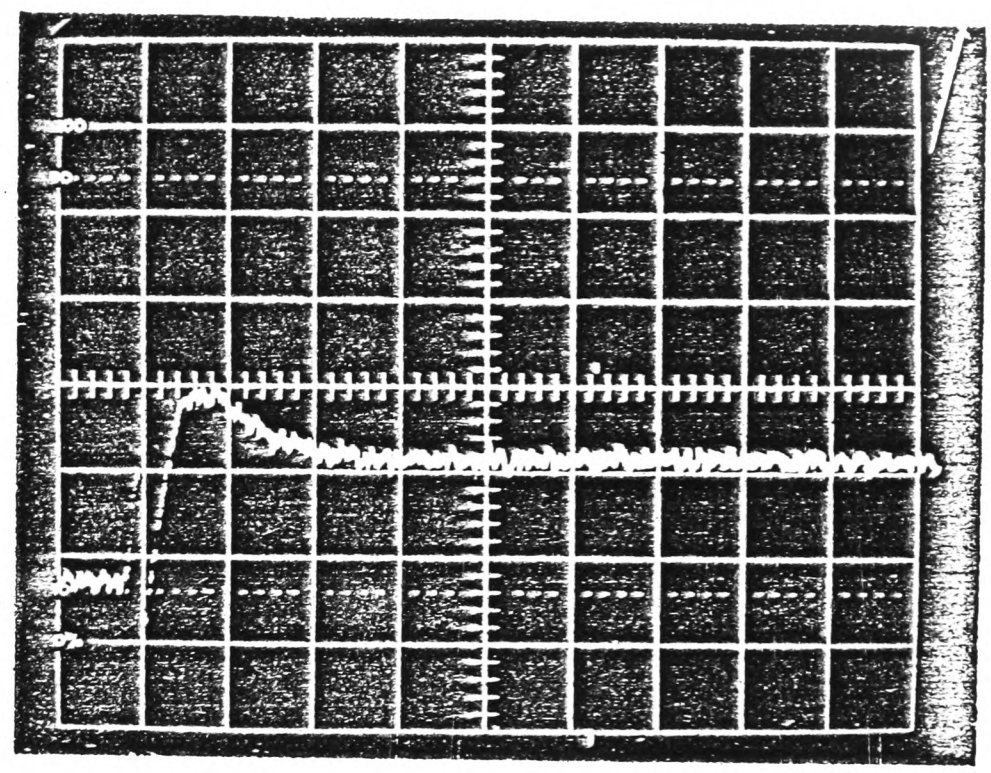
The inclusion of the [Ar] term assumes that the results are in the low pressure region of unimolecular decay. This is verified by the results of Schecker and Wagner [147]. The activation energy obtained by us of 59±3 kcal.mol^{-1} [6] agrees well with the value of 61 kcal.mol^{-1} obtained by them in the low pressure region.

It was only at temperatures approaching 4000 K that clear information could be obtained on the initial vibrational distribution of the CO product. At lower temperatures, the population of each level rose more slowly than the populations of lower levels. v=0 as studied with a 1->0 line rose the fastest. This suggests an overpopulation in v=0 relative to a Boltzmann distribution at the translational temperature. If the CO were born in such a Boltzmann distribution, the populations of all levels would rise at the same rate.

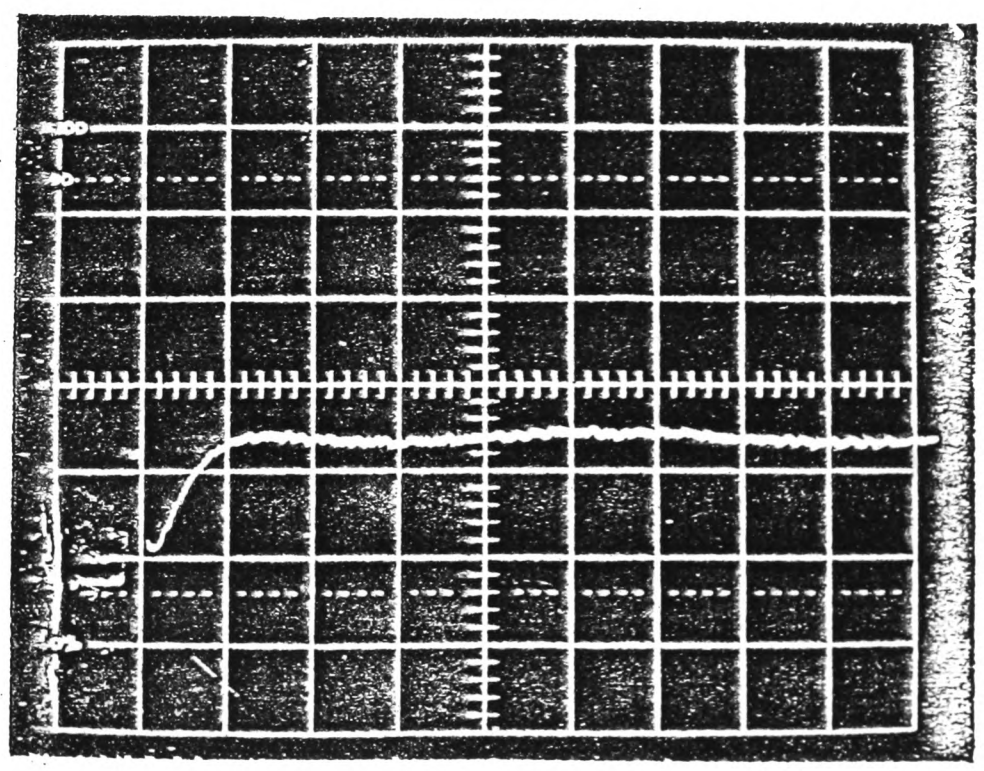
An overpopulation in v=0 is hard to observe compared to other possible overpopulations, because a relatively large fraction is in v=0 at equilibrium. At room temperature, where 99.997 % of CO is in v=0 at equilibrium, an overpopulation would be impossible to observe. The fraction in v=0 falls to 99 % at 670 K and 90 % at 1340 K.

An overpopulation in v=0 was directly observed by seeing the population rise and then fall to equilibrium at temperatures above 3500 K (where 59 % is in v=0 at equilibrium). In figure 9.1 a typical trace is shown, together with a 2->1 trace obtained under similar conditions. Both have a timescale of 5μs/div. The conditions are detailed below, for 0.5 % OCS in Ar:

FIGURE 9.1



1-20P(5)-1



2-1AP(5)

laser line	T_2 /K	p_2 /torr	vertical scale /mv.div^{-1}
1->0P(9)	3870	280	10
2->1P(9)	3762	300	20

Initially the (v=0) population rises rapidly as it is produced in the decomposition, then it falls as energy transfer to higher vibrational levels occurs. The (v=1) population rises on a similar timescale to that of the fall of (v=0). As a check on this interpretation of the results, experiments with higher percentages of OCS but the same temperature were performed. This change increased the vibrational relaxation rate relative to the dissociation rate, and as a result for 10 % OCS in Ar no overpopulation was visible. For 5 % OCS it was just visible as a kink in the curve for the rise of population in (v=0).

As the temperature is well above 2800 K, we can be sure that all CO molecules are formed from the unimolecular dissociation and not from the abstraction process (9.4). The two traces shown in figure 9.1 were used to estimate a lower limit for the fraction born in (v=0). The upper limit is unity, as we have no firm evidence that any molecules are born in higher vibrational levels. As the calculation is approximate, it is assumed that the gain is given by:

$$G_v(t) = \ln[(I_o - \Delta I)/I_o] = A(n_v - n_{v+1}) \qquad (9.5)$$

i.e. the different degeneracies and populations of the upper and lower rotational levels are ignored. The absorption coefficient A is calculated from the known final experimental conditions, and final equilibrium gains, for both 2->1 and 1->0 traces. The populations are then worked out at the time t_m when the 1->0 trace has just reached its

maximum, as follows. We assume that at t_m, $n_2 = 0$, and hence calculate n_1 from equation (9.5) for the 2->1 trace. From n_1 we get n_0 from (9.5) and the 1->0 trace. The result is that, whereas at final equilibrium, $n_0 = 0.56$, $n_1 = 0.25$, and $n_2 = 0.11$ (w.r.t. $\Sigma n_v=1$), at t_m $n_0 = 0.55$ and $n_1 = 0.06$ (the other 0.4 is still OCS). The ratio of n_0 to n_1 is thus 9:1 instead of 2:1 for final Boltzmann equilibrium at the translational temperature. At least 90 % of the CO is born in (v=0). The vibrational temperature of the CO when it is born is therefore less than 1400 K, at a translational temperature of 3800 K.

9.7 Discussion

The discussion will be divided into two parts: (i) given that the CO is born with an overpopulation in (v=0) do the conditions required to achieve this tie in with the expected decomposition and energy transfer rate constants? and (ii) can the fact that the CO is born vibrationally cold be explained from unimolecular decomposition theory?

In order to investigate (i), the numerical integration computer program of section 5.5 was extended. All the CO-Ar (VT) processes and CO-CO (VV) processes were left in. However the CO(v=0), instead of being present initially, was formed by decomposition of OCS, and an extra differential equation, describing the change in population of OCS, was introduced. The decomposition rate constant could be varied relative to the vibrational rate constants. An OCS-CO (VV) rate constant was also included. Differences in population $n_v - n_{v+1}$ were again calculated to compare with laser absorption traces.

If all the CO molecules begin in (v=0), the situation is similar to the vibrational relaxation of CO following shock-heating. The CO-CO (VV) processes make no contribution to the increase of vibrational energy of the CO, but ensure that it progresses through a continuous

series of Boltzmann distributions. OCS-CO (VV) processes tend to drive the CO vibrational temperature towards the OCS vibrational temperature, which equals the translational temperature, but the concentration of OCS falls rapidly. CO-S (VT) processes become more important with time.

It was not possible to carry out a precise fit of rate constants to the results without making full allowance for the slight change in temperature due to the occurrence of the reaction. This was not done, as it would have necessitated a vast increase in the complexity of the computations. However it is clear that a realistic choice of rate constants can explain the results. An overpopulation of the correct degree is produced with the dissociation rate constant k_D 10 times the CO-Ar (VT) rate constant k_{01} (this is in accord with extrapolations of our experimental results for k_D [6] and Millikan's for $(p\tau)_{CO-Ar}$ [135]), and with an OCS-CO (VV) rate constant with 100 times the value of k_{01}. After the maximum has been reached, the fall in (n_0-n_1) is less rapid than found experimentally. The inclusion of CO-S (VT) processes, which grow in rate as the dissociation proceeds, might correct this. As the CO is only 0.5 % of the mixture, this would require the CO-S relaxation time to be over 200 times faster than the CO-Ar one. At 4000 K, the CO-O relaxation time, as measured by Center [148], is 900 times faster than the CO-Ar relaxation time, so this is not unreasonable.

It is generally found from the computer and experimental results that the 2->1 trace appears to reach equilibrium earlier than the 1->0 one. This is because of the behaviour of the population of individual vibrational levels as the vibrational temperature is raised. n_0 falls constantly, but n_1 rises to a maximum fractional value of 0.25 at 4400 K then falls. For a large range of vibrational temperatures the fractional population in (v=1) is almost constant so the 2->1 trace changes little. n_1 itself appears to reach equilibrium even sooner than

$n_1 - n_2$.

The observation of CO born vibrationally cold in the decomposition of OCS contrasts with the observation of N_2 born vibrationally hot in the decomposition of N_2O [142] as discussed in section 9.3. This difference is explicable, as will now be described.

The electronic groundstates of OCS, CO, N_2O and N_2 are singlets but those of S and O are triplets. The reactions are thus both in the spin-forbidden class of dissociation of diatomics:

$$OCS + Ar \rightarrow CO + S(^3P) + Ar \qquad (9.6)$$

$$N_2O + Ar \rightarrow N_2 + O(^3P) + Ar \qquad (9.7)$$

The $S(^1D)$ state which correlates directly with the ground-state of the OCS molecule lies higher in energy, so the potential energy diagram for the dissociation of OCS, with the C-S bond-length as the x-coordinate and the C-O bond-length fixed, exhibits curve crossing. So does that for N_2O, with the difference that the upper state for N_2O is purely repulsive whereas that for OCS has a small well [149]. The situation is shown in figure (9.2). The occurrence of curve-crossing modifies the usual unimolecular scheme (RRKM theory) for the dissociation of species A:

$$A_{sing} \overset{+M}{\rightleftharpoons} A^*_{sing} \rightleftharpoons A_{trip} \overset{+M}{\rightleftharpoons} A^*_{trip} \rightarrow A^{\#} \rightarrow \text{Products} \qquad (9.8)$$

Here $A^{\#}$ is the transition state, and * indicates internal excitation. The third step may not be necessary.

For N_2O, dissociation follows immediately after the singlet-triplet transition as the triplet state is unstable and repulsive. Energy is

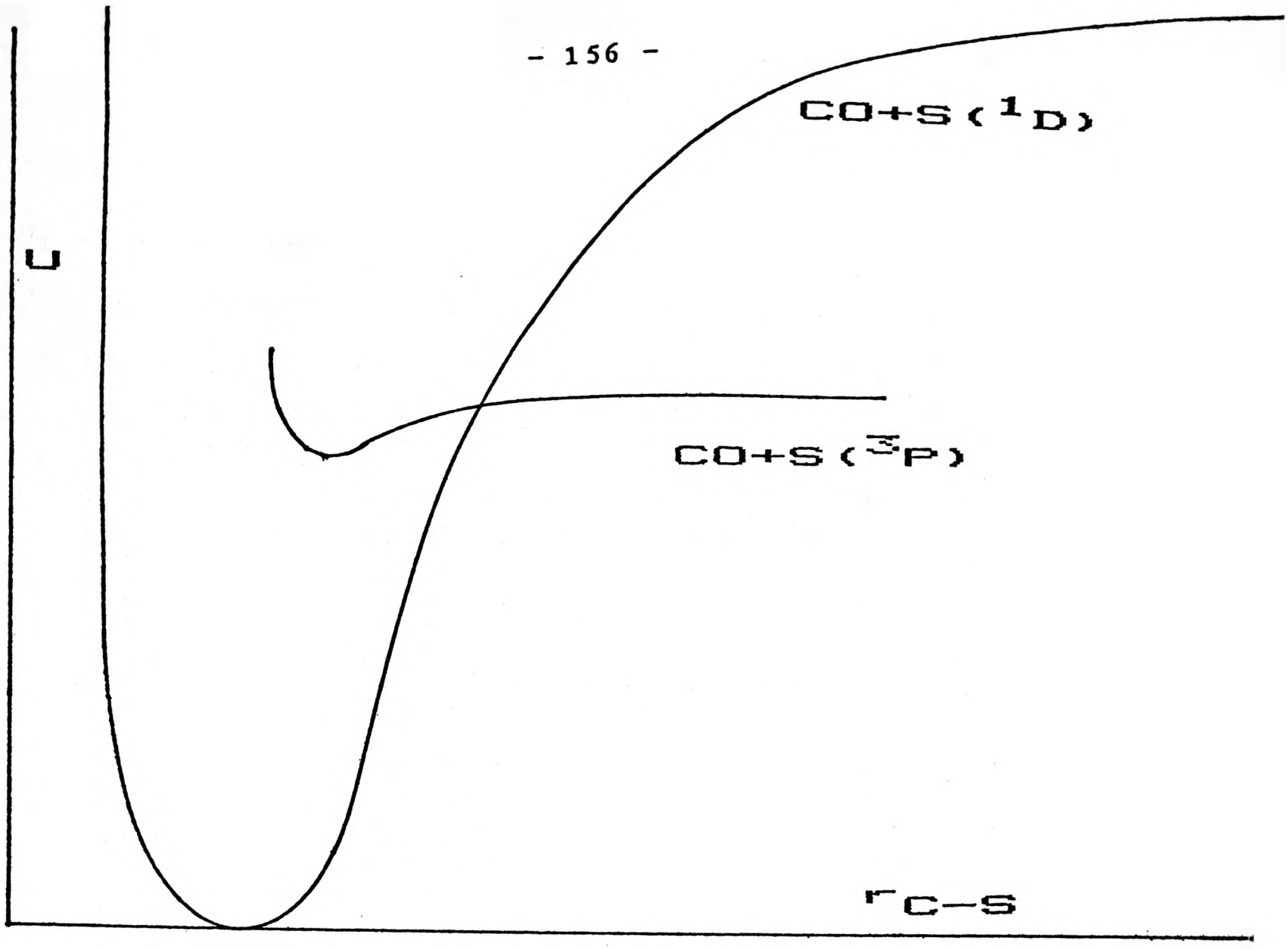
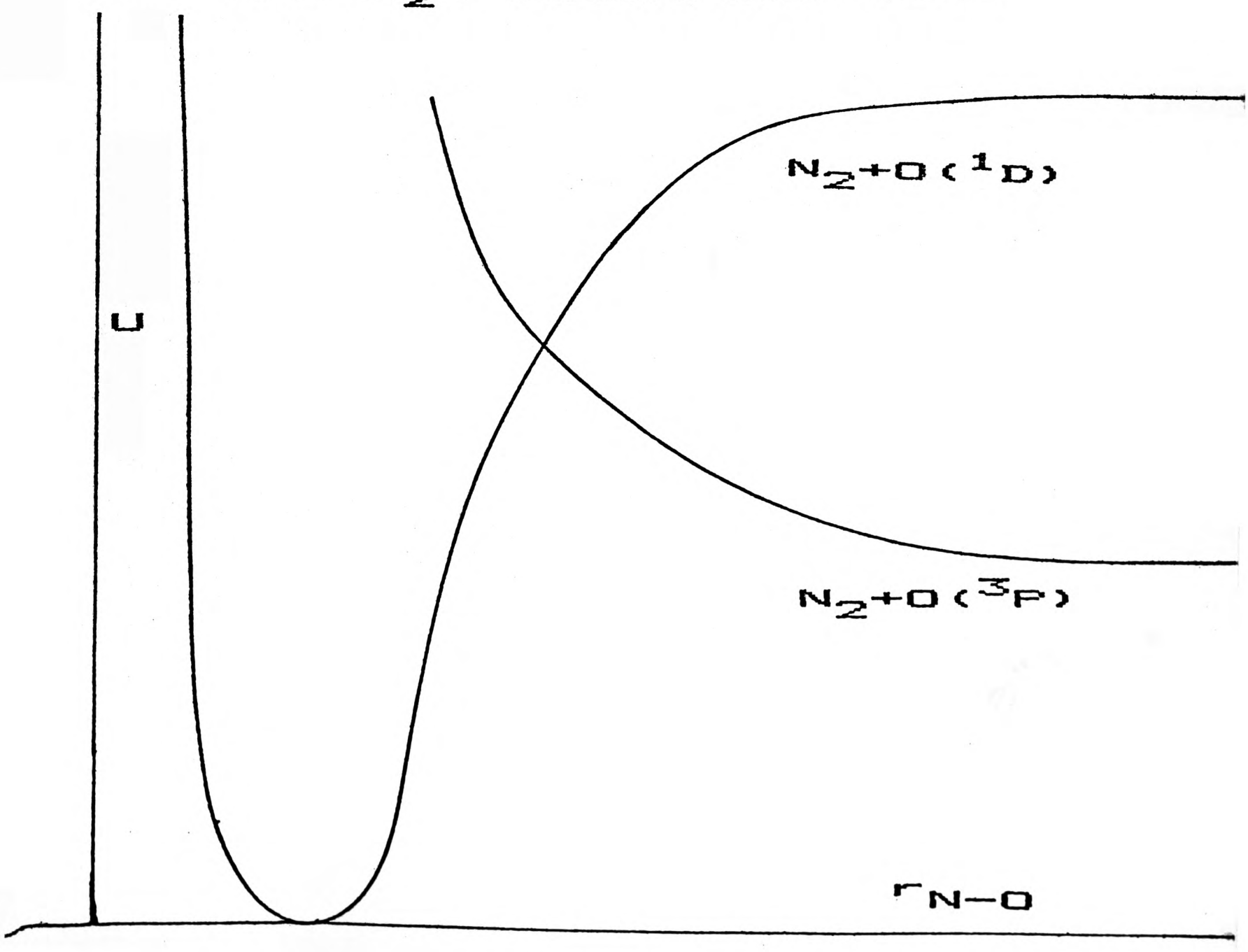


FIGURE 9.2

OCS AND N_2O DECOMPOSITIONS



released as the dissociation occurs and some is evidently gained by the N_2 vibration. The second collisional activation is not necessary. For OCS, the crossover occurs at an energy below the dissociation energy, and further energy must be put into the C-S bond before the break occurs. Troe and Wagner [150] state that in this case the extra energy required comes from the rotational energy of the OCS, so the second collisional excitation process is again unnecessary. It seems likely that energy also moves from the mainly C-O vibration ν_3 to the mainly C-S vibration ν_1, at this point and thus the CO is born vibrationally cold.

To summarise, from the different shapes of the potential curves we can see that, between the curve-crossing and the completion of the dissociation, the N_2 from N_2O can gain vibrational energy but the CO from OCS loses vibrational energy.

Experimental support for the dissociation occurring via curve-crossing into the ground atomic state rather than into the ^1D state is as follows [149]:

(i) The activation energy is not large enough compared to the energy required to reach that state, but does correlate with the energy required to reach the ^3P state.

(ii) The high pressure limit is reached at a much lower pressure than for spin-allowed dissociation of triatomics such as NO_2.

(iii) The pre-exponential factor in the high pressure limit expression for the rate constant is low compared to the spin-allowed dissociation of triatomics.

(ii) and (iii) follow as the rate constant k_3 of the normal unimolecular scheme,

$$A \underset{k_2[M]}{\overset{k_1[M]}{\rightleftharpoons}} A^* \xrightarrow{k_3} \text{Products} \qquad (9.9)$$

is lower than for direct dissociation as it includes a curve-crossing probability which is less than unity.

Our measurements have been in the low pressure region. It is interesting to speculate on whether CO would be born cold in the high pressure limit. The activation energy observed by Schecker and Wagner [147] is higher in the high pressure region (68 kcal.mol^{-1}) than the low pressure region (61 kcal.mol^{-1}). This is generally the case for unimolecular reactions, as explained in the following paragraph.

The experimental activation energy is a measure of the difference between the average energy of the reactant molecules and the average energy of the transition states. In RRKM theory molecules with enough energy to react are called energised molecules. These may proceed to transition states or be deactivated by a collision. In the high pressure limit, many of the energised molecules are deactivated before they can react. Therefore a greater proportion of the transition states come from energised molecules with higher energies which proceed more rapidly to transition states. The higher energy of transition states may well be reflected in higher internal energy of the products, so in general products would be expected to be born with a higher vibrational temperature in the high pressure limit. Spin-forbidden reactions are a special case however, and very little work has been done on energy disposal following thermally-initiated decomposition reactions, so we cannot be sure.

We shall return to the question of energy disposal in thermally-initiated unimolecular reactions in chapter 11 on current and future experiments. Meanwhile the OCS decomposition has provided what is possibly the first-ever observation of a product born vibrationally cold in a chemical reaction.

CHAPTER 10 - THE CO ISOTOPE EXCHANGE

10.1 Introduction

A study of the reaction

$$^{12}C^{18}O + {}^{13}C^{16}O \rightleftharpoons {}^{12}C^{16}O + {}^{13}C^{18}O \qquad (10.1)$$

was a logical follow-up to the work on CO vibrational relaxation recounted in chapter 6, for vibrational excitation of the reactants was thought to play a crucial role in the mechanism [151]. Here was a case where we might be able to determine non-equilibrium vibrational distributions in both reactants and products, making full use of our insight into vibrational relaxation processes to rationalise the results.

The experiments were more difficult than any others attempted in this work, and conclusive results were not obtained. Impurities were evidently to blame. However, significant advances in our understanding of the reaction did result. Firstly the contribution of two earlier studies will be described.

10.2 Previous Studies

The reaction was previously studied by Bar-Nun and Lifshitz [151], using a single-pulse shock tube (section 2.10), and by Bopp, Kern and O'Grady [152], using a shock tube with a time-of-flight mass spectrometer (section 2.11). The papers were published in 1968 and 1975 respectively.

Bar-Nun and Lifshitz found the activation energy too low for a mechanism via the dissociation of CO. The concentration of the argon

diluent was involved in the rate law, so more than one step was involved. They proposed a mechanism, the 'VEX' mechanism, in which, firstly, one molecule of CO is excited to a critical vibrational level, in the rate-determining step, and, secondly, the isotope exchange takes place between this molecule and another one. The latter step has a four-centre transition state. The following expression was found for the rate of exchange:

$$\text{rate} = k_b[CO]^{1.45}[Ar]^{0.55} \qquad (10.2)$$

with $k_b = 10^{14.36\pm0.42} \cdot e^{(-76\pm5)x10^3/RT}\ cm^3 mol^{-1} s^{-1}$.

From an analytical treatment of the kinetic equations, they were able to explain their rate law with a model in which the critical level lies between v=7 and v=10, and the order with respect to CO is greater than 1 either because some of the vibrational excitation is due to CO, or because the exchange itself is partially rate-limiting.

The products of the reaction were analysed by mass spectrometry. Experiments were carried out in the temperature range 2000-2675 K.

Since they used the single-pulse technique, Bar-Nun and Lifshitz had to assume that the product growth was exponential, but could obtain no evidence for this, as pointed out in section 2.10.

Bopp et al, using time-of-flight mass spectrometry, found that the product rise was exponential. They did not investigate the reaction orders but assumed that Bar-Nun and Lifshitz's applied. They carried out experiments on two different mixtures, E1 with 8 % CO, 11 % H_2, 1 % Ar and 80 % Ne, and E2 with 8 % CO, 20 % Kr and 72 % Ar. The second mixture had a relaxation time about 6 times as long as the first, but they obtained identical results for the rate of isotope exchange for

each mixture. They found this 'not surprising' despite the involvement of the diluent in the rate law.

Bopp et al's experiments were at higher temperatures than the earlier work, in the range 2900-4650 K. However the data could be plotted with that of Bar-Nun and Lifshitz on one Arrhenius plot, and the resultant activation energy had the lower value of 55.47 ± 0.89 kcal.mol^{-1}, corresponding to a critical level of v=5 to 7 according to Bar-Nun and Lifshitz's model. The pre-exponential factor became $10^{12.58 \pm 0.07}$.

Bopp at al. also conducted important non-shock-tube experiments on the exchange. They saturated the mixture E2 with mercury vapour and irradiated it using mercury lamps at room temperature. Such mercury-photosensitisation had been shown previously to produce vibrationally excited CO in the levels v=2-9, but with the isotopic mixture no exchange was observed. This they took to show that translational as well as vibrational energy is required for the exchange.

10.3 Discussion of Previous Work

After our work on vibrational relaxation of CO, we are in a position to understand more fully the mechanism postulated for the exchange.

At first sight, it seems that, since the vibrational relaxation time is known to be much faster than the exchange (~30 times for 1.7 % CO at 4000 K), vibrational relaxation of CO cannot be rate-determining. However, supposing the critical level is v=8, at 4000 K vibrational relaxation corresponds to 0.2 % of the molecules reaching v=8, whereas isotope exchange to equilibrium requires 25 % of the molecules to reach v=8; the latter is likely to take longer. This was pointed out by

Bar-Nun and Lifshitz in their earlier paper on isotope exchange in N_2 [32].

There seems to be no reason why, given that, say, 8 vibrational quanta are required in order that the isotope exchange may take place, all 8 vibrational quanta should be in the same molecule. A collision, for instance, between two molecules in the v=4 level is equally probable to a collision between one in v=0 and one in v=8 (only exactly equal for simple harmonic oscillators). Bar-Nun and Lifshitz [32] assumed one molecule was in v=0 to simplify their mathematics. They made further assumptions. Their treatment assumes a steady-state in the population of the critical level. They did not consider how long it would take for that steady-state to become established, so did not justify their assumption that the product concentration rises exponentially. Their neglect of the reverse isotope exchange is only justified at early times. We shall not detail the analytical treatment of Bar-Nun and Lifshitz here, as a comparison of the results with a numerical integration, involving fewer approximations, is more profitable.

If the vibrational relaxation is complete before significant isotope exchange occurs, as is the case experimentally, then the CO will be in a Boltzmann distribution at the translational temperature. Reaction from the critical level will tend to deplete the population in that level. (VT) and (VV) processes will tend to preserve the Boltzmann distribution. True, in the vibrational relaxation of CO following shock-heating, (VV) processes have no role to play, but this is only because the (VT) rate constants are such that relaxation via a continuous series of Boltzmann distributions is ensured. Once an outside process is added, which tends to destroy the Boltzmann distribution, the (VV) processes will be instrumental in opposing this. Therefore the outside process - the isotope exchange - must be faster

than the (VV) processes to deplete upper levels.

If the isotope exchange were not faster than the (VV) processes, the Boltzmann distribution would be preserved. The overall rate of the exchange process depends on the exchange rate constant times the fraction of molecules in the critical level. If the Boltzmann distribution were preserved despite the occurrence of the exchange, the fraction of molecules in the critical level would be constant at a particular temperature, so the overall rate would depend only on the rate of exchange and not on the vibrational relaxation. The reaction would be zero-order with respect to argon or other diluent in this case. The important conclusion of this argument is that the observation of a dependence of the reaction rate on the concentration of diluent means that the isotope exchange rate is faster than the (VV) rate. Since both rates depend on $[CO]^2$, this means that the isotope exchange rate constant is greater than the (VV) rate constant i.e. when two CO molecules collide with sufficient energy, it is more probable that they will exchange atoms than that they will exchange vibrational quanta. This might seem unlikely, but only a full consideration of the CO/CO potential hypersurface would bring certainty. In fact Smith and Wood [153] showed from trajectory calculations that, for an atom-diatomic exchange e.g. $H + H_2 \rightarrow H_2 + H$, atom exchange can be more rapid than vibrational energy transfer.

The results of Bar-Nun and Lifshitz and their interpretation of them in terms of the VEX mechanism imply that the isotope exchange is indeed faster than the (VV) processes. Evidently both (VT) and (VV) processes are important in the population of the critical level as the rate law is rate = $k_b[CO]^{1.45}[Ar]^{0.55}$. If (VT) alone were important it would be $k_b[CO]^1[Ar]^1$, and if (VV) alone $k_b[CO]^2$. In the dilute mixtures of Bar-Nun and Lifshitz (0.3 % and 1.7 %), the (VT) and (VV)

rates are comparable, so the involvement of each is sensible.

The potential surface for the reaction must be very nearly symmetrical, the reactants and products only differing isotopically, so if vibrational energy is necessary for the reactants, then the products must be born with the same vibrational energy. Therefore the isotope exchange does not remove vibrational energy from the system, so does not involve a change in vibrational temperature. Thus (VT) steps are not absolutely necessary to repopulate the critical level, but are of comparable importance to (VV) steps in sufficiently dilute mixtures.

Given that Bar-Nun and Lifshitz have established that vibrational relaxation is involved in the rate, the observation by Bopp et al. [152] that changing the vibrational relaxation time by a factor of 6 (by changing the diluent) does not effect the rate must be surprising. Yet Bopp et al. found this 'not surprising'. (They do not say why they decided to investigate this effect in the first place.) They stated that it was 'not surprising since the rate of exchange was in all experiments observed under the condition of vibrational equilibration'. This does not follow. As has been said above, vibrational equilibration corresponds to only a small percentage reaching upper levels, not the large percentage which pass through upper levels to react. Further, the Bar-Nun and Lifshitz reaction orders, which Bopp et al. assume, are inexplicable unless the overall rate depends on the rate of vibrational relaxation.

Bopp et al's paper is thus self-contradictory and brings the Bar-Nun and Lifshitz mechanism into question. However Bar-Nun and Lifshitz's reaction orders would not be expected to apply over a range of temperatures and concentrations beyond those of their own experiments. Since Bopp et al. used a higher percentage of CO (8 %), it may be that a rate law rate = $k[CO]^2$ is consistent with the VEX

mechanism in their case. Thus the VEX mechanism is not totally disproved by their findings. They should not, however, have assumed Bar-Nun and Lifshitz's reaction orders.

Bopp et al's paper contains useful information for formulating an acceptable mechanism. It shows that the results of Bopp et al. and of Bar-Nun and Lifshitz form a consistent set, and derives an energy of activation. The lack of exchange in the room temperature mercury photosensitisation experiment shows that vibrational energy alone cannot cause the exchange. Bopp et al. believed that a combination of vibrational and translational energy was required.

An alternative explanation of the mercury photosensitisation result is that the isotope exchange does not occur via the VEX mechanism at all, but by some other path which becomes more rapid at higher temperatures.

The obvious alternative is an atomic-chain mechanism:

$$^{12}C^{18}O + ^{16}O \rightleftharpoons ^{12}C^{16}O + ^{18}O \qquad (10.3)$$

$$^{13}C^{16}O + ^{18}O \rightleftharpoons ^{13}C^{18}O + ^{16}O \qquad (10.4)$$

The O-atoms are catalytic, so could come from a low-concentration impurity. The most likely source of O atoms is the reaction:

$$CO + O_2 \rightarrow CO_2 + O \qquad (10.5)$$

Bar-Nun and Lifshitz did not calculate the rate of this reaction for their known O_2 impurity concentration, but dismissed the O-atom mechanism on the basis of their observed order, which was not consistent with the known variation in their O_2 level. Bar-Nun and Lifshitz did

show that $O_2 + Ar \rightarrow 2O + Ar$ was slower than process (10.5). We shall return to the atomic mechanism in discussing our own results.

Bar-Nun and Lifshitz's results depend on the assumption that the product growth was exponential. If in reality there was an induction time, their rate constants and orders would be without meaning. Bopp et al. observed that the product growth was indeed exponential (which is linear at early times), but it is not clear how certain they were of the position of their time origin. Unfortunately they did not publish one of their traces of concentration against time or say over which part of the reaction they obtained their rate constant. The same group (Kern and coworkers) studied other isotope exchanges including $^{28}N_2 + {}^{30}N_2$ [154], $^{32}O_2 + {}^{36}O_2$ [155] and $H_2 + D_2$ [156] and found a zero initial slope in each of these cases. No reason was given for why the CO case should be different.

Comparison with the case of $H_2 + D_2$ provides reason to doubt the VEX mechanism. Early shock tube experiments e.g. [156] by the single-pulse and time-of-flight techniques on this system supported a VEX mechanism. However Lifshitz, Bidani and Carroll have recently published a paper [67] entitled 'The reaction $H_2 + D_2 \rightleftharpoons 2HD$. A long history of erroneous interpretation of shock tube results.' In it they clearly show that the apparent rate of the H_2/D_2 exchange has decreased over the years as successive investigators have used cleaner shock tubes. In their own ultraclean (see section 2.20) shock tube, Lifshitz et al. monitored the H atom concentration using ARAS (see section 2.17) and only observed HD production when they also observed H atoms.

As Lifshitz at al. point out, the VEX mechanism for $H_2 + D_2$ has also come into theoretical disrepute. Calculations of the $H_2 + D_2$ potential have failed to reveal any pathway via a 4-centre transition state with a lower activation energy than the dissociation energy of H_2.

Therefore the process is predicted to go via an atomic chain.

There is no reason why the case of the CO/CO potential should be expected to be different. Consideration of the overlap of p-orbitals in a hypothetical square transition state shows that the system would be anti-aromatic, involving 8 electrons, i.e destabilised. Indeed bimolecular reactions proceeding via 4-centre transition states are very rare, though not unknown. (An example is the elementary step $2HI \rightarrow H_2 + 2I$, the rate of which is enhanced by vibrational excitation of the HI [157].)

H atoms are a particularly difficult species to exclude from a shock tube as they can be formed from pump-oil molecules which have backstreamed into the tube. In the case of the CO exchange, H atoms cannot act as a catalyst, but C atoms could start a chain similar to the O-atom chain, and other hydrocarbon fragments may also be able to produce C or O from CO. Traces of water could initiate reaction via $H_2O+M \rightarrow OH+H+M$, $OH+CO \rightarrow CO_2+H$, $CO_2+M \rightarrow CO+O+M$. It is not difficult to suppose that a combination of other impurities and the O-atom chain from traces of O_2 could explain the results, given Lifshitz et al's work on the $H_2 + D_2$ system, and the doubts cast on the VEX mechanism by the results of Bopp et al. Bar-Nun and Lifshitz's reaction orders can be explained by some impurities originating in the CO samples, while some originate in the Ar sample or are knocked off the walls by the total gas pressure (largely Ar).

10.4 Experimental Conditions

Our shock tube is not ultraclean, so we were unable to carry out the ideally conclusive experiment of repeating the conditions of previous workers under very clean conditions and achieving no conversion, thus disproving the VEX mechanism. It was likely that our

results would be capable of interpretation by both VEX and atomic chain mechanisms. Computer models for both of these were set up, to compare with the results.

The immediate goal was to see whether we could obtain results consistent with those of other workers, in terms of the overall timescale of events, shape of curve for product growth and order with respect to CO and Ar.

When reactants are very expensive, as in this experiment, the incident shock technique has a major disadvantage relative to the reflected shock technique in that, in order to obtain given post-shock conditions, a greater initial pressure p_1 is required. Therefore we were very restricted in the number of shocks that could be run.

On the other hand, our method is much more direct than the time-of-flight technique and especially the single-pulse technique, and we normally expect it to provide more reliable results, although not as reliable as those obtained in the new ultraclean tubes. The single liquid-nitrogen trap between each of the diffusion pumps and the shock tube test section will not be sufficient to keep every pump-oil molecule out of the shock tube. However this is expected to be less of a problem for incident-shock than for reflected-shock studies. When the former technique is used, there is little time for molecules, which have been knocked off the walls by the shock wave, to diffuse into the main body of the test gas before the gas is probed.

It was apparent that our experiment would have to be done at a temperature above 4000 K for the process to be complete in our observation time, if the previous investigators' rate law was obeyed.

Initially a 1.7 % CO (50:50 isotope mix) in Ar mixture was used. The pressure had to be high enough for the process to be complete before

the arrival of the contact surface. At high pressures and temperatures, the noise is found to be larger, presumably because of unstable flow conditions. The driver pressures used in this experiment (up to 200 P.S.I. of hydrogen) were the highest used in all the experiments reported in this thesis. Line-broadening was greater than usual (~0.04 cm^{-1}) and with 4 isotopes of CO involved, there was a large chance of absorption by neighbouring lines. In calculating the optimum lines, the Dunham coefficients of Todd et al. [104] for $^{12}C^{16}O$, $^{13}C^{16}O$ and $^{12}C^{18}O$ had to be supplemented by those of Ross et al. [158] for $^{13}C^{18}O$.

This experiment was the most difficult to do of those considered in this thesis. Before changing conditions, one or more dummy shocks were run, with B.O.C. cp grade CO replacing the isotopic mixture, to ensure that the selected diaphragm produced the desired post-shock conditions. This also served to obtain the vibrational relaxation time of CO under these conditions, and check that after the relaxation the absorption did not change because of flow non-idealities. (The vibrational relaxation times were too fast to be determined accurately but consistent with Millikan's CO-Ar results.)

10.5 Results

B.O.C. research grade argon, 99.9995 % pure, was used as diluent in all experiments. After the experiments had been completed, the remaining $^{12}C^{18}O$ and $^{13}C^{16}O$ samples were analysed by mass spectrometer in the University of Oxford Clarendon Laboratory. The results were surprising, not to say bizarre. There was found to be a total of more than 3 % O_2 in the combined CO samples, including some $^{16}O^{17}O$ remarkably. According to the suppliers, B.O.C. / Amersham International (see below), the isotopic purities were 97.5 and 99.95 % respectively,

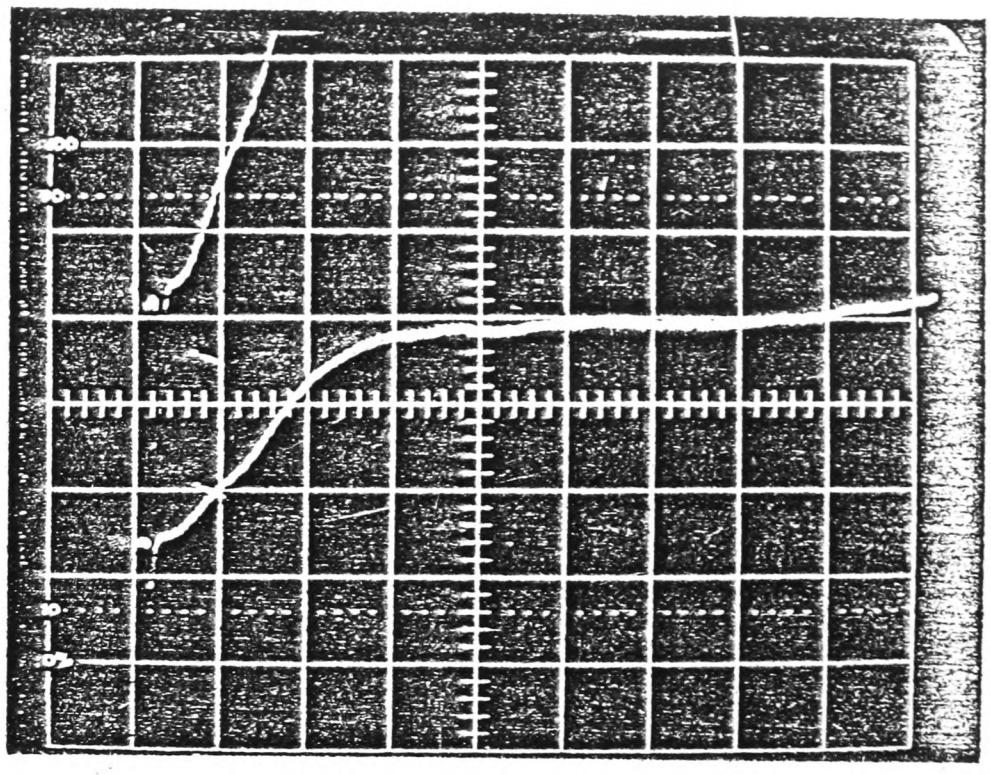
more pure than those used by the previous workers, and we had tacitly assumed that the chemical purity would be better also. The manufacturers could not explain the presence of $^{16}O^{17}O$. Communications with the manufacturers were hindered by the purchase of B.O.C.'s Prochem business by Amersham International, neither company wishing to assume responsibility for the gas purity. The mass 28 / mass 32 ratio shows that leakage of air was not responsible for impurities.

Given the high level of O_2, it is extremely likely that the isotope exchange proceeds via an atomic chain mechanism in our experiments. This does not make the results inconsequential, as we shall see.

The initial conditions chosen were T_2~4500 K, p_2~1600 torr, using a 3->2P(9) laser line, and mixture composition 1.7 % CO (50:50 isotope mix), 98.3 % Ar, chosen to match one of Bar-Nun and Lifshitz's mixtures. The signal-to-noise was unsatisfactory here, so it was repeated with 3.4 % CO. The result obtained is shown in figure 10.1, top trace. The experiments were carried out before the installation of the transient recorder and computer. The initial jump is due to the presence of $^{12}C^{16}O$ in the reactant samples, plus a chance coincidence with a product transition.

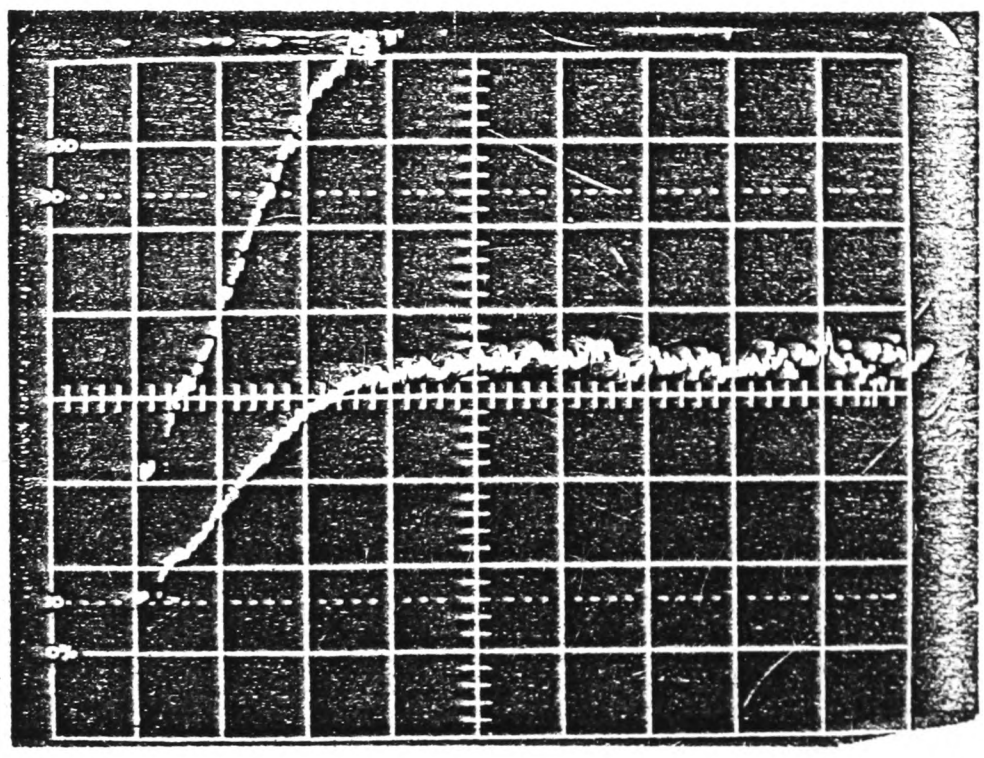
A very important result is provided immediately: after the initial jump, the trace shows zero initial slope for the growth in the population of the exchange products. This contradicts Bopp et al's results. The overall timescale of our results is consistent with that of Bopp et al, so there is no question that we were observing a much more rapid process. The presence of an 'induction time' is in fact to be expected, for either an atomic or a molecular mechanism, for a process going via more than one step with the first step (at least partially) rate determining. This is because the O-atom concentration, or population of the critical vibrational level, builds up before the

FIGURE 10.1



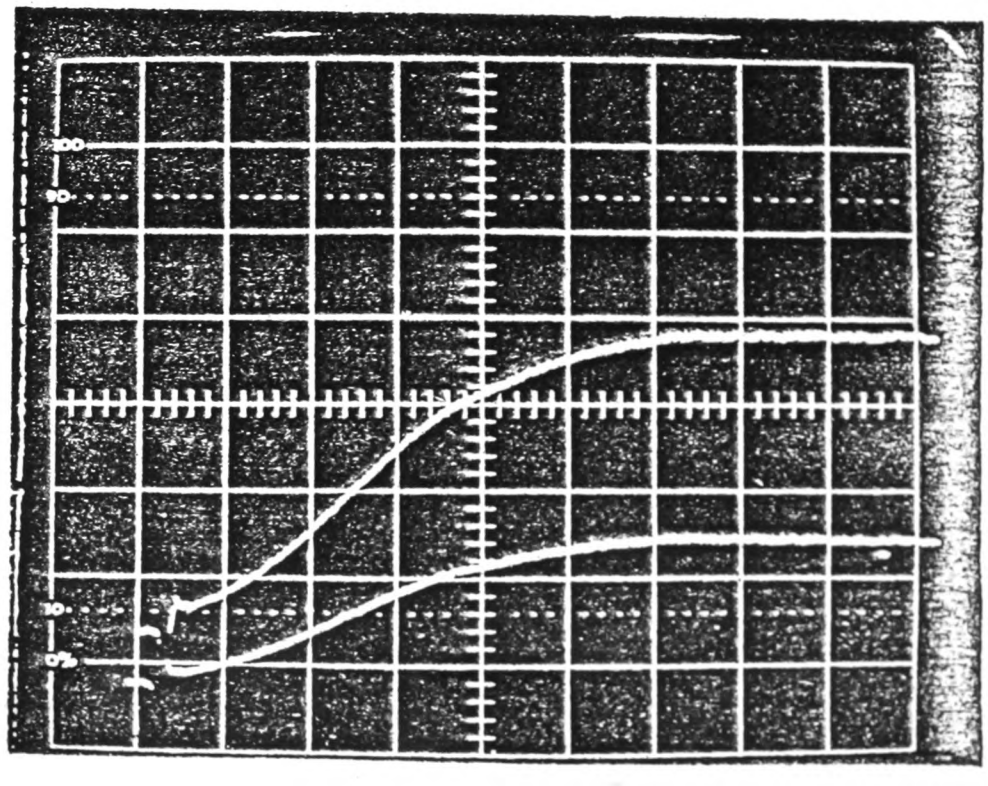
$P_{CO}=67$

$P_{Ar}=360$



$P_{CO}=61$

$P_{Ar}=1495$



$P_{CO}=139$

$P_{Ar}=750$

maximum rate of reaction is reached.

The observation of a non-exponential product growth had immediate ramifications. There was now no simple way to determine a rate constant from the experimental trace, so we could not directly test Bar-Nun and Lifshitz's experimental rate law. The rate constants derived by the previous workers have no precise meaning, but must be taken as a guide to the rate of the overall process.

It is surprising that Bopp et al. did not observe zero initial slope. Our method could not show a schlieren spike, corresponding to the time origin, and then a zero initial slope, when a zero initial slope does not exist, so we believe that Bopp et al's results are wrong and ours right in this respect.

It was not possible for us to go on to deduce values for the order of reaction with respect to CO and Ar, but we could test the qualitative changes brought about by changes in the partial pressure of CO and Ar at constant temperature. It was decided to reduce p_{Ar} as far as possible for constant p_{CO} and see whether the rate decreased.

For each shock, the time for the laser absorption trace to reach (1-1/e) of its final equilibrium value was recorded. This gave a guide to the overall rate. Since these figures should not be overinterpreted, they are not listed here. Attempts were made to extract more meaningful data, e.g. by plotting log(-gain) against time and trying to extract an induction time and subsequent rate constant, but no self-consistent set of figures was forthcoming.

Eighteen $^{12}C^{18}O/^{13}C^{16}O/Ar$ shocks were fired. The post-shock temperature was held approximately constant. The hottest and coldest shocks were at 4703 K and 4164 K; twelve of the shocks had temperatures between 4340 and 4550 K. The temperature quoted is that calculated for

vibrationally relaxed CO; the isotope exchange was assumed not to change the temperature, as the specific enthalpy of each isotope was assumed equal to that of $^{12}C^{16}O$. Calculations assuming that the vibration is simple harmonic show that the differences in specific enthalpy between the isotopes are less than 1 % at all temperatures.

With the partial pressure of CO in the range 56-67 torr, the partial pressure of Ar was varied from 1495 to 88 torr. This should have made the overall process 5 times slower, according to Bar-Nun and Lifshitz's $[Ar]^{0.55}$ dependence. The decrease in rate observed by us was by less than a factor of 2. p_{Ar} could not be reduced to zero, because of the resultant arrival of the contact surface before the completion of reaction.

Varying the total pressure for constant composition increased the rate but apparently not quite as much as expected for an overall reaction order of 2.0.

The shape of the overall curve did not change markedly with p_{CO} or p_{Ar}. Some sample results are shown in figure 10.1. The change in size of the initial jump is due to a change in the magnitude of the pressure-broadening altering the effect of a close frequency coincidence.

Repeating the same experiment on different days gave good reproducibility, even when the $^{12}C^{18}O$ bulb was replaced with a new one. Increasing pre-shock pumping time to 4 hours did not significantly reduce the rate.

All shocks were run with the laser on 3->2P(9) except one with it on 5->4P(11) which gave a thoroughly consistent result. Different product levels are not expected to rise at different rates, certainly for the atomic mechanism. Owing to the lack of materials and large

possibility of failure due to chance coincidences, no further lines were tried. A single experiment to monitor a reactant transition, running the laser on $^{13}C^{16}O$ failed as absorption by product and reactant occurred to approximately equal extents, giving a rapid rise followed by a horizontal line.

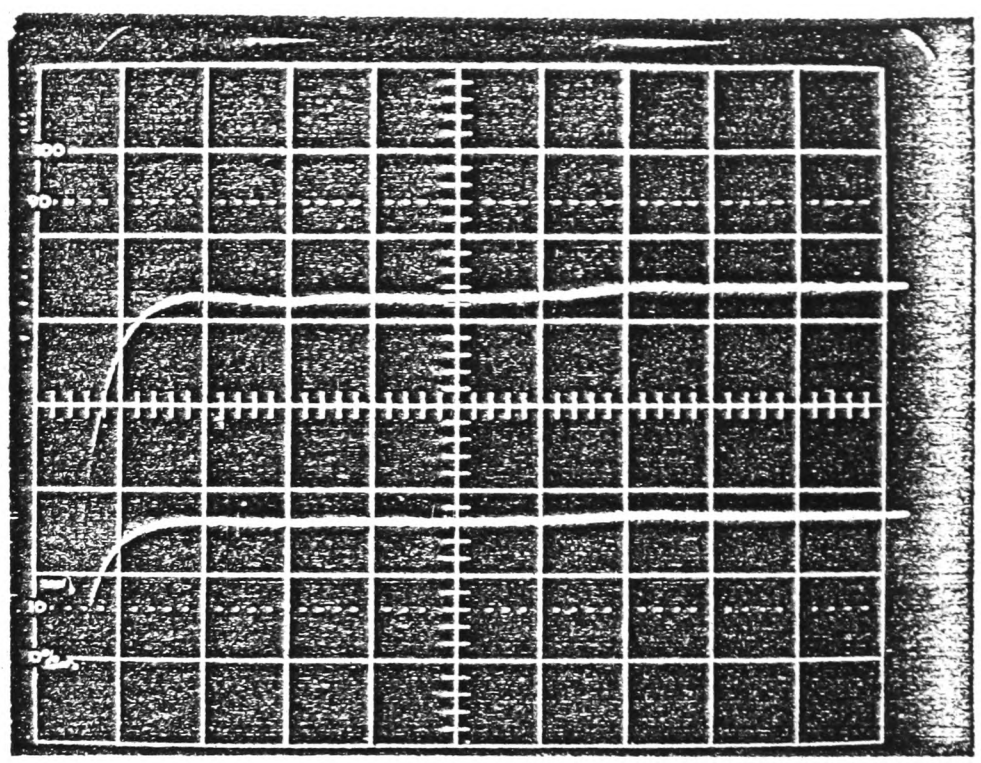
The times corresponding to (1-1/e) of equilibrium were in general agreement with Bopp et al's rates. A smaller dependence on [Ar] than expected is shown. All our results except the two with highest p_{CO} are faster than their best-fit straight line, although in our temperature range their own results tend to lie above that line also.

In order to investigate the isotope exchange under conditions where an atomic mechanism was clearly responsible, two experiments were carried out with N_2O added to the $^{12}C^{18}O/^{13}C^{16}O/Ar$ mixture. The compositions were 69 % Ar, 30.7 % CO (50:50 isotope mix), 0.306 % N_2O and 68.7 % Ar, 31.2 % CO, 0.076 % N_2O; pressures were 401 and 395 torr; temperatures were 4473 and 4439 K. N_2O is often used in shock tube experiments as a source of O atoms, e.g. [46]. The rate of its decomposition is well known [149]; under our conditions it is fast compared to the exchange. The two N_2O result are shown in figure 10.2. The rise is now approximately exponential, since the O-atom concentration reaches its equilibrium (100 % dissociation of N_2O) value very rapidly. That there is a very short induction-time is shown by the fact that the schlieren spike rises and falls before the signal rise. For processes that happen immediately the gas is shock-heated, e.g. the population of level v=1 in a vibrational relaxation experiment, the signal does not fall to the baseline following the spike.

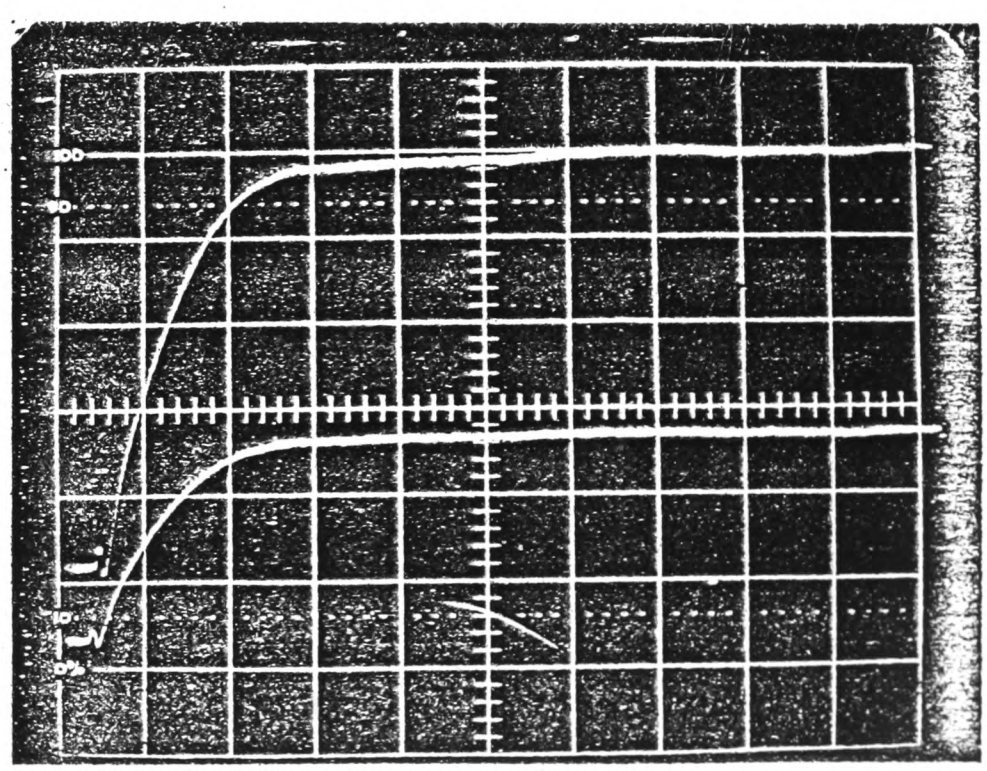
The system with added N_2O had comparatively simple kinetics to be modelled by the computer numerical integration program. The modelling of the results is discussed in the next section.

FIGURE 10.2

0.306 % N_2O



0.076 % N_2O



10.6 Modelling of Isotope Exchange

The N_2O results were modelled using the following scheme:

$$N_2{}^{16}O + M \xrightarrow{k_D} N_2 + {}^{16}O + M \qquad (10.6)$$

$${}^{16}O + {}^{12}C{}^{18}O \underset{k_{iso}}{\overset{k_{iso}}{\rightleftharpoons}} {}^{18}O + {}^{12}C{}^{16}O \qquad (10.7)$$

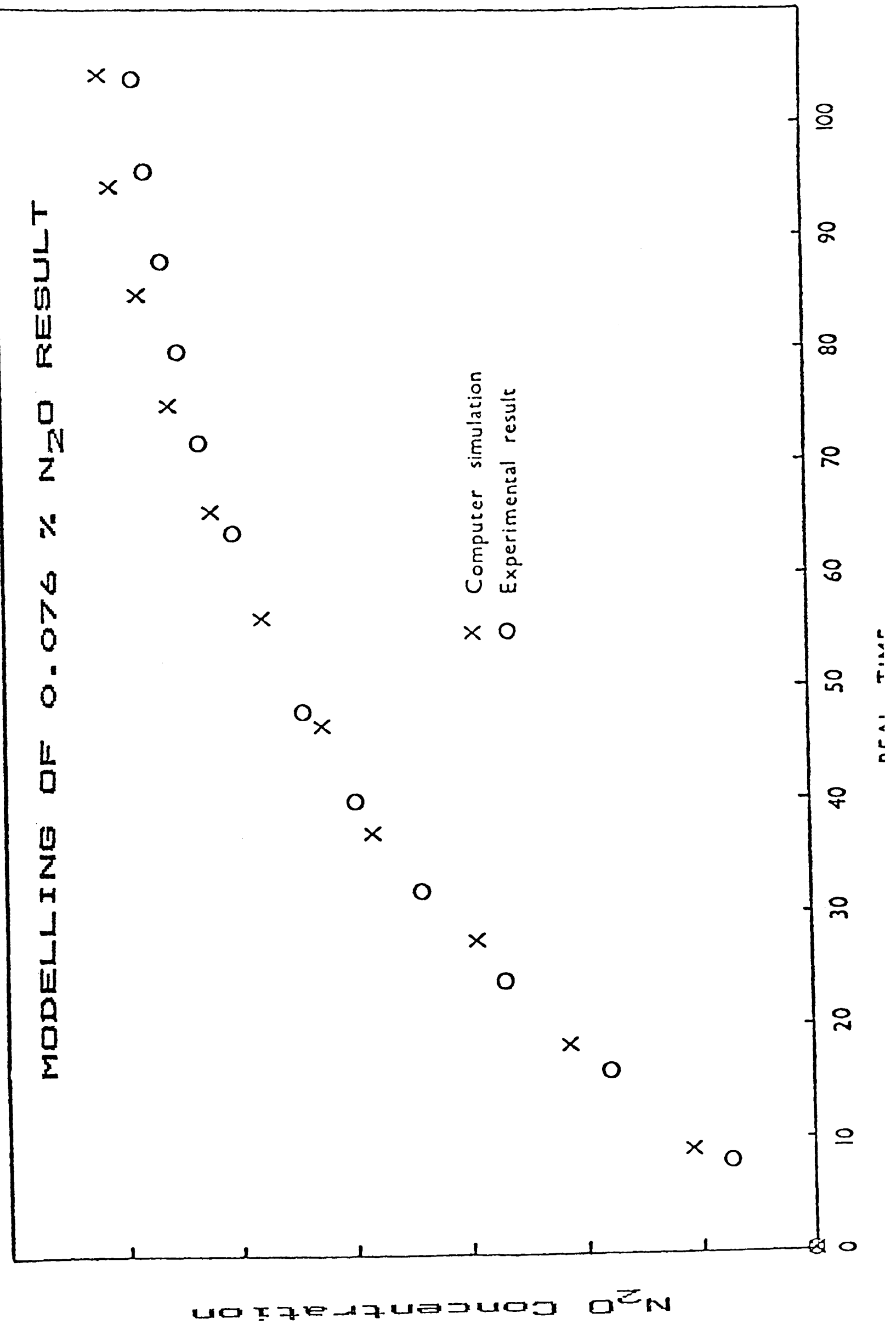
$${}^{18}O + {}^{13}C{}^{16}O \underset{k_{iso}}{\overset{k_{iso}}{\rightleftharpoons}} {}^{16}O + {}^{13}C{}^{18}O \qquad (10.8)$$

For k_D, the value of $5x10^{14}e^{-58,000/RT}$ $cm^3mol^{-1}s^{-1}$ (all activation energies in kcal per mole) as given in Troe and Wagner [149] was used. The reverse reaction was not allowed for as dissociation is 100 % under our conditions. For k_{iso}, the value of $6.2x10^{10}e^{-6,900/RT}$ $cm^3mol^{-1}s^{-1}$, obtained by Jaffe and Klein [159], was used.

The model program of section 5.5 was adapted. For this case the subroutine containing the differential equations was completely altered. Reference to different vibrational levels of CO was eliminated. The simulation was run for the conditions of the 0.076 % N_2O result (CO:N_2O=400:1) and the excellent fit obtained is shown in figure 10.3. Our result is thus consistent with the rate constants previously obtained, so the atomic mechanism certainly applies with added N_2O.

The computer simulation shows that it takes 20 μs for the O-atom concentration to reach 99 % of its final value. Vibrationally-excited N_2 from the N_2O decomposition could not be responsible for reaction, as there is an insignificant quantity of it. Each N_2 molecule can only pass its vibrational energy to CO once, whereas the O-atoms start a

FIGURE 10-3


MODELLING OF 0.076 % N2O RESULT
Computer simulation
Experimental result
N2O Concentration
0
10
20
30
40
50
60
70
80
90
100

chain so are effective despite being in such a small quantity.

It was now attempted to model the results in the absence of N_2O. First the possibility of the exchange being initiated by the decomposition of CO,

$$CO + Ar \rightarrow C + O + Ar \qquad (10.9)$$

was considered. The mechanism of the decomposition of CO is complex [160,161], but equation (10.9) as it stands is responsible for the initial rate as measured by Fairbairn [161] - the rate constant is $10^{-10}T^{1/2}e^{-256,000/RT}$ $cm^3molecule^{-1}s^{-1}$. The model program shows that this is seven orders of magnitude too low to explain our results.

Attention therefore switched to O-atoms generated by:

$$CO + O_2 \rightarrow CO_2 + O \qquad (10.10)$$

The rate constant of this has been measured by Sultzmann et al. [162] as $3.5x10^{12}e^{-51,000/RT}$ $cm^3mol^{-1}s^{-1}$. Again the reverse rate constant was not included in the model as the equilibrium is so far to the right, CO being in vast excess over O_2. The assumption of 0.3 % O_2 in the mixture (i.e. $CO:O_2$=100:1) was necessary to give a reasonable fit.

The model was now adjusted to simulate one of Bar-Nun and Lifshitz's results. Their shock no. 55 was chosen. By their own reckoning, 70 ppm of O_2 were present. Again using Sultzmann et al's rate constant for process (10.10) and Jaffe and Klein's for (10.7)/(10.8), the model gives 7 % conversion after 880 ms. 13 % conversion was observed by Bar-Nun and Lifshitz. Clearly the atomic mechanism should not have been utterly dismissed. A small adjustment in one of the rate constants, or the presence of 150 ppm of O_2, would

explain their result entirely as due to the atomic mechanism.

The VEX mechanism was also modelled. In this case individual levels v=0 to v=8, of reactants and products, were considered. This was an adaptation of the existing program with all the (VT) and (VV) processes kept in. An isotope exchange step was added, it being assumed that any collision between two molecules having 8 vibrational quanta between them could lead to exchange. The vibrational states of the products were assumed to be the same as those of the reactant molecules. A reasonable fit to the results could be obtained but only with the isotope exchange rate constant greater than the (VV) rate constant. A similar fit could have been obtained with lower isotope exchange rate constant but less than 8 quanta required. It would only be possible to distinguish the possibilities by comparing experimental results and computer calculations carried out over a range of temperatures. Since it is clear that a chain mechanism is responsible for our results, this matter was not pursued further.

10.7 Discussion and Conclusion

The mass spectral analysis showed more than enough O_2 present in the isotopes to explain our results. In fact the slowness of our results is puzzling, given the presence of so much O_2. The analysis is in doubt itself because of the presence of $^{16}O^{17}O$ to the bewilderment of ourselves and the suppliers. It used the last of our $^{12}C^{18}O$ sample so could not be repeated. An exact fit of theoretical rate constants to our results is thus impossible.

We are certain that our results can be explained by an atomic chain mechanism, and believe this also applies to the results of previous investigators. The principle reasons for this are:

1) A atomic chain initiated by $CO + O_2 \rightarrow CO_2 + O$ can explain the

results of Bar-Nun and Lifshitz and of ourselves, with realistic initial quantities of O_2. The activation energy of the CO/O_2 process, 51 ± 7 kcal.mol^{-1}, agrees with the activation energy for the isotope exchange process, 55 ± 1 kcal.mol^{-1}.

2) It has been shown on both experimental and theoretical grounds that the analogous $H_2 + D_2 \rightarrow 2HD$ reaction proceeds via an atomic chain mechanism.

3) The results of Bopp et al. cast doubt on the VEX mechanism, in that (i) they found that the rate of exchange does not depend on the identity of the diluent, and (ii) they failed to observe exchange in the mercury photosensitisation experiment.

Our observation that the process has an induction time conflicts with Bopp et al, but is to be expected for either VEX or atomic mechanism.

It is not intended to doubt that any bimolecular reaction proceeds via a 4-centre transition state. Isotope exchange reactions represent a special class for which the potential hypersurface is very nearly symmetrical with respect to reactants and products. Where the products are chemically different to the reactants, the barrier on the potential energy surface may be early, or late, and the situation will be different.

10.8 Future Work

Extremely pure gases are clearly required for a conclusive investigation, and a reaction as sensitive to impurities as this one is probably best done in an ultraclean shock tube. It is the intention of this group to remove samples of test gas immediately before shocks are fired, and subsequently analyse the samples in the mass spectrometer in the Clarendon laboratory, as a regular procedure, to test our

'cleanliness'. This has not yet begun, as at present there is nobody available in Oxford who knows how the mass spectrometer works and who can teach us. It will be worthwhile to investigate the exchange further, as long as the concentration of impurities are precisely known.

It is certainly possible for us to study the isotope exchange initiated by known amounts of O-atom producers, as we did with N_2O. A detailed investigation of the N_2O-initiated exchange would not be very interesting, as it seems that it would only confirm the values of the previously determined rate constants of a simple mechanism. Our two N_2O results indeed do this already. An investigation of the $CO+O_2$-initiated exchange would be more interesting. The mechanism may be more complex than that given above. The various processes included by Pilling and Noyes [163] in their model of the CO/O_2 explosion should be considered. For instance the CO_2 formed in reaction (10.10) can decompose, producing another O-atom. Also, is reaction (10.10) really a bimolecular reaction with a four-centre transition state, as it is written? Pilling and Noyes did include it as the initial step in their model, but with a smaller rate constant.

Future work in general will be considered in the final chapter.

10.9 Postscript

Very recently (June 1984), a third paper on the CO isotope exchange, by Rockwood, Bahler and McCullough [164] has been published. The authors agree with many of the arguments put forward here. They updated Bopp et al's photosensitisation experiments, and concluded that exchange did not take place from levels $v \leq 9$. They doubted that the VEX mechanism occurred via higher levels, but could not prove this. (It seemed more likely that in the photosensitisation experiment the exchange observed occurred via formation of CO_2 from electronically

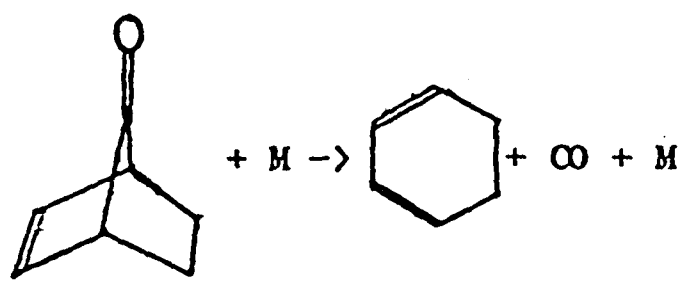
excited CO.) They did not do shock tube experiments of their own, but they modelled Bar-Nun and Lifshitz's and Bopp at al's results. Like us they concluded an atomic mechanism could explain the former results, but were puzzled by Bopp et al's. Their model could not reproduce the exponential rise of product. Our own observation of a zero-initial slope under similar conditions is therefore important.

CHAPTER 11 -CURRENT AND FUTURE WORK

11.1 Unimolecular Decompositions

Following the successful completion of the OCS experiment (chapter 9), it was decided to pursue studies of other unimolecular decompositions that produced CO. Attempts to determine the vibrational distribution of CO from the decomposition of CO_2 were unsuccessful as (i) all low CO laser lines are also absorbed by hot CO_2, and (ii) the decomposition of CO_2 is slower than that of OCS, and thus could not be made fast relative to energy transfer in the product CO. Rate constants for the decomposition were obtained however [6].

A reaction was sought which gave CO cleanly (i.e. no alternative products) and which was believed to be genuinely unimolecular. To fulfill the latter condition, it is a help if the other decomposition product is stable. Radical products e.g. S from OCS, may react with the parent as in $OCS + S \rightarrow CO + S_2$ and provide an alternative to unimolecular decay. Attention switched to relatively large organic molecules which might give stable products. The first reaction studied was:



$$+ M \rightarrow + CO + M \qquad (11.1)$$

The reactant is norbornen-7-one (bicyclo[2,2,1]hept-2-ene-7-one). The reaction had been observed before in the gas-phase and was known to be clean. The decomposition is classified by the Woodward-Hoffman rules as a cheletropic reaction, and allowed as a concerted process [165].

Norbornenone was studied rather than the simpler analogue 3-cyclopentenone because no information was found on the thermal decomposition of the latter. The decomposition of cyclopropenone to give acetylene and CO was impractical because of the tendency of the reactant to polymerise [166].

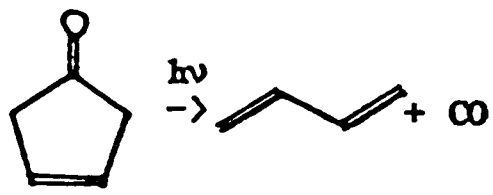
It is not certain whether reaction (11.1) is exothermic or endothermic, as there are no details on the thermochemistry of norbornenone (or of its vibrational frequencies from which the specific enthalpy could be estimated) and therefore it had to be assumed that the vibrational relaxation and the reaction were isothermal in calculating the shock tube conditions. Very dilute mixtures (< 1 %) were employed to minimise the error. The data analysis to calculate decomposition rate constants was as for the OCS decomposition, but making use of the transient recorder and computer.

The potential energy surface for a reaction like (11.1) is very different from that for the decomposition of OCS. The principal difference is that both products are stable, so there is a hump in the graph of potential energy against reaction co-ordinate. Therefore energy is released as the transition state passes over to the products, and whether the CO is born vibrationally excited is a point of interest.

The results of the experiment are discussed elsewhere [167-169]. They are outlined here in so far as is necessary for a discussion of future work. Experiments were carried out in the low-pressure region and fall-off region. The CO was found to be born vibrationally cold. This result may be explained as follows. In the low-pressure limit, where collisional activation is rate limiting, the molecules that undergo decomposition will only just have enough energy to surmount the barrier. All the energy will be concentrated in the breaking bonds, with none left over for the CO vibration. At the transition state, the CO is

almost free already, with its equilibrium bond-length i.e the products are already 'decoupled'. As the decomposition proceeds further and energy is released, it does not therefore go into the CO vibration and since the fragments are decoupled inter-fragment (VV) does not occur.

The deduction that the energy released after the transition state does not go into the vibration of CO, has also been made by Sonobe, Fletcher and Rosenfeld [9] who studied the 'photofragmentation' of 3-cyclopentenone:



(11.2)

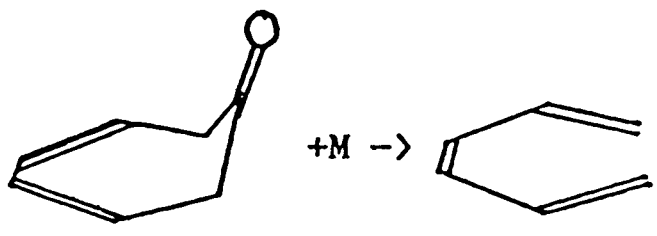
Their technique differs from ours in that the energy to surmount the barrier is provided by a laser pulse, rather than thermally. In their case, more than enough energy is provided, and the CO is born vibrationally hot. The energy in the CO corresponds to its statistical share of the energy difference between the laser energy and the barrier height, so again it seems that the energy release as the potential surface goes downhill after the barrier is not into the CO vibration.

Since the subject of energy disposal in unimolecular decompositions is of great current interest, and since the Simpson group is the only one looking at thermal rather than photolytic decompositions, it is likely that the group will carry out further investigations of reactions similar to (11.1).

An investigation of 3-cyclopentenone would complement the work of Sonobe et al. very neatly. In their technique the reactant is excited to an electronically excited state by the laser pulse, but Sonobe et al. believe that internal conversion to the ground electronic state occurs

when the geometry is still reactant-like, so the decomposition would occur from the same potential surface in both shock tube and photolysis experiments. It is unlikely that the result of the shock tube experiment will be markedly different from the the result for the similar molecule norbornenone. Indeed Dolbier and Frey [170] concluded that the thermal decomposition of 3-cyclopentenone had a product-like transition state, which is consistent with the discussion of the mechanism for norbornenone. They measured the entropy of activation in a kinetic study in the gas-phase using product analysis.

The unimolecular phase of the shock tube section of the Simpson group could well be brief. Experiment and theory are beginning to suggest that the birth of vibrationally cold products is normal from thermally-induced unimolecular decompositions. Experiments verifying this for molecule after molecule will become progressively less interesting. It will soon become sensible only to carry out experiments on decompositions for which there is some theoretical grounds for expecting a different result - such a molecule is 3,5-cycloheptadienone, on which Carpenter has proposed that we perform an experiment [171]. This is an isomer of norbornenone and gives hexatriene and CO:



(11.3)

The major difference is that the transition state for the concerted decomposition of 3,5-cycloheptatriene (CHT) involves a 4n delocalised electron system, whereas for 3-cyclopentenone (CP) there is a 4n+2 electron system. According to the Woodward-Hoffman rules, the concerted

decomposition of CHT must involve a conrotatary motion of the CH_2 groups adjacent to the expelled CO [165]. This is a larger rotation than the disrotatary motion of the CH_2 groups in CP. Carpenter suggests that the CO bond energy is not very well coupled to the energy of this rotation. In the low pressure limit, there is a lot of time for rearrangement of internal energy before deactivation or activation, so if energy can flow rapidly from the C-O vibration to where it is needed for the decomposition to take place, then it will, and the CO will be born vibrationally cold. In this case, if energy flow from the C-O vibration to the CH_2 rotation is slow, the CO may be born hot.

The thermal decomposition of N_2O (section 9.3) is an example where a vibrationally hot product was said to be produced. This result has been called into doubt by Troe [172], but in any case the potential energy surface for triatomics is different from that for large molecules. For triatomics, the diatomic fragment is the larger one, and the only one that can possess vibrational and rotational energy. For the diatomic to be born vibrationally cold, all the energy release must go into translation and rotation.

For norbornenone, as well as the vibrational product distribution, activation energies have been calculated, and the pressure-dependence of the reaction investigated [168]. If an experiment is limited to an investigation of the vibrational product distribution, it can be carried out rapidly, and it will be more interesting to carry out investigations of vibrational product distributions for several molecules, rather than detailed kinetic studies for a few. Traditional kinetic parameters are most useful in the high-pressure region, which is often difficult to reach, particularly behind the incident shock. Detailed studies of unimolecular kinetics are perhaps best left to reflected shock workers e.g. the comparative-rate single-pulse technique [33] (see section 2.10)

or workers using incident and reflected shocks to obtain a wide pressure range. e.g [173].

As well as decompositions forming CO, studies of decompositions giving other diatomic molecules which can be monitored with the CO laser are possible. DCl has been monitored by us, as described in chapter 7. Therefore the elimination of DCl from deuterated vinyl chloride is a possibility. The potential surface here is quite different here as the D-Cl bond is a new one. However preliminary investigations have failed to find a good coincidence with a 1->0 transition in DCl.

We have found a good coincidence with a 1->0 transition of NO using the 7->6P(13) line of $^{12}C^{16}O$. The line monitored is the $^2\Pi_{3/2}$ 1->0P(39/2) line in NO [57]. For NO, a good coincidence with a 2->1 line has not been found, but use of the 1->0 line would make it possible to observe any overpopulation in v=0 from the decomposition, for example that of CF_3NO. The rate of decomposition of CF_3NO has been studied in a shock tube by Glanzer et al. [174]. Roellig et al. [175] have performed a vibrational analysis of the newly-born NO following photofragmentation of CF_3NO.

The observation of the vibrational product distribution implies nothing about the rotational product distribution. Rotational relaxation is generally very fast, so any non-equilibrium distribution will generally become equilibrated before it can be observed. However see section 11.3 for remarks on possible observation of rotational effects.

While on the subject of decompositions, note that the decomposition of CO itself [160,161] occurs at temperatures too high for us to work at in conditions of good flow. A study would not be a neat follow-up to our vibrational relaxation work anyway, as the mechanism is not via

vibrational ladder-climbing as for N_2 [134], but is thought to proceed either via C_2, or via an electronically excited state of CO [160].

11.2 General Reaction Kinetics

There are numerous systems involving CO that could be studied, including the oxidation of most carbon-containing molecules. Therefore there is a need for criteria to decide which reactions should be investigated.

The system should be one on which there is interest, on practical or theoretical grounds. To make the best use of our shock tube / CO laser combination, the experiment should obtain information that could not be obtained by an alternative technique. The observation of different vibrational levels is the best example of this. Observation of one isotope of CO in the presence of others is performed more directly than by time-of-flight mass spectrometry. An isotope exchange could not be studied by emission, due to the overlap of bands from the different isotopes. Generally, CO may be observed by emission or absorption. The latter is more sensitive so is an improvement, even when specific vibrational levels are not of interest.

The system must be one which is not so complex that no useful information can be obtained. An ever-present danger is absorption by other species, of which CO_2 is prominent. CO_2 does not absorb CO laser radiation at room temperature, but does at shock tube temperatures when higher levels are populated. Reactions forming significant quantities of CO_2 should be avoided. However correction for CO_2 absorption should be easier than correction for CO_2 emission, as the identity of the species responsible is known more precisely.

Where the interest is in rate constants rather than vibrational

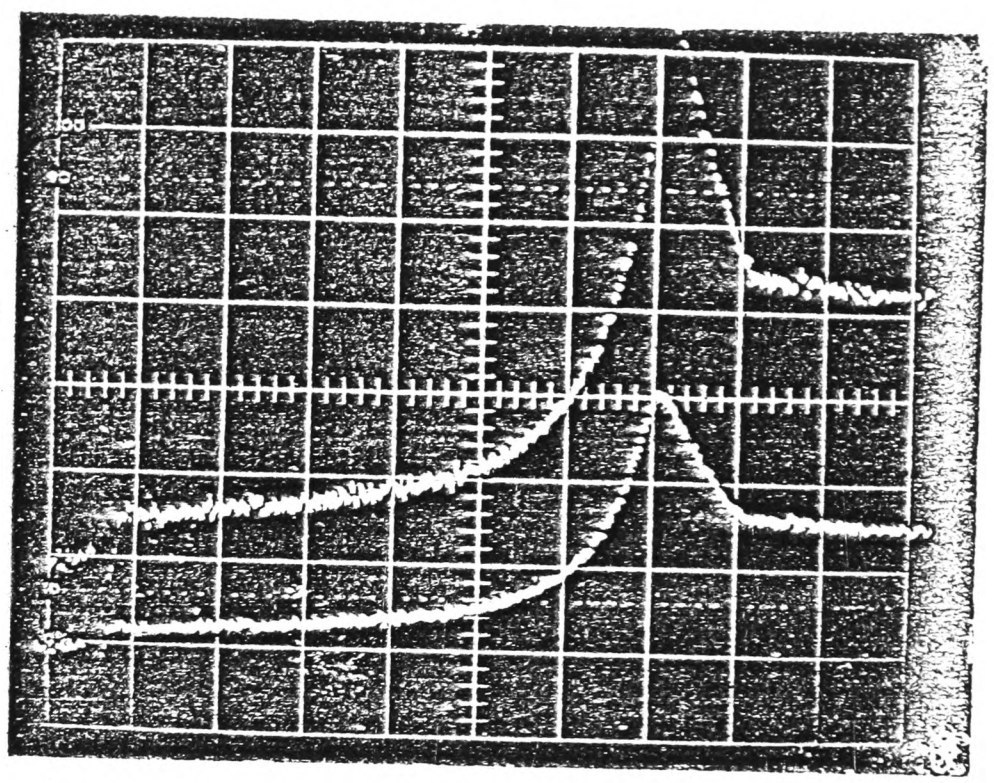
distributions, reactions known to be sensitive to small quantities of impurity should be avoided, as the shock tube is not 'ultraclean'. Thus our CO_2 decomposition rate constants [6], for instance, while agreeing with much early work [149], produce an activation energy significantly below that of recent extremely careful work [176] which measured the initial rate. On the other hand results that we have obtained on the OCS decomposition, on CO/CO, CO/Ar and DCl/DCl vibrational relaxation times, and on the rate of the CO/CO isotope exchange in the presence of added N_2O, are in good agreement with accepted rate constants.

The avoidance of impurity effects is more important in experiments where the results are of theoretical interest e.g. the value of the activation energy for the CO_2 decomposition, than in those whose results are of practical interest e.g. studies of processes important in combustion. This is because impurities are present in the real world as well as in the shock tube. However it is important to know the nature and quantities of the impurities and increased use of mass spectral analysis will be vital here (see chapter 10).

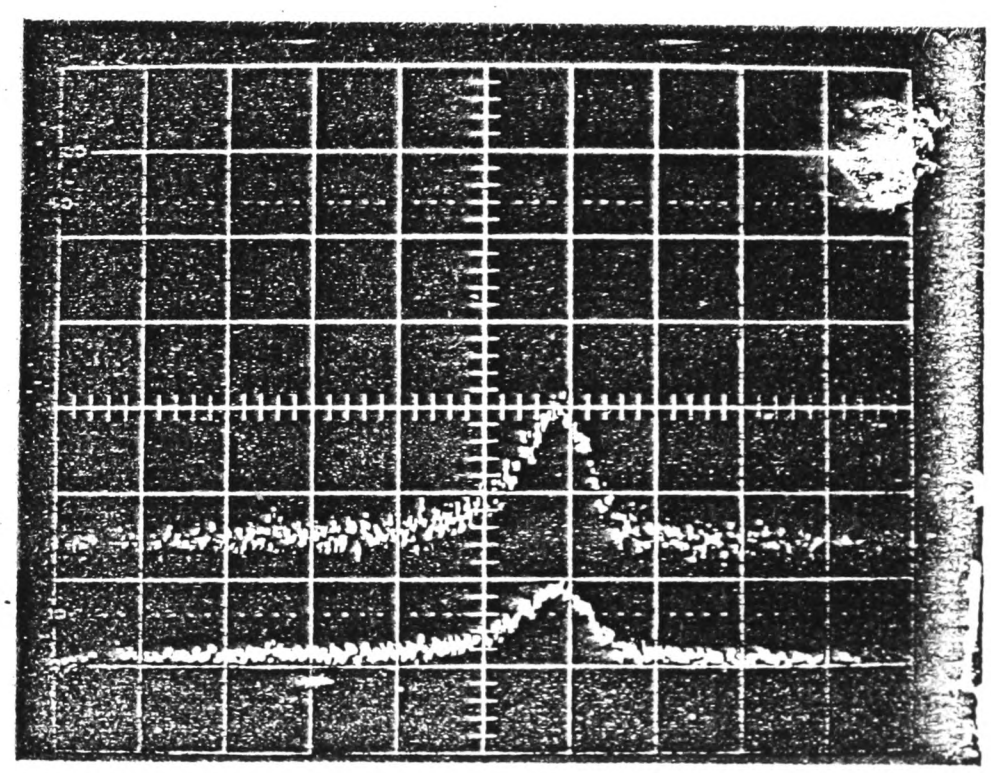
One system which has been looked at in a preliminary manner is $CS_2 + O_2$. This was chosen because it is a reaction known to produce vibrationally excited CO, as it is the basis for the CO chemical laser. It made a welcome change from observing CO born in v=0. Two results are shown in figure 11.1, monitoring the 4->3 and 15->14 bands of CO. A 1 % CO, 4.3 % CO_2 and 94.7 % Ar mixture was used. There is a long induction time before the CO is born. The 15->14 absorption returns to the baseline but the 4->3 falls to the value corresponding to to the appreciable equilibrium population in v=3 at the temperature of the experiment (~2000 K). It is likely that the CO is born in very high levels, and that the population cascades down into the lower levels. However it would be difficult to experimentally observe different delay

FIGURE 11.1

CS_2 OXIDATION



4->3P(10)



15->14P(8)

times before different levels are formed. Because of the rapidity of (VV) energy transfer, time delays between the formation of successive levels will be very short, also conditions are not exactly reproducible from shock to shock. An attempt to circumvent this was made by using the 9->8P(9) laser line, which monitors both v=8,J=9 and v=1,J=46 (see section 4.8), in the hope that the rise and fall of population in v=8, followed by the rise in population of v=1, would be seen. This was not observed, with only one rise being seen. So it is unlikely that precise information on vibrational level distributions could be obtained, as has been at lower temperatures in the reaction initiated by a pulsed electric discharge [177] (the distribution peaks at v=13). Dibble and Bowen [60], using reflected shocks and a rather primitive CO laser, shocked a 5 % CS_2, 95 % O_2 mixture and observed positive gain at 860 K and 500 torr, but only after a 660 μs induction time. Their results were irreproducible. For us to repeat these experiments would be impossible, as the contact surface would intervene before the induction time was complete.

If we cannot observe the vibrational product distribution, in this case, we can certainly obtain kinetic information e.g. the length of the induction time. A previous study of the reaction in a shock tube [178] gave results that could not be explained by any plausible mechanism so there is scope for further investigations.

Of more practical interest than the CS_2/O_2 reaction, and to be given precedence by us, is the study in collaboration with British Gas of some processes which are important in combustion, firstly the decomposition of formaldehyde. This is a complex process, important because CH_2O is an intermediate in the oxidation of methane (see e.g. [179]). Dean et al. [180] used infrared emission from CH_2O to follow the decomposition in a shock tube, and explained the results in terms of

the following mechanism:

$$CH_2O + M \rightleftharpoons CHO + H + M \qquad (11.3)$$

$$CH_2O + H \rightleftharpoons CHO + H_2 \qquad (11.4)$$

$$CHO + M \rightleftharpoons H + CO + M \qquad (11.5)$$

$$CHO + H \rightleftharpoons CO + H_2 \qquad (11.6)$$

They found that the direct route

$$CH_2O + M \rightleftharpoons CO + H_2 + M \qquad (11.7)$$

was not significant, but this was a controversial point as the discussion at the end of their paper shows. We can obtain complementary information by monitoring the CO product, and also repeat their determination of the CH_2O decay using a chance coincidence. The CHO concentration is expected to be too low to be monitored by infrared absorption. If conditions under which vibrational relaxation of the CO is slow compared to its formation can be obtained, the initial product distribution of the CO will be examined too. Its interpretation will be complicated as CO is formed by processes (11.5), (11.6) and possibly (11.7), but the information could turn out to be vital. In a reaction where the mechanism is as complex as this, the mechanism of the photolysis, as investigated by Houston and Moore [8], will be quite different. Houston and Moore obtained the vibrational distribution of the CO product.

If this study is successful, logical follow-ups are the oxidation of CH_2O (by O_2 and/or O atoms from N_2O), and the decomposition and

oxidation of glyoxal, CHO-CHO.

The isotope exchange studies discussed in section 10.8 are not to be forgotten.

11.3 Further Energy Transfer Work

Vibrational relaxation time measurements using the techniques developed in chapter 8 can be readily made. The relaxation of CO by numerous additives could be studied, but kinetics experiments are considered to be of greater interest. More novel would be the determination of relaxation times for N_2 by various additives. This could be done by monitoring CO added to the mixture, with the N_2 in excess. (VT) energy transfer would then be dominated by N_2, and (VV) processes would hold the CO/N_2 system in a quasi-equilibrium. The vibrational temperature of the CO could be obtained from the experimental gain as in chapter 8. The vibrational temperature of the N_2 at that time would be given by Treanor's equation (9.2), and then $F(T_{vib})$ could be plotted for N_2.

The possibility of observing rotational energy transfer effects requires consideration. Generally, rotational energy transfer is too fast to be observed in our experiments, and any species being monitored may safely be assumed to be rotationally equilibrated. However this may not be the case where very high rotational levels are involved, and the gaps between successive levels are greater. The rotational levels that are normally monitored by our CO laser are J=7-13, levels lower than the most populated level, which is J~20 at 2000 K. What is required is a chance coincidence that enables observation of a much higher J level of the 1->0 vibrational band - this could be monitored for CO shock-heated from room temperature, or CO born in a decomposition. The population of a higher level will be more sensitive to the rotational temperature.

Unfortunately there is no such sure-fire coincidence; the best is perhaps the 13->12P(17) line of $^{12}C^{16}O$ monitoring the 1->0P(70) line of $^{13}C^{16}O$ but the laser does not normally run on this line, and the Dunham coefficients may not be reliable for energies of levels up to J=70. To produce high J-lines, a higher than liquid nitrogen temperature is required, but at higher temperatures a different gas mixture, possibly including xenon, is necessary. Xenon is absolutely necessary for CO lasers which operate at room temperature. Our laser was designed for use at liquid nitrogen temperatures and has never been run at higher temperatures.

As chance would have it, there are more coincidences involving the expensive isotope $^{12}C^{17}O$, either in the laser or in the test gas. The frequencies show that 6->5P(13) of $^{12}C^{16}O$ can be used to monitor 1->0P(36) of $^{12}C^{17}O$, and 8->7P(9) of $^{12}C^{17}O$ can be used to monitor 1->0P(45) of $^{13}C^{16}O$. No viable coincidence exists to monotor a high J-level of the 1->0 band of $^{12}C^{16}O$, which is unfortunate as it therefore requires an isotopically-substituted parent compound to obtain information on the rotational product distribution from a decomposition.

11.4 Changes to Apparatus and Data Analysis

There are enough experiments to do to keep the shock tube / CO laser combination in use for several years. However it is a good plan to study a reaction by more than one technique. If results from more than one technique agree, those results have greater authority. The possible use of intra-cavity dye laser spectroscopy with the shock tube was mentioned in section 2.19. The proposal to develop the technique of SIDLS was given an alpha grade by the S.E.R.C. but lack of funds meant that the money was not forthcoming. As the dye laser would have to be built specially with a cavity sufficiently long to take the width of the

shock tube, use of a shared facility is not possible. It was intended to use SIDLS to monitor the CHO radical in the pyrolysis and oxidation of formaldehyde, and NHO and C_2 are other species that the technique could be applied to. This would have provided totally new information on the kinetics of fundamental reactions.

A less ambitious plan is to build an OH lamp to monitor OH in combustion processes. OH is not involved in the pyrolysis of formaldehyde [180] but is in its oxidation [46].

Eventually the CO laser could be replaced by a tunable diode laser as used by Hanson [56]. This has the advantage that the range of available frequencies is continuous.

The shock tube is likely to remain in its present form. A new tube would require many months of work characterising the flow conditions as was done for the present tube. It may be possible to keep the present driver section and dump tank but replace the test section with one of identical dimensions but 'ultraclean' design.

The logical future development of the data analysis is for direct fitting of the results to a model of the system. (At present the results analysis and numerical integration are completely separate and output is compared by eye.) This will require a link from our North Star Advantage microcomputer to the P.C.L.'s Norsk Data minicomputer. The numerical integration could involve the Rankine-Hugoniot equations as well as the kinetic equations, and this would produce point-to-point values of the temperature, pressure and density as well as species concentrations. An article by Gardiner, Walker and Wakefield [181] describes the necessary mathematics. Note that when it is known that the vibrational energy levels are not in Boltzmann equilibrium at the translational temperature, the equilibrium value of the enthalpy cannot

be used.

11.5 Conclusions

The possibilities for studies of energy transfer in triatomics had become exhausted. Meanwhile new technical developments had been made, and so the carbon monoxide infrared laser had been brought in to replace the laser schlieren system. The question was, what possibilities were there with the new system?

The opportunity was taken to carry out a detailed investigation of vibrational energy transfer in the diatomic molecule carbon monoxide. This followed on neatly from what had gone before, but was also a necessary precursor of what was to come. The results were in accord with the established theories, but confusion, arising from the erroneous experimental results of others and their misinterpretation of the theories, had to be cleared up, and to further this cause the experiments were extended to deuterium chloride.

Having paused to establish a technique for the ready determination of vibrational relaxation rates, the work moved into the wider fields of chemical kinetics. The first investigation was of the relatively simple decomposition of carbonyl sulphide. The direct determination of the vibrational product distribution was a novel piece of work for a thermally-induced decomposition. This experiment aroused great interest, and a follow-up program of investigations into the unimolecular decomposition of larger molecules is underway.

Another investigation that the technique seemed particularly suitable for was into the scrambling of atoms between isotopes of carbon monoxide. This ran into trouble from impurities, but not without producing further evidence in favour of an atomic chain mechanism.

A wide range of reactions has been considered for future work, and studies of the pyrolysis and oxidation of formaldehyde are set to begin.

The technique is now well established. Time-dependent vibrational spectroscopy has been shown to bring insight on diverse problems of chemical interest. The future looks bright.

REFERENCES

[1] J. P. Martin, M. R. Buckingham, J. A. Chenery and C. J. S. M. Simpson, Chem. Phys. 74 (1983) 15.

[2] A. J. Aherne, J. P. Buxton, J. A. Chenery, A. Fakhr and C. J. S. M. Simpson, Chem. Phys. Lett. 98 (1983) 93.

[3] E. W. Montroll and K. E. Shuler, J. Chem. Phys. 26 (1957) 454.

[4] C. C. Rankin and J. C. Light, J. Chem. Phys. 46 (1967) 1305.

[5] C. C. Chow and E. F. Greene, J. Chem. Phys. 43 (1965) 324.

[6] J. A. Chenery, A. Fakhr, M. I. Wood and C. J. S. M. Simpson, Chem. Phys. Lett. 96 (1983) 143.

[7] M. C. Lin, Chem. Phys. 7 (1975) 433.

[8] P. L. Houston and C. B. Moore, J. Chem. Phys. 65 (1976) 757.

[9] B. I. Sonobe, T. R. Fletcher and R. N. Rosenfeld, Chem. Phys. Lett. 105 (1984) 322.

[10] M. R. Driels, J. Sound and Vibration 84 (1982) 563.

[11] D. Barschdorff, Phys. Fluids 18 (1975) 529.

[12] A. W. Hodgson and J. C. Mackie, J. Colloid and Interface Science 83 (1981) 547.

[13] W. H. Beck and J. C. Mackie, J. Phys. D 11 (1978) 1249.

[14] S. Nakajima, K. Kosasa, Y. Maruyama and S. Kawai, Spect. Acta 37B (1982) 685.

[15] S. K. Kanoo and S. Jois, Proc. Ind. Nat. Sci. Acad. 46A (1980) 456.

[16] R. E. Dannerberg, A.I.A.A. J. 14 (1976) 1183.

[17] I. I. Glass and W. S. Liu, J. Flu. Mech. 84 (1978) 55.

[18] R. J. Stalker, Aero. Q. 17 (1966) 351.

[19] C. J. S. M. Simpson, K. B. Bridgman and T. R. D. Chandler, J. Chem. Phys. 49 (1968) 509.

[20] O. Laporte and M. J. Yoder in Shock Tube Research, Proceedings of 8th International Shock Tube Symposium, London (1971).

[21] M. W. Matthew and J. Steinwandel, J. Aerosol Sci. 14 (1983) 755.

[22] E. F. Greene and J. P. Toennies, Chemical Reactions in Shock Waves, Arnold, London (1964).

[23] R. L. Belford and R. A. Strehlow, Ann. Rev. Phys. Chem. 20 (1969) 247.

[24] A. Lesage, S. Sahal-Brechot and M. H. Miller, Phys. Rev. A16 (1977) 1617.

[25] M. F. Weisbach and C. Chackerian Jr, J. Chem. Phys. 59 (1973) 4272.

[26] M. Frenklach, S. Taki, C. K. Li Kwok Cheong and R. A. Matula, Comb. Flame 51 (1983) 37.

[27] W. R. Seeker, T. W. Lester and J. F. Merklin, Rev. Sci. Inst. 51 (1980) 1523.

[28] A. E. Nasser and R. A. East, Int. J. Heat and Mass Trans. 23 (1980) 515.

[29] S. Fujikawa, T. Akamatsu, J. Yahara and H. Fujioka, App. Sci. Res. 38 (1982) 363.

[30] J. P. Appleton, J. Chem. Phys. 47 (1967) 3231.

[31] A. Lifshitz, S. H. Bauer and E. L. Resler Jr, J. Chem. Phys. 38 (1963) 2056.

[32] A. Bar-Nun and A. Lifshitz, J. Chem. Phys. 47 (1967) 2878.

[33] W. Tsang, in Shock Waves in Chemistry, ed. A. Lifshitz, Marcel Dekker, New York (1981).

[34] S. C. Khandelwal and G. B. Skinner, in Shock Waves in Chemistry, ed. A. Lifshitz, Marcel Dekker, New York (1981).

[35] R. D. Kern and G. G. Nika, J. Phys. Chem. 75 (1971) 171.

[36] C. J. S. M. Simpson, K. B. Bridgman and T. R. D. Chandler, J. Chem. Phys. 49 (1968) 513.

[37] J. H. Kiefer, M. Z. Al-Alami and J. C. Hajduk, Applied Optics 20 (1981) 221 and 2042.

[38] J. H. Kiefer and J. C. Hajduk, Shock Tubes and Waves, Proceedings of the 12th International Symposium on Shock Tubes and Waves, Jerusalem

(1979), p. 97.

[39] J. H. Kiefer, M. Z. Al-Alami and K. A. Buclach, J. Phys. Chem. 86 (1982) 808.

[40] C. J. S. M. Simpson, T. R. D. Chandler and A. C. Strawson, J. Chem. Phys. 51 (1969) 2214.

[41] P. D. Gait, D. Phil. Thesis, University of Oxford (1974).

[42] J. H. Kiefer, in Shock Waves in Chemistry, ed. A. Lifshitz, Marcel Dekker, New York (1981).

[43] J. Heppner, W. Liese, G. J. Deppe and H. Quakulinsky, J. Phys. E12 (1979) 105.

[44] Y. Hidaka, H. Kawano and M. Suga, Bull. Chem. Soc. Japan 55 (1982) 351.

[45] Y. Hidaka, T. Kataoka and M. Suga, Bull. Chem. Soc. Japan 47 (1974) 2166.

[46] A. M. Dean, R. L. Johnson and D. C. Steiner, Comb. Flame 37 (1980) 41.

[47] P. Borrell and G. E. Millward, J. Chem. Soc. Faraday II 69 (1973) 1060.

[48] D. J. Seery, J. Chem. Phys. 58 (1973) 1796.

[49] J. A. Chenery, Part II Thesis, University of Oxford (1981).

[50] W. J. Hooker and R. C. Millikan, J. Chem. Phys. 38 (1963) 214.

[51] A. L. Myerson and W. S. Watt, J. Chem. Phys. 49 (1968) 425.

[52] R. Lohr and P. Roth, Ber. Bunsen 85 (1981) 153.

[53] T. Just in Shock Waves in Chemistry, ed. A. Lifshitz, Marcel Dekker, New York (1981).

[54] R. K. Hanson, S. Salimian, G. Kychakoff and R. A. Booman, Applied Optics 22 (1983) 641.

[55] D. J. Eckstrom and D. Bershader, J. Chem. Phys. 57 (1972) 632.

[56] R. K. Hanson, Applied Optics 16 (1977) 1479.

[57] R. K. Hanson, J. P. Monat and C. H. Kruger, J. Quant. Spec. and

Rad. Trans. 16 (1976) 705.

[58] M. Y. Louge and R. K. Hanson, Int J. Chem. Kin. 16 (1984) 231.

[59] C. Chackerian Jr. and M. F. Weisbach, J. Chem. Phys. 59 (1973) 807.

[60] R. W. Dibble and J. R. Bowen, J. Chem. Phys. 65 (1976) 2028.

[61] R. M. Siddles, D. Phil. Thesis, University of Oxford, to be published (198?)

[62] G. H. Atkinson, Private communication.

[63] S. J. Harris, Applied Optics 23 (1984) 1311.

[64] J. F. Bott and N. Cohen, Recent Developments in Shock Tube Research, Proceedings of 9th International Shock Tube Symposium, Stanford (1973) P.251.

[65] M. M. Maricq, E. A. Gregory, C. T. Wickham-Jones, D. J. Cartwright and C. J. S. M. Simpson, Chem. Phys. 75 (1983) 347.

[66] J. W. Glaser and S. Lederman, A.I.A.A. J. 21 (1983) 85.

[67] A. Lifshitz, M. Bidani and H. F. Carroll, J. Chem. Phys. 79 (1983) 2742.

[68] A. Lifshitz, M. Bidani and H. F. Carroll, Rev. Sci. Int. 52 (1981) 622.

[69] P. Borrell, P. M. Borrell, M. D. Pedley and K. R. Grant, Proc. Roy. Soc. A367 (1979) 395.

[70] R. B. Klemm, T. Tanzawa, E. G. Skolnik and J. V. Michael, 18th Symp. (Int.) Comb. (1981) 785.

[71] A. Fontijn, W. Felder and J. J. Houghton, 16th Symp. (Int.) Comb. (1976) 871.

[72] J. F. Griffiths and A. Perche, 18th Symp. (Int.) Comb. (1981) 893.

[73] G. Kychakoff, R. D. Howe, R. K. Hanson and J. C. McDaniel, Applied Optics 21 (1982) 3225.

[74] C. J. S. M. Simpson, T. R. D. Chandler and F. W. J. Clutterbuck, J. Phys E2 (1969) 99.

[75] P. Brechignac and J. P. Martin, I.E.E.E. J. Quantum Elec. 12 (1976)

80.

[76] J. P. Martin, These de Docteur es Sciences Pysiques, Universite de Paris-Sud (1979).

[77] M. L. Bhaumik, W. B. Lacina and M. M. Mann, I.E.E.E. J. Quantum Elec. 8 (1972) 150.

[78] B. Sidney, R. M. McInville and H. A. Hassan A.I.A.A. J. 14 (1976) 923.

[79] C. E. Treanor, J. W. Rich and R. G. Rehm, J. Chem. Phys. 48 (1968) 1798.

[80] G. E. Caledonia and R. E. Center, J. Chem. Phys. 55 (1971) 552.

[81] C. J. S. M. Simpson, T. R. D. Chandler and K. B. Bridgman, Phyics of Fluids 10 (1967) 1894.

[82] C. J. S. M. Simpson, unpublished work.

[83] J. H. Kiefer and R. W. Lutz, J. Chem. Phys. 44 (1966) 658.

[84] C. J. S. M. Simpson and T. R. D. Chandler, Proc. Roy. Soc. A317 (1970) 265.

[85] C. J. S. M. Simpson and J. M. Simmie, Proc. Roy. Soc. A325 (1971) 197.

[86] C. J. S. M. Simpson, P. D. Gait and J. M. Simmie, Chem. Phys. Lett. 22 (1973) 144.

[87] C. J. S. M. Simpson, P. D. Gait and J. M. Simmie, Recent Developments in Shock Tube Research, Proceedings of 9th International Shock Tube Symposium, Stanford (1973) p.352.

[88] A. J. Andrews, M. E. Crowther, T. J. Price, C. J. S. M. Simpson and P. D.Gait, Modern Developments in Shock Tube Research, proceedings of 10th Internatioal Shock Tube Symposium, Kyoto (1975) p.569.

[89] C. J. S. M. Simpson, P. D. Gait and J. M. Simmie, Proc. Roy. Soc. A348 (1976) 57.

[90] C. J. S. M. Simpson, P. D. Gait and J. M. Simmie, Proc. Roy. Soc. A348 (1976) 73.

[91] C. J. S. M. Simpson, P. D. Gait and J. M. Simmie, J. Chem. Soc. Faraday II 72 (1976) 417.

[92] C. J. S. M. Simpson, P. D. Gait, T. J. Price and M. G. Foster, Chem. Phys. 68 (1982) 293.

[93] C. J. S. M. Simpson, T. J. Price and M. E. Crowther, Chem. Phys. Lett. 34 (1975) 181.

[94] C. J. S. M. Simpson, J. Chem. Phys. 58 (1973) 5844.

[95] C. J. S. M. Simpson, P. D. Gait and J. M. Simmie, Chem. Phys. Lett. 47 (1977) 133.

[96] M. G. Foster and C. J. S. M. Simpson, J. Chem. Soc. Faraday II 75 (1979) 509.

[97] J. M. Jackson, P. A. Lewis, M. P. Skirrow and C. J. S.M. Simpson, J. Chem. Soc. Faraday II 75 (1979) 1341.

[98] K. C. Lapworth, J. Phys. A2 (1969) 415.

[99] Joint Army Navy Air Force Thermochemical Tables, 2nd edition, Washington (1971).

[100] J. T. Davies and J. M. Vaughan, Astrophysics J. 137 (1963) 1302.

[101] J. A. Dowling, S. Silverman, W. S. Benedict and J. W. Quinn, J. Res. Nat. Bur. Stan. 75A (1971) 469.

[102] H. J. Werner, Mol. Phys. 44 (1981) 111.

[103] D. Williams, D. C. Wenstrand, R. J. Brockman and B. Curnutte, Mol. Phys. 20 (1971) 769.

[104] T. R. Todd, C. M. Clayton, W. B. Telfair, T. K. McCubbin, Jr. and J. Pliva, J. Mol. Spec. 62 (1976) 201.

[105] J. D. Lambert, Vibrational and Rotational Relaxation in Gases, Clarendon Press, Oxford (1977).

[106] L. Landau and E. Teller, Phys. Zeit. der Sowjetunion 10 (1936) 34.

[107] R. N. Schwartz, Z. I. Slawsky and K. F. Herzfeld, J. Chem. Phys. 20 (1952) 1591.

[108] D. L. Matthews, J. Chem. Phys. 34 (1961) 639.

[109] K. F. Herzfeld and T. A. Litovitz, Absorption and Dispersion of Ultrasonic Waves, Academic Press, New York (1959).

[110] B. Stevens, Collisional Activation in Gases, The International Encyclopaedia of Physical Chemistry and Chemical Physics, Topic 19 Volume 3, Pergamon, Oxford (1967).

[111] J. T. Yardley, Introduction to Molecular Energy Transfer, Academic Press, New York (1980).

[112] H. A. Bethe and E. Teller, Ballistic Research Labs, Aberdeen Proving Ground, Maryland, Report X-117 (1945).

[113] M. J. Pilling, Science Progress, 63 (1976) 397.

[114] D. J. Kewley, J. Phys. B8 (1975) 2565.

[115] R. D. Sharma and C. A. Brau, J. Chem. Phys. 50 (1969) 924.

[116] G. Hancock and I. W. M. Smith, Applied Optics 10 (1971) 1827.

[117] H. T. Powell, J. Chem. Phys. 63 (1975) 2635.

[118] W. D. Breshears and P. F. Bird, J. Chem. Phys. 50 (1969) 333.

[119] C. B. Moore, J. Chem. Phys. 43 (1965) 2979.

[120] E. A. Gregory, M. R. Buckingham, D. Z. Clayton, F. J.Wolfenden and C. J. S. M. Simpson, Chem. Phys. Lett. 104 (1984) 393.

[121] R. Herman and R. J. Rubin, Physics of Fluids 2 (1959) 547.

[122] N. W. Bazley, E. W. Montroll, R. J. Rubin and K. E. Shuler, J. Chem. Phys. 28 (1958) 700 ; 29 (1958) 1185.

[123] H. Teitelbaum, Can. J. Chem. 61 (1983) 1267.

[124] K. N. C. Bray, J. Phys. B1 (1968) 705.

[125] J. W. Rich and R. G. Rehm, 11th Symp. (Int.) Comb. (1967) 37.

[126] G. M. Jursich and F. F. Crim, J. Chem. Phys. 74 (1981) 4455.

[127] H. Teitelbaum, Can. J. Chem. 61 (1983) 1276.

[128] H. Teitelbaum, Can. J. Chem. 61 (1983) 1253.

[129] W. D. Breshears, Chem. Phys. Lett. 20 (1973) 429.

[130] K. Glanzer and J. Troe, J. Chem. Phys. 63 (1975) 4352.

[131] K. Glanzer, Chem. Phys. 22 (1977) 367.

[132] M. Windsor, N. Davidson and R. Taylor, 7th Symp. (Int.) Comb. (1959) 80.

[133] J. H. Kiefer and J. C. Hajduk, Chem. Phys. 38 (1979) 329.

[134] J. P. Appleton, M. Steinberg and D. J. Liquornik, J. Chem. Phys. 48 (1968) 599.

[135] R. C. Millikan, J. Chem. Phys. 40 (1964) 2594.

[136] R. C. Millikan, J. Chem. Phys. 38 (1963) 2855.

[137] K. P. Huber and G. Herzberg, Molecular Spectra and Molecular Structure IV. Constants of Diatomic Molecules, van Nostrand, New York (1979).

[138] C. Carruthers and H. Teitelbaum, to be published.

[139] K. E. Shuler, J. Chem. Phys. 30 (1959) 1631.

[140] J. A. Coxon and J. F. Ogilvie, J. Chem. Soc. Faraday II 78 (1982) 1345.

[141] E. F. Greene, Private Communication.

[142] A. I. Demin, E. M. Kudryavtsev, Y. A. Kulagin and N. N. Sobolev, Sov. Phys. JETP Lett. 18 (1973) 149.

[143] H. A. Olschewski, J. Troe and H. Gg. Wagner, Ber. Bunsen. 70 (1966) 450.

[144] B. E. Holmes and D. W. Setser, in Physical Chemistry of Fast Reactions Volume II, Reaction Dynamics ed. I. W. M. Smith, Plenum, New York (1980).

[145] I. W. M. Smith, Kinetics and Dynamics of Elementary Gas Reactions, Butterworths, London (1980), chapter 6.

[146] A. J. Hay and R. L. Belford, J. Chem. Phys. 47 (1967) 3944.

[147] H. G. Schecker and H. Gg. Wagner, Int. J. Chem. Kin. 1 (1969) 541.

[148] R. E. Center, J. Chem. Phys. 58 (1973) 5230.

[149] J. Troe and H. Gg. Wagner, in Physical Chemistry of Fast Reactions Volume 1, Gas Phase Reactions of Small Molecules, ed. B. P. Levitt, Plenum, London (1973).

[150] J. Troe and H. Gg. Wagner, Ber. Bunsen. 71 (1967) 937.

[151] A. Bar-Nun and A. Lifshitz, J. Chem. Phys. 51 (1969) 1826.

[152] A. F. Bopp, R. D. Kern, and B. V. O'Grady, J. Phys. Chem. 79 (1975) 1483.

[153] I. W. M. Smith and P. M. Wood, Mol. Phys. 25 (1973) 441.

[154] J. M. Bopp, R. D. Kern and T. Niki, J. Phys. Chem. 81 (1977) 1795.

[155] A. F. Bopp. R. D. Kern, T. Niki and G. M. Stack, J. Phys. Chem. 83 (1979) 2933.

[156] R. D. Kern and G. G. Nika, J. Phys. Chem. 75 (1971) 1615.

[157] H. Horiguchi and S. Tsuchiya, Int. J. Chem. Kin. 13 (1981) 1085.

[158] A. H. M. Ross, R. S. Eng and H. Kildal, Opt. Comm. 12 (1974) 433.

[159] S. Jaffe and F. S. Klein, J. Chem. Soc. Far. Trans. 62 (1966) 3135.

[160] J. P. Appleton, M. Steinberg and D. J. Liquornik, J. Chem. Phys. 52 (1970) 2205.

[161] A. R. Fairbairn, Proc. Roy. Soc. A312 (1969) 207.

[162] K. G. P. Sultzmann, B. F. Myers and E. R. Bartle, J. Chem. Phys. 42 (1965) 3969.

[163] M. J. Pilling and R. M. Noyes, Int. J. Chem. Kin. 11 (1979) 821.

[164] A. L. Rockwood, D. L. Bahler and E. A. McCullough, Jr., J. Chem. Phys. 80 (1984) 6052.

[165] T. L. Gilchrist and R. C. Store, Organic Reactions and Orbital Symmetry, Cambridge, 2nd edition (1979), section 4.2

[166] J. P. Buxton, Part Two Thesis, University of Oxford (1983).

[167] R. H. Sohm, Part Two Thesis, University of Oxford (1984).

[168] J. P. Buxton, R. H. Sohm and C. J. S. M. Simpson, Chem. Phys. to be published.

[169] J. P. Buxton, D. Phil. Thesis, University of Oxford, to be published (1986?)

[170] W. R. Dolbier and H. M. Frey, J. Chem. Soc. Perkin II (1974) 1674.

[171] B. K. Carpenter, Private Communication.

[172] J. Troe, Private Communication.

[173] D. C. Astholz, J. Troe and W. Wieters, J. Chem. Phys. 70 (1979) 5107.

[174] K. Glanzer, M. Maier and J. Troe, Chem. Phys. Lett. 61 (1979) 175.

[175] M. P. Roellig, P. L. Houston, M. Asscher and Y. Haas, J. Chem. Phys. 73 (1980) 5081.

[176] J. H. Kiefer, J. Chem. Phys. 61 (1974) 244.

[177] S. Tsuchiya, N. Nielsen and S. H. Bauer, J. Phys. Chem. 77 (1973) 2455.

[178] J. Hardy and W. C. Gardiner, Jr, Symp. (Int.) Comb. (1976) 985.

[179] C. T. Bowman, 15th Symp. (Int.) Comb. (1974) 869.

[180] A. M. Dean, B. L. Craig, R. L. Johnson, M. C. Schultz and E. E. Wang, 17th Symp. (Int.) Comb. (1978) p. 577.

[181] W. C. Gardiner, Jr, B. F. Walker and C. B. Wakefield, in Shock Waves in Chemistry, ed. A. Lifshitz, Marcel Dekker, New York (1981).